Hélio Jacinto da Cruz Neto

Active Control of Stick-Slip Oscillations in Oil-well Drilling Systems

São Carlos

2022

Hélio Jacinto da Cruz Neto

Active Control of Stick-Slip Oscillations in Oil-well Drilling Systems

Thesis presented to São Carlos School of Engineering, University of São Paulo, as part of the requirements for the degree of Doctor of Science - Post-graduate Program in Mechanical Engineering.

Concentration area: Dynamics and Mechatronics

Advisor: Marcelo Areias Trindade

São Carlos
2022

CORRECTED VERSION
ORIGINAL VERSION
AVAILABLE ON
MECHANICAL
ENGINEERING
DEPARTMENT AT
EESC-USP.

Catalog card prepared by Patron Service at "Prof. Dr. Sergio Rodrigues Fontes" Library at EESC/USP

Cruz Neto, Hélio Jacinto da
C957a Active control of stick-slip oscillations in oil-well drilling systems / Hélio Jacinto da Cruz Neto; Dissertation Thesis directed by Marcelo Areias Trindade. -- São Carlos, 2023.

Doctoral (Dissertation) - Graduate Program in Mechanical Engineering and Research Area in Dynamic and Mechatronics -- São Carlos School of Engineering of the University of São Paulo, 2022.

1. Stick-slip. 2. Drill string. 3. Negative damping coefficient. 4. Optimal static output feedback. 5. Negative damping control. 6. Global stability. I. Title.

Elena Luzia Palloni Gonçalves – CRB 8/4464

FOLHA DE JULGAMENTO

Candidato: Engenheiro **HELIO JACINTO DA CRUZ NETO.**

Título da tese: "Controle ativo de oscilações de *Stick-Slip* em sistemas de perfuração de poços de petróleo"

Data da defesa: 02/02/2023.

Comissão Julgadora	**Resultado**
Prof. Titular **Marcelo Areias Trindade** **(Orientador)** (Escola de Engenharia de São Carlos/EESC-USP)	APROVADO
Prof. Dr. **Rubens Sampaio Filho** (Pontifícia Universidade Católica do Rio de Janeiro/PUC-RJ)	Aprovado
Prof. Dr. **Thiago Gamboa Ritto** (Universidade Federal do Rio de Janeiro/UFRJ)	APROVADO
Prof. Associado **Rodrigo Nicoletti** (Escola de Engenharia de São Carlos/EESC-USP)	Aprovado
Prof. Dr. **Juan Francisco Camino** (Universidade Estadual de Campinas/UNICAMP)	Aprovado

Coordenador do Programa de Pós-Graduação em Engenharia Mecânica:
Prof. Associado **Adriano Almeida Gonçalves Siqueira**

Presidente da Comissão de Pós-Graduação:
Prof. Titular **Murilo Araujo Romero**

Acknowledgements

Countless people contributed directly or indirectly to the development of this work, and the brevity of this section is perhaps not enough to express my gratitude to them accordingly. Still, I would like to dedicate a few words of thanks to some people that my poor memory allows me to remember.

Professor Marcelo Trindade was one of the cleverest people I encountered during my development as a researcher, and I am very grateful for the opportunity I had to work with him. Our several discussions on research topics and beyond have contributed enormously to my professional development. I hope our collaboration will last for a long time.

I wish I could properly describe all the support I received from my family, especially my parents, Aparecida and José, and my sister, Isabel. Everything I have become today has solid foundations in the teachings and examples I received from my parents, which I will carry with me for the rest of my life. I am deeply grateful for the emotional and financial support they have given me over all these years.

During the entire period of my doctorate, I had great support from Nathália, who closely followed the development of this project. I am genuinely grateful for all the patience and care I have received from her, especially in these last few years that we have been living together. Her loving presence made all the difference.

I thank my laboratory colleagues for the opportunities to learn about several interesting research topics, as well as, of course, the several chess games we played.

I thank the employees of the mechanical engineering department, especially Iara and Ana Paula (in memoriam), for their help with all additional aspects of the graduate program.

I thank the jury for taking the time to read, evaluate and give suggestions to this thesis.

Lastly, I would like to thank the financial support from Coordenação de Aperfeiçoamento de Pessoal de Nível Superior (CAPES), essential for the development of this work.

List of Figures

List of Tables

List of abbreviations and acronyms

WOB	Weight-On-Bit
BHA	Bottom-Hole-Assembly
DOF	Degree Of Freedom
FE	Finite Element
ODE	Ordinary Differential Equation
PDE	Partial Differential Equation
PI	Proportional-Integral
LQR	Linear Quadratic Regulator
OSOF	Optimal Static Output Feedback
LQG	Linear Quadratic Gaussian
ARE	Algebraic Riccati Equation
SQP	Sequential Quadratic Programming

Abstract

Cruz Neto, H.J. Active Control of Stick-Slip Oscillations in Oil-well Drilling Systems. Doctoral Thesis - São Carlos School of Engineering, University of São Paulo, São Carlos, 2022.

Rotary drilling systems are subjected to harmful interactions between the drilling structure, borehole and rock formation, leading to torsional stick-slip vibrations that can decrease drilling efficiency and cause drill string component failures. A proper way to reduce these detrimental failures is to design an active controller that efficiently mitigates vibrations with the constraint of using the limited amount of real-time data available in field operations. In this context, this thesis proposes two novel control techniques relying only on simple linear combinations of measured signals to mitigate drill string torsional vibrations and improve drilling performance. Since the measured signals are of paramount importance for the effectiveness of the proposed techniques, this work also investigates which signals are relevant for feedback with the aim of ensuring asymptotic stability. The first proposed control technique relies on a work developed by the author during his master's degree, and consists of determining the control gain of an output feedback controller (OSOF) such that its performance is as close as possible to that of a full state feedback controller (LQR). The second proposed control technique derives from the negative damping coefficient concept developed in this thesis, and aims to enlarge the limits of drill string safe operation by minimizing the value of the negative damping coefficient for which the operating point is asymptotically stable. The proposed controllers are applied to a representative drill string torsional dynamics model, modeled using the finite element method with non-regularized dry friction. The model developed contemplates the particular aspects regarding the application of the proposed controllers, such as the reformulation of the equations of motion as a stabilization problem and the addition of an integral action. Simulations reveal that the proposed controllers perform better than an optimized PI controller both in the case of known parameters and in the presence of uncertainties. Furthermore, sensitivity analyses indicate a seeming global stability of the closed-loop system equipped with one of the proposed controllers, in addition to very low sensitivity of performance with respect to parameter variations. Results motivate further investigations of the apparent global stability provided by the proposed controller and practical implementation of the developed strategies.

Keywords: Stick-slip. Drill string. Negative damping coefficient. Optimal static output feedback. Negative damping control. Global stability.

Resumo

Cruz Neto, H.J. Controle Ativo de Oscilações de Stick-Slip em Sistemas de Perfuração de Poços de Petróleo. Tese (Doutorado) - Escola de Engenharia de São Carlos, Universidade de São Paulo, São Carlos, 2022.

Sistemas de perfuração rotativa estão sujeitos a interações nocivas entre a estrutura de perfuração, o poço e a formação rochosa, levando a vibrações torcionais que podem diminuir a eficiência da perfuração e causar falhas nos componentes da coluna de perfuração. Uma maneira adequada de reduzir essas falhas prejudiciais é projetar um controlador ativo que mitiga as vibrações, com a restrição de usar somente a quantidade limitada de dados em tempo real disponíveis nas operações de campo. Neste contexto, esta tese propõe duas novas técnicas de controle, as quais são baseadas apenas em simples combinações lineares de sinais medidos, com o objetivo de mitigar as vibrações torcionais da coluna de perfuração e melhorar o desempenho da perfuração. Visto que os sinais medidos são de suma importância para a eficácia das técnicas propostas, este trabalho também investiga quais sinais são relevantes para realimentação com o objetivo de garantir estabilidade assintótica. A primeira técnica de controle proposta baseia-se no trabalho desenvolvido pelo autor durante seu mestrado e consiste em determinar o ganho de controle de um controlador com realimentação de saída (OSOF) de modo que seu desempenho seja o mais próximo possível de um controlador com realimentação de estado completo (LQR). A segunda técnica de controle proposta deriva do conceito de coeficiente de amortecimento negativo desenvolvido nesta tese e visa ampliar os limites de operação segura da coluna de perfuração através da minimização do valor do coeficiente de amortecimento negativo para o qual o ponto de operação é assintoticamente estável. Os controladores propostos são aplicados a um modelo representativo da dinâmica torsional da coluna de perfuração, modelado através do método dos elementos finitos com atrito seco não regularizado. O modelo desenvolvido contempla aspectos particulares da aplicação dos controladores propostos, como a reformulação das equações de movimento como um problema de estabilização e a adição de uma ação integral. Simulações revelam que os controladores propostos desempenham melhor que um controlador PI otimizado tanto no caso de parâmetros conhecidos quanto na presença de incertezas. Adicionalmente, análises de sensibilidade indicam uma aparente estabilidade global do sistema equipado com um dos controladores propostos, além de baixa sensibilidade do desempenho com relação a variações de parâmetros. Os resultados motivam investigações futuras sobre a aparente estabilidade global fornecida pelo controlador proposto e a implementação prática das estrágias desenvolvidas.

Palavras-chave: Stick-slip. Coluna de perfuração. Coeficiente de amortecimento negativo. Realimentação ótima estática de saída. Controle de amortecimento negativo. Esta-

bilidade global.

Contents

1 Introduction

This chapter contextualizes the problems of vibrations in rotary drilling systems, presents an overview of drill string models and active control techniques implemented for this problem, and states the objectives and motivations of this thesis.

1.1 Oil exploration and the drill string problem

Oil has a wide range of applications, such as the manufacture of agricultural fertilizers, plastics, pharmaceuticals, fuels, among others. Despite the recent trend for the development and use of renewable energies, the growing demand in all of the aforementioned areas incited an increase in world crude oil and lease condensate production to around 82 million barrels a day in 2019, as depicted in Figure 1. Although the COVID-19 outbreak caused an economic crisis that led to a drop in oil consumption and production in 2020 (International Energy Agency, 2020), recent data indicate a resumption of production after a reduction in the pandemic severity in 2022 (U. S. Energy Information Administration, 2022). The overall expansion in production is also observed at the national level. Since the announcement of oil traces in the pre-salt layer in 2006 and the beginning of its exploration in 2008 to the present day, Brazil has moved from the fifteenth to the eighth position in the rank of world largest crude oil and lease condensate producers (U. S. Energy Information Administration, 2022). In 2021, Brazil had an average production of 2.90 million barrels per day and, according to the public company *Empresa de Pesquisa Energética*, oil production is expected to increase to 4 million barrels per day in 2024 (Brasil, Ministério de Minas e Energia, Empresa de Pesquisa Energética, 2017). This increase in production and demand has been reflected in research and development, so that oil and gas companies have increased investments in this area in order to increase efficiency at all stages of oil exploration (TAUHATA, 2018). The entire process of oil exploration can be divided in several stages (THOMAS, 2001), which can be summarized as:

1. Prospecting: the process of identifying a geological structure that could be a potential hydrocarbon reservoir. The most common techniques used to identify oil and gas reservoirs are: a) seismic prospecting, which generates seismic waves and uses their reflection to create a map of the geologic structure; b) gravity prospecting, which measures spatial variations in the Earth's gravitational field to identify low density rocks that may indicate the presence of oil and gas; c) magnetic prospecting, which identifies sedimentary basins and their thickness; and d) geochemical prospecting,

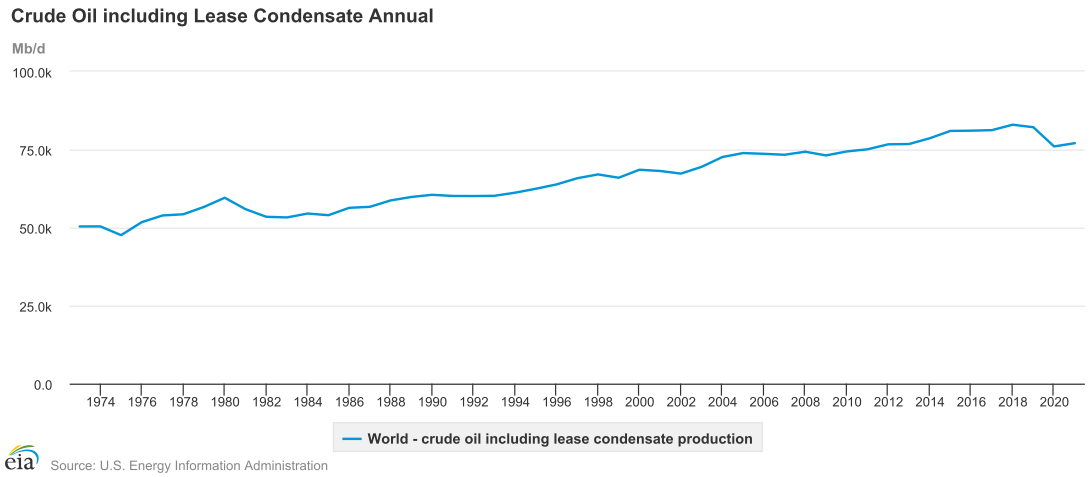

Figure 1 – World annual production of crude oil and lease condensate since 1973.

which analyzes the chemical composition of underground water and the content of dissolved gases and organic matters within it (GACI; HACHAY, 2017).

2. Drilling: Upon identification of a potential reservoir, a drilling rig is constructed in a suitable region. A drilling system is used to create a borehole that connects the drilling rig and the oil reservoir.

3. Cementing and testing: upon reaching a certain depth, the drill pipe is removed and a steel pipe is pushed to the bottom of the well to inject cement up along the sides of the well to protect the integrity of the hole and the surrounding area. The drilling and cementing processes are alternated until the oil reservoir is reached. Tests are performed in order to ensure well impermeability.

4. Well completion: encompasses the operations to get the well ready for production after the drilling process. Well completion should be performed to optimize production and minimize future maintenance. At this stage, components such as the Christmas Tree, production tube and subsurface safety valves are installed (BELLARBY, 2009).

5. Fracking: a technique of well stimulation in which the rock formation is fractured by means of a pressurized liquid. Fracking is not strictly necessary for oil and gas extraction, however, it considerably increases well-reservoir exchanges and generates adequate flow rates, especially for gas extraction (CHARLEZ, 1997). In 2010, it was estimated that 60% of the wells practiced hydraulic fracturing (MONTGOMERY; SMITH, 2010).

6. Production: After all the steps mentioned, oil and gas production begins. In the introductory phase, the reservoir pressure is sufficient to push the oil to the surface, whilst in the following phases, some mechanisms such as water and gas injection,

oil heating and carbon dioxide flooding are used to increase reservoir pressure and decrease fluid viscosity, making oil and gas recovery feasible (TZIMAS et al., 2005).

These steps constitute a part of the oil and gas industry known as upstream, which deals with exploration and production. There are still midstream and downstream sectors, which deal with transportation, refinement, marketing and distribution of oil and gas derivatives. This work is dedicated to analyze the drilling process, focusing on the dynamic behavior of the drilling structure. A schematic representation of a drilling rig is shown in Figure 2.

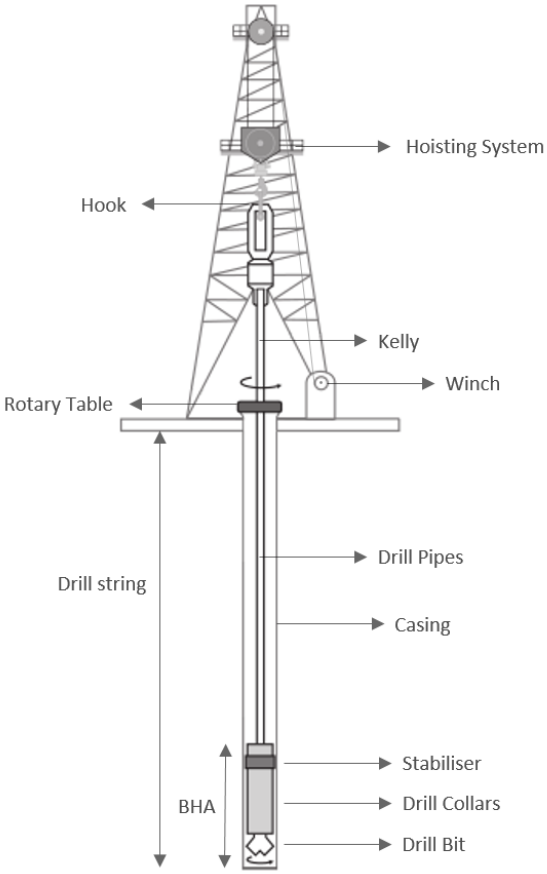

Figure 2 – Basic components of a rotary drilling system. Adapted from: (LIU, 2015)

The conventional technique in oil and gas industry for opening a borehole in a rock formation is the rotary drilling. From a dynamics perspective, the rotary drilling mechanism can be described as a composition of the hoisting and rotating systems. In the rotating motion, a motor applies torque to the rotary table, which has a large rotary inertia to prevent sudden changes in drilling angular velocity. The torque is transmitted to the cutting device, called drill bit, through the drill string, which is a slender and long structure composed of several drill pipes. At the bottom of the drill string, there are the drill collars, which are thick-walled, high-density pipes designed to apply weight-on-bit (WOB) and prevent buckling, and also the stabilizers, which help to keep the assembly

centered in the hole. In conjunction with the drill bit, these elements constitute the lower part of the drill string called bottom-hole-assembly (BHA), as shown in Figure 2.

The vertical motion of the drill string is controlled by a block-and-tackle hoisting system. Powered by an electric or diesel engine, the winch pulls the drill lines that are attached to the traveling block. Below the traveling block, there are the hook and the swivel, which cushion the impacts caused by moving loads and separate the rotary and stationary elements. The swivel is linked to the kelly, a hexagonal or square steel bar that is connected to the drill string and slides freely vertically through the interior of the rotary table. The element that allows the kelly to free-slide in the vertical direction and makes its connection to the rotary table is the kelly bushing. As the drilling progresses, drill pipes are added below the kelly, increasing the drill string size. The downward speed and WOB are controlled by a winch braking system.

Another important component of a drilling rig is the hydraulic system. Using a hydraulic pump, the drilling fluid is injected into the drill string through the swivel. The role of the drilling fluid, which basically consists of water with viscosifiers and weighting materials, is to cool and lubricate the bit and transport the cuttings from the bottom to the surface. Upon reaching the surface, the fluid is treated by eliminating solids and gases and by adding chemicals to adjust its properties, after which it is again injected into the drill string (JANSEN, 1993; THOMAS, 2001).

The numerous factors involved in the drilling process enrich the drill string dynamics, which may manifest multiple vibration modes. Due to the slender and flexible nature of the drill string structure, the vertical and rotational movements associated with the drilling process, and mass imbalance, the drill string may exhibit three primary types of vibration: torsional, axial and lateral. Other key components in the drill string dynamics are its interaction with the environment, e.g., the contact with the borehole and the cutting process between the drill bit and the rock formation. These interactions can intensify vibrations, giving rise to phenomena such as bit-bouncing, stick-slip and whirling, which are extreme examples of coupled vibrations dominated by axial, torsional and lateral motions, respectively (GHASEMLOONIA; RIDEOUT; BUTT, 2015). As a model that integrates all different phenomena involved in the drill string dynamics makes the analysis and design of techniques to mitigate vibration cumbersome or even unfeasible, the focus of this work is the modeling and control of drill string torsional (stick-slip) vibrations.

The stick-slip phenomenon is a persistent oscillation that alternates between the stick phase, in which the drill bit reaches a complete standstill, and the slip phase, in which the drill bit angular velocity may reach a value much higher than the nominal speed. Since vibrations are one of the main factors for drill string failure, and consequently delays and increased costs in oil production (DONG; CHEN, 2016; JARDINE; MALONE; SHEPPARD, 1994), it is of great interest for the oil and gas industry to mitigate them. Several

approaches have been proposed to model and control drill string torsional vibrations, most relying on active and passive vibration control techniques. The following sections attempt to present an overview of the research in modeling and active control of torsional vibrations in rotary drilling systems. Axial vibrations are also covered to some degree since they can also influence the torsional behavior of the drill string. Whirling motion is prevalent at higher angular speeds and generally does not occur simultaneously with stick-slip (LEINE; CAMPEN; KEULTJES, 2002), therefore, it is not analyzed. For other approaches to the vibration control of these systems, the reader may consult the reviews in (DONG; CHEN, 2016; ZHU; TANG; YANG, 2014).

1.2 Research on drill string torsional vibrations

The aspects regarding experiments and modeling of the drill string torsional dynamics are presented in subsection 1.2.1, while the main active control techniques proposed to mitigate vibrations are analyzed in subsection 1.2.2.

1.2.1 Modeling

Initially, the efforts employed to address the problems of drill string failures were directed toward material strength rather than evaluating the dynamic behavior of the structure (GRANT; TEXTER, 1941; SAYE; RICHARDSON, 1954). One of the first studies to investigate the dynamic causes of drill string failures was carried out by (FINNIE; BAILEY, 1960), who presented measurements indicating the occurrence of axial and torsional vibrations. In an accompanying paper (BAILEY; FINNIE, 1960), the authors also presented an analytical model to predict the real system behavior and correlate it with the measured data. The behavior of the drill string was represented by the dynamic equations of a rod in torsion and a bar in extension, with models in both directions uncoupled. Contact, friction and damping were neglected. The authors tried to correlate the measured frequencies with the natural frequencies of the model for typical boundary conditions, such as clamped and free ends. The attempt to establish this relationship was unsatisfactory, and the authors alluded that the measured frequencies might not be related to the system's natural frequencies and that possible factors not represented in the model could affect the results.

A slight improvement in the study of axial and torsional dynamics was done by (DAREING; LIVESAY, 1968). The authors considered the same model as Bailey and Finnie, but with the addition of viscous damping and a harmonic displacement at the drill bit as a boundary condition. Experimental tests indicated that the occurrence of vibrations depended almost completely on the formation being drilled and simulations have shown that shock subs placed above the bit with softer spring constants were more

effective in reducing vibration amplitudes.

The models proposed so far considered systems with constant parameters and boundary conditions that could only describe natural and forced vibrations in linear systems. Another type of periodic response that is present only in nonlinear systems is the self-excited vibration (ANDRONOV; VITT; KHAIKIN, 1966). These vibrations occur in the absence of any outside periodic source and their amplitude and frequency are independent of initial conditions. From a nonlinear dynamics perspective, these vibrations can be understood as limit cycles occurring in autonomous systems.

One type of self-excited vibration present in mechanical systems is the stick-slip. Studies on stick-slip vibrations date back to the late thirties, when (BOWDEN; LEBEN, 1939) identified friction-induced oscillations in a block and belt system. A decade later, (DUDLEY; SWIFT, 1949) proposed a model considering friction with a velocity weakening dependence (the force is a function of the velocity with negative slope) that was able to predict stick-slip oscillations for the same system. However, the comprehension that torsional vibrations observed in drill strings could be the result of a similar mechanism came only in the 1980s, with the article by (BELOKOBYL'SKII; PROKOPOV, 1982). Indeed, this was the first article to recognize the periodic response observed in drilling operations as stick-slip vibrations. The authors considered a one degree of freedom (DOF) torsional pendulum to represent the inertia and stiffness properties of the drill string, and friction with a velocity weakening dependence to model the bit-rock interaction. Given these hypotheses, the equations of motion of the drill string were the same as those for the conveyor belt system. These considerations were used to predict the occurrence of stick-slip oscillations, calculate the periods of these oscillations, and evaluate how the friction parameters could affect the properties of the oscillations. After the publication by Belokobyl'skii and Prokopov, several other studies adopted the friction law with a velocity weakening component to model the bit-rock interaction (SALDIVAR et al., 2016). This velocity weakening dependence of the torque on bit was confirmed later in numerous laboratory and field measurements (BRETT, 1992; PAVONE; DESPLANS, 1994; ERTAS et al., 2013; KAPITANIAK et al., 2015; RITTO; AGUIAR; HBAIEB, 2017).

Another approach to model the bit-rock interaction (RICHARD; GERMAY; DETOURNAY, 2007; GERMAY; DENOËL; DETOURNAY, 2009) consists of a model without a velocity weakening torque on bit, that exhibits stick-slip oscillations via a regenerative effect caused by the cutting process and coupling between the axial and torsional modes. Although this approach suggests that the velocity weakening effect is not an intrinsic property of the bit-rock interaction but rather a consequence of mode coupling and the cutting process, the conclusion that the combination of these factors still produces a torque on bit with a velocity weakening effect justifies its inclusion in a model considering only the torsional mode.

Despite the differences in the models for predicting stick-slip vibrations, both approaches mentioned previously considered the bit-rock interaction as their primary source. Other important factors for a proper assessment of the impacts of vibrations on the drill string and its components are the models for the drill string itself and its other interactions with the environment. Regarding the drill string, some studies that focused on vibration or deformation analyses considered large deformations or non-linear stress-strain relationships (TUCKER; WANG, 1999a; TRINDADE; WOLTER; SAMPAIO, 2005), while those concerned also with the controller synthesis generally adopt the simplifying hypotheses of small deformations and linear stress-strain relationships. The latter can be divided into the ones that maintain the continuum description (distributed parameter models) of the drill string and those that consider spatial discretization methods, which are further divided into lumped parameter methods and series discretization methods (mostly the finite element (FE) method) (MEIROVITCH, 1997).

The majority of the models for the drill string rely on lumped parameter methods (GHASEMLOONIA; RIDEOUT; BUTT, 2015). Similar to the pioneering article by Belokobyl'skii and Prokopov, some researchers (KYLLINGSTAD; HALSEY, 1988; LIN; WANG, 1991; RUDAT; DASHEVSKIY, 2011) examined the one DOF torsional pendulum with a constant velocity at the top to identify safe operating values for some drilling parameters, such as the WOB and rotary table angular speed. Although this model can predict the influence of some parameters on the drill string dynamics, it cannot be used for controller synthesis (in the case in which torque is the control input) due to the absence of a top rotary inertia to which an input torque can be applied. Therefore, several studies on active vibration control (JANSEN; VANDENSTEEN, 1995; SERRARENS et al., 1998; ABDULGALIL; SIGUERDIDJANE, 2004; NAVARRO-LOPEZ; SUAREZ, 2004; CANUDAS-DE-WIT et al., 2005; RITTO; GHANDCHI-TEHRANI, 2019) consider the two DOF torsional pendulum. In most of these models, a motor variable (torque, voltage) is designed using active control techniques to actuate on the top rotary inertia and influence the drill string dynamics. Other studies (NAVARRO-LOPEZ; LICEAGA-CASTRO, 2009; KREUZER; STEIDL, 2012; WASILEWSKI et al., 2019; LOBO et al., 2022) considered lumped parameter models with more degrees of freedom to represent better the influence of higher-order modes.

In the case of models based on series discretization methods, the most frequent example (perhaps the only one) is the finite element method. Many studies (KHULIEF; AL-NASER, 2005; KHULIEF; AL-SULAIMAN; BASHMAL, 2007; SAMPAIO; PIOVAN; LOZANO, 2007; RITTO; SOIZE; SAMPAIO, 2009; LIU et al., 2020) consider FE models to analyze the influence of parameters or uncertainties in the drilling process, whereas only a few use these models for controller synthesis (MONTEIRO; TRINDADE, 2017; TRINDADE, 2020). FE models are suitable for complex geometries and boundary conditions, and their potential to aggregate these features in automated computational algo-

rithms allows a feasible development of a representative model. Moreover, some important factors in drill string dynamics, such as wave propagation time and the stick phase duration are represented better using infinite-dimensional or multimodal models (TUCKER; WANG, 1999a), and field observations indicate the influence of higher-order modes in drill string vibrations (RUNIA; DWARS; STULEMEIJER, 2013). The combination of these factors with the possibility of obtaining a suitable model (described by ordinary differential equations (ODE)) for the design of several standard control techniques favors representations using the FE method.

Other researchers consider distributed parameter models (described by partial differential equations (PDE)) to design controllers. Although this representation eliminates the problems related to the limited frequency bandwidth of discretized models, the control techniques for these systems are restricted, and their limitations generally require other simplifications or assumptions. For instance, some models simplify the bit-rock interaction using periodic or linear functions (BRESCH-PIETRI; KRSTIC, 2014; WANG; TANG; KRSTIC, 2020), some neglect the inertia of the BHA (SAGERT et al., 2013), and several consider measurements of variables at the drill-bit for controller feedback, such as the torque on bit or the bit angular velocity or displacement (SALDIVAR et al., 2013; SAGERT et al., 2013; BRESCH-PIETRI; KRSTIC, 2014; SALDIVAR; MONDIÉ; VILCHIS, 2016; WANG; TANG; KRSTIC, 2020). These assumptions may oversimplify the model, not reproducing some important phenomena observed in practice, and reduce the applicability of controllers. Further discussions on the types of sensors and actuators used in the controller design are presented in the next section.

The last aspects of drill string modeling involve other sources of energy dissipation, such as internal damping and interactions with the drilling fluid and the borehole. The majority of the models (YIGIT; CHRISTOFOROU, 2006; LIU et al., 2014; GHASEMI; SONG, 2018; VAZIRI; KAPITANIAK; WIERCIGROCH, 2018; TRINDADE, 2020) concerned with controller synthesis adopt a simplified representation of energy dissipation sources, given by a constant viscous damping matrix. Although a simple equivalent viscous damping may not accurately reproduce the structural damping and the fluid-structure interaction, it provides a reasonable method to introduce damping effects in the model and allows a suitable drill string representation for controller design. Other articles propose more detailed models for the fluid-structure interaction (PAÏDOUSSIS; LUU; PRABHAKAR, 2008; RITTO; SOIZE; SAMPAIO, 2009) and friction torque between the drill string and the borehole (AARSNES; SHOR, 2018; VROMEN et al., 2019).

1.2.2 Active control

A widely employed method for mitigating vibrations in drill strings is active control. An active feedback control system is characterized by the presence of sensors, which

measure the variables of interest of the structure, a controller, which processes and combines the measured signals, and actuators, which act on the structure, according to the rules prescribed by the controller, to modify its dynamics and achieve a specified degree of performance and robustness. The function that describes how the measured signals are combined to generate the control action is often called a control law, which can be designed using several different control techniques. For some of these techniques, the control action is a simple linear combination of measured signals specified a priori (static output feedback) and for others, it requires measurements of all dynamic variables that describe the behavior of the system (state feedback). Some alternatives to the latter use state observers to feed back unmeasured states, which implies a dynamic control action, i.e., the control action is a solution of a differential equation involving the measured signals and inputs. All these techniques have been applied to the drill string problem. Instead of listing all the control techniques employed for this problem, this section describes and gives a few examples of control techniques that can be implemented using certain sensors, starting with the elementary ones and progressing as the number of sensors and controller complexity increase.

The first and most basic control technique to be employed in the rotary drilling process is the proportional-integral (PI) (LOBO et al., 2022; TRINDADE, 2020) control. In the PI control, the output variable (measured signal) is the angular velocity of the rotary table, which is compared with a reference value yielding an error. Then, the control action is defined as a sum of a term proportional to the error and another proportional to the integral of the error. The proportionality constants are the control gains and must be carefully designed to yield an effective control action. An important distinction between the PI control and other control techniques is that the former only specifies the signals used in the control action, but not how they are combined (the control gain values). Standard methods for the PI control gains design for general systems are Ziegler-Nichols tuning rules, pole placement, fuzzy logic, and so forth (JOHNSON; MORADI, 2005). Specifically for the drilling problem, some researchers propose to determine the PI control gains to achieve good performance according to a meaningful criterion for the drilling process. For instance, (KYLLINGSTAD; NESSJØEN, 2009) proposes a technique for finding PI control gains that reduce torsional wave reflections, and (MONTEIRO; TRINDADE, 2017) suggests to find PI control gains that minimize the average deviation from the drill bit target angular velocity.

Although the PI control effectively uses two signals for feedback: one directly measured (velocity) and another obtained via integration (displacement), it only needs one sensor that measures the rotary table velocity. The first alternatives for the PI control suggested monitoring another quantity on the rotary table and using only this new component for feedback or combining it with a PI controller. (HALSEY; KYLLINGSTAD; KYLLING, 1988) proposes to control the top velocity using the torque at the rotary table

for feedback, and select the new control parameters to reduce torsional wave reflection. Recognizing that the electric current of the rotary drive motor is proportional to the torque at the rotary table, (JAVANMARDI; GASPARD, 1992) made a slight change in the previous work by measuring the electric current instead of the torque. This modification was patented by Shell as soft-torque in the early nineties. Using also the electric current for feedback, (JANSEN; VANDENSTEEN, 1995) proposes to design the control gains to increase the damping along the drill string, instead of minimizing reflections of torsional waves. Afterwards, (TUCKER; WANG, 1999b) analyzed the effects of measuring the shear strain at the top of the drill string and using it for feedback together with the PI controller. The authors showed that using this new quantity for feedback improved the torsional waves absorption when compared to the soft-torque.

The control techniques discussed so far use only measurements at the rotary table and simple linear combinations of these signals for feedback. Subsequently, some researchers studied the application of general control techniques, involving either measurements along the drill string or surface measurements combined with state observers. Examples of works using linear controllers with static state feedback are (CHRISTOFOROU; YIGIT, 2003), which uses the linear quadratic regulator (LQR), and (CANUDAS-DE-WIT et al., 2005; YIGIT; CHRISTOFOROU, 2006), which use pole placement for the velocity controllers. All these works use the bit angular velocity for feedback, and (CHRISTOFOROU; YIGIT, 2003; YIGIT; CHRISTOFOROU, 2006) additionally consider measuring the difference between the bit and rotary table angular displacements. Despite using quantities that may not be accessible, the mentioned techniques have the benefit of guaranteeing asymptotic stability and stability margins. Examples of works also using state feedback but applying nonlinear control techniques are (ABDULGALIL; SIGUERDIDJANE, 2004), which uses feedback linearization, and (LIU, 2015; NAVARRO-LOPEZ; LICEAGA-CASTRO, 2009), which develop sliding mode controllers. All state variables are incorporated in the controller on feedback linearization, including even the torque on bit. Moreover, controllers based on feedback linearization may wastefully cancel nonlinearities that contribute to stability and have poor robustness properties (FREEMAN; KOKOTOVIC, 1996). Although the sliding mode controller ensures a larger stability region than the linear controllers and uses fewer state variables than the feedback linearization controller, it still assumes knowledge of the drill bit angular velocity for feedback.

An alternative for the state feedback controllers is the adoption of state observers to estimate unmeasured variables. Most of the studies cited previously mentioned this possibility, yet none analyzed the effects of the observer on performance and stability. Design and analyses of output-based controllers were carried out by (BESSELINK et al., 2016; VROMEN et al., 2017). Although these controllers only use surface measurements, their complex structure requires the solution of differential equations for the control action and a model for the observer, which may produce time delay, lower stability margins, and

spillover (PREUMONT, 2011).

The final aspects addressed for the control system are the number and types of actuators. Most of the works mentioned above considered a single actuator represented by some motor variable, usually torque or voltage. In a few other studies (SALDIVAR; MONDIÉ; VILCHIS, 2016; TOUMI et al., 2017; MLAYEH; TOUMI; BEJI, 2018), the control variable was the angular speed provided by the motor, and there was a mismatch between this velocity and the angular velocity at the top of the drill string. Other researchers (YIGIT; CHRISTOFOROU, 2006; CANUDAS-DE-WIT; RUBIO; CORCHERO, 2008; MONTEIRO; TRINDADE, 2017) proposed to combine the control torque with manipulation of the hook load, using effectively two actuators. While adding this new control action may indeed improve performance, it is necessary to evaluate the hook response speed and the influence of axial dynamics on the WOB. To assess the performance of a collocated actuator, (TUCKER; WANG, 2003) analyzed the effects of an actuator at the drill bit on the rate of penetration and robustness of the closed-loop system. In general, one might expect that adding sensors or actuators should improve system performance given an efficient controller design. However, it is important to emphasize the feasibility and complexity of the proposed approaches, as well as an adequate evaluation of the controller's performance using a representative model.

1.3 Motivations and objectives

The concise research review conducted previously identified fundamental aspects in the areas of modeling and control of torsional vibrations in drill strings: 1) important factors in drill string dynamics, such as wave speed of propagation and the stick phase duration are better represented using infinite-dimensional or multimodal models, and field observations indicate the influence of higher-order modes in drill string vibrations; 2) the variables that characterize the bit-rock interaction are rarely known and are subject to changes according to the rock formation lithology, therefore, uncertainties must be considered either in the controller design or in a sensitivity analysis; 3) although some complex control strategies involving the measurement of all system states or the estimation of unmeasured states using dynamic observers may provide a better performance, they rely on assumptions that are not feasible for typical drilling rigs. The design of an effective controller with a wide range of applications in a variety of oil wells must consider not only performance but constraints such as limited information and a restricted ability for transmitting real-time data over long distances.

Given these observations, the primary objective of this thesis is to propose novel control techniques to mitigate torsional vibrations of drill strings with the constraint of employing only simple linear combinations of measured signals. Considering that the mea-

sured signals are of paramount importance for the effectiveness of the proposed techniques, another objective of the present work is to investigate which signals might be relevant for feedback with the aim of ensuring asymptotic stability and good performance. To properly evaluate the control techniques developed, the last objective of this thesis is to compare them with each other and with a PI controller by performing numerical simulations of a model that considers the fundamental aspects identified previously: the continuum nature of the drill string and the uncertainties in the bit-rock interaction. This comparison encompasses stability, performance and applied torque in cases where the system parameters are known and in the presence of uncertainties.

1.4 Outline

Chapter 2 presents a mathematical model to represent the drill string torsional dynamics. Initially, a distributed parameter model obtained from the linear theory of thin rods is spatially discretized using the FE method. To reduce computational effort, a modal reduction is performed, retaining only the modes within a relevant frequency bandwidth. Then, the equations of motion are transformed to a state space representation and further reformulated for controller design.

Chapter 3 describes the typical behavior of the drill string in the open- and closed-loop configurations. First, the open-loop equilibria are determined, and a linear stability analysis of the operating point is performed, identifying the key factors that cause instability. Then, stick-slip oscillations are illustrated for the closed-loop system using different types of controllers.

Chapter 4 deals with the controller design. The beginning of this chapter is devoted to the analysis of which signals are relevant for measurement (output matrix design) presuming that the control action is a simple linear combination of the measured signals. Once the output matrix structure is established, two novel control techniques are proposed, the first focusing on nominal performance and the second on robustness.

Chapter 5 and Chapter 6 analyze the performance of the proposed control techniques through numerical simulations. The former presents results considering nominal operating conditions, in which the model parameters are known, while the latter investigates the effects of initial conditions and parameter variations on performance and stability of the proposed controllers.

Chapter 7 summarizes the main results and give recommendations for future research.

2 Drill string model

This chapter presents a mathematical model to represent the drill string torsional dynamics. Initially, a distributed parameter model obtained from the linear theory of thin rods is spatially discretized using the FE method. To reduce computational effort, a modal reduction is performed, retaining only the modes within a relevant frequency bandwidth. Then, the equations of motion are transformed to a state space representation, and reformulated by shifting the operating point to the origin and adding the error integral as a state. This reformulation is used in the following chapters for dynamic analysis and design of control laws.

2.1 Model

The torsional dynamics of the drilling system is represented in a simplified way considering three main components: the rotary table, the bottom hole assembly (BHA) and the drill string, which are schematically represented in Figure 3. The stabilizers, drill collars and drill bit are represented compactly by the BHA, which is modeled as a rigid body with rotary inertia J_b. The rigid body hypothesis is also assumed for the rotary table, which has a rotary inertia J_t. The drill string is modeled as a thin rod using the fundamental torsional-deformation assumptions (CRAIG; KURDILA, 2006):

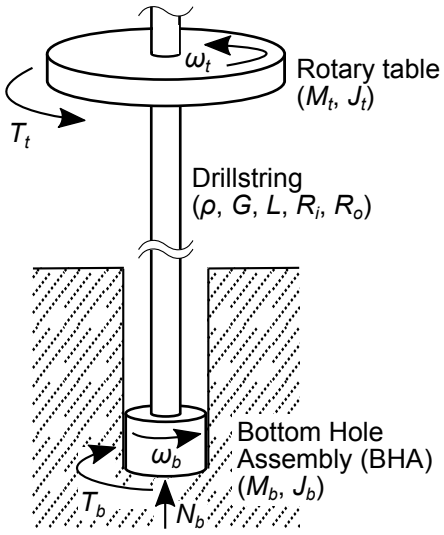

Figure 3 – Basic components of a rotary drilling system. Source: (MONTEIRO; TRINDADE, 2017).

- The longitudinal axis remains straight and inextensible;

- Every cross section remains plane and perpendicular to the longitudinal axis;
- Radial lines remains straight and radial as the cross section rotates about the longitudinal axis.

Additionally, the material is considered linear elastic – there is a linear relationship between shear stress and shear strain – with constant properties. Presuming these hypothesis and applying Newton's Laws or the extended Hamilton's principle, the equations of motion are derived as

$$G\frac{\partial^2\theta(x,t)}{\partial x^2} = \rho\frac{\partial^2\theta(x,t)}{\partial t^2}, \tag{2.1}$$

in which G is the shear modulus of elasticity, ρ is the mass density, $\theta(x,t)$ denotes the angular displacement of the cross section at position x and time t, and x is measured from the top end. For convenience, the rotary table and drill bit speeds are defined (Figure 3) as $\omega_t = \dot{\theta}\,(0,t)$ and $\omega_b = \dot{\theta}\,(L,t)$. As Eq. (2.1) is defined by a homogeneous differential operator of order two, there must be one boundary condition to be satisfied at each end of the drill string. Using the diagram shown in Figure 3, the boundary conditions are written as:

$$GI\frac{\partial\theta(x,t)}{\partial x} - J_t\ddot{\theta}(x,t) + T_t = 0, \qquad at\ \ x = 0, \tag{2.2a}$$

$$GI\frac{\partial\theta(x,t)}{\partial x} + J_b\ddot{\theta}(x,t) + T_b = 0, \qquad at\ \ x = L, \tag{2.2b}$$

in which I is the second moment of area, T_t denotes the torque applied by the motor to the rotary table and T_b is the reaction torque applied by the rock formation to the drill bit. The torque applied by the motor will be considered as a control input variable, which will be determined later in the controller design. The reaction torque is modeled as frictional force using the Karnopp's model with an exponential decaying friction term, which was initially proposed by (NAVARRO-LOPEZ; SUAREZ, 2004). The torque expression is given in Eq. (2.3) and illustrated in Figure 4.

$$T_b = \begin{cases} T, & \text{for } |\omega_b| \leq \delta \text{ and } |T| \leq a_2 N_b, \\ a_2 N_b sgn(T), & \text{for } |\omega_b| \leq \delta \text{ and } |T| > a_2 N_b, \\ \left[a_1 + (a_2 - a_1)e^{-\beta|\omega_b|}\right] N_b sgn(\omega_b), & \text{for } |\omega_b| > \delta. \end{cases} \tag{2.3}$$

The values a_1 and a_2 are called dynamic and static frictions coefficients, respectively, β is a positive exponential friction coefficient, T is the torque transmitted by the drill string to the bit, N_b is the normal force applied to the bit, ω_b is the bit angular speed and $\delta = 10^{-4}$ (MONTEIRO; TRINDADE, 2017) is the width of the stick phase region,

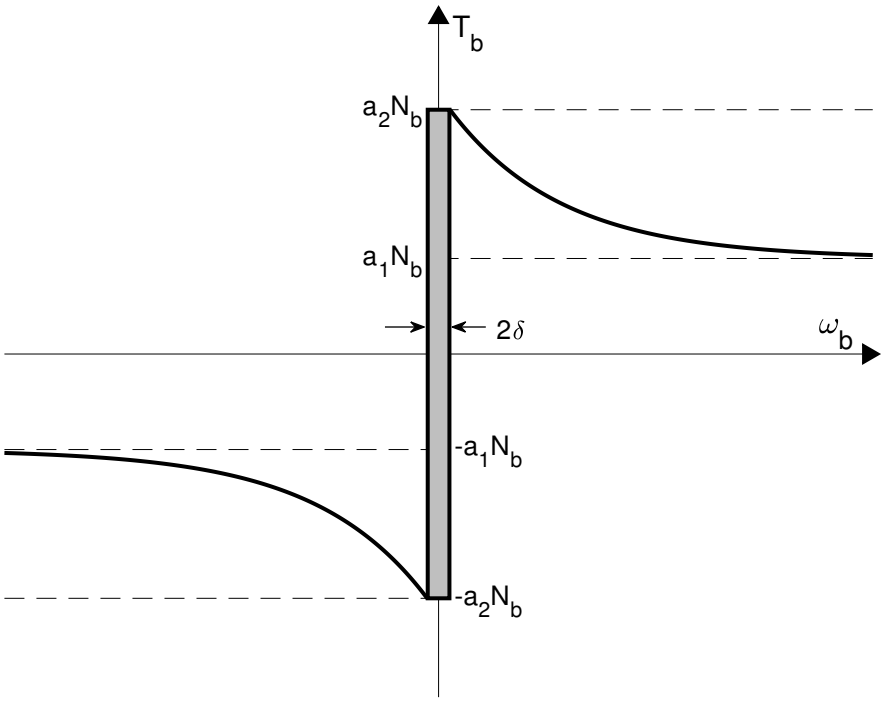

Figure 4 – Karnopp's model with an exponential decaying friction term.

introduced for numerical integration purposes. Assuming a quasi-static movement in axial direction, the normal force N_b can be approximated by the difference between the weight of the complete drilling assembly and the vertical force in the top cable. The difference between these forces is called Weight-on-Bit (WOB) and is assumed constant.

Although there are methods for dynamic analysis and control design for systems described by partial differential equations (KRSTIC; SMYSHLYAEV, 2008; TRÖLTZSCH, 2010), these methods are limited and require assumptions that may misrepresent some physical phenomena and restrict or make unfeasible the controller's implementation, as discussed in subsection 1.2.1. Therefore, to apply conventional numerical integration algorithms and, in some sense, more flexible methods for dynamic analysis, the dependence on the spatial variable in Eqs. (2.1)-(2.2) is eliminated, such that the model described by Eqs. (2.1)-(2.3) is transformed into a system of ODEs. Three different methods are usually employed to eliminate the space dependence: the method of d'Alembert, using the general solution of the wave equation, lumping parameter methods and series discretization methods. The first method adopts the general solution of the wave equation, given by an "up-moving wave" and a "down-moving wave", and replaces it in the boundary conditions. Although this method has the advantage of providing an input-output model that has a one-to-one correspondence with the solution of the former PDE, it results in a delayed differential equation, which has similar problems for the dynamic analysis and controller design as the methods for PDEs. The second and third methods are traditionally employed in structural problems and transform the boundary value problem into a

system possessing a finite number of ODEs. Although some components of the solution are lost in this transformation, these components are associated with higher frequencies, which are rarely excited for torsional dynamics in drilling processes. The advantages of series discretization methods over lumped parameters methods are the convergence properties and automated implementation of computational models. Detailed analysis of series discretization methods is outside the scope of this document, here we only describe the conditions used to apply the FE method to the drill string problem.

The numerical values of general properties of the considered drilling system were taken from (TUCKER; WANG, 2003). In order to analyze this system for other WOB operating conditions, (MONTEIRO; TRINDADE, 2017) determined additional values for the friction coefficients that still approximate the phenomenological model proposed by (TUCKER; WANG, 2003). All these parameters are indicated in Table 1 and Table 2.

Table 1 – Numerical values of the drilling system general parameters.

Drill string mass density (kg/m^3)	8010
Drill string shear modulus (GPa)	79.6
Drill string length (m)	3000
Drill string inner radius - R_i (m)	0.0543
Drill string outer radius - R_o (m)	0.0635
BHA effective rotary inertia $(kg.m^2)$	394
Driving table effective rotary inertia $(kg.m^2)$	500

Table 2 – Dry friction parameters for different values of WOB.

WOB (kN)	80	100	120	140	160
a_1 (m)	0.037	0.032	0.029	0.026	0.025
a_2 (m)	0.057	0.070	0.079	0.085	0.089
β $(s.rad^{-1})$	0.082	0.093	0.097	0.098	0.099

To represent this system using a FE model, a regular mesh was constructed and refined until there was a negligible variation in the natural frequencies up until 6 Hz, which, by rounding up, implied in the use of 30 elements. This frequency bandwidth was set based on (DONG; CHEN, 2016), which indicates that the frequency range of torsional vibrations is 0.1∼5 Hz. Hermite cubics were used as interpolation functions to improve convergence. A modal reduction was performed (assuming a free-free boundary condition) to reduce computational effort (for some simulations, modal reduction reduces simulation time by 200 times), retaining only the thirteen modes that were within the range of 6 Hz (including a rigid body mode). The approximate eigenfunctions were determined to allow sensors positioning along the drill string in the controller design. These functions were calculated as in the Rayleigh-Ritz method since, except for convergence and embedding properties of mass and stiffness matrices, the FE method can be treated as a Rayleigh-Ritz method (MEIROVITCH, 1997). The mode shapes and corresponding natural frequencies

of the flexible modes are depicted in Figure 5. Finally, to represent general dissipation sources, a modal damping factor of 1% was added for each mode. One should note that this type of damping does not provide energy dissipation for the rigid body mode, since its corresponding natural frequency is null. An alternative to add damping for the rigid body mode is to use Rayleigh damping with a positive proportionality constant for the mass matrix. Adding more damping to the system actually increases the regions of safe operation (the reasons for this claim will become apparent in chapter 3) and, the model adopted in this thesis, where only modal damping is considered, can be regarded as a critical case (harder to control). The system equations in modal coordinates are

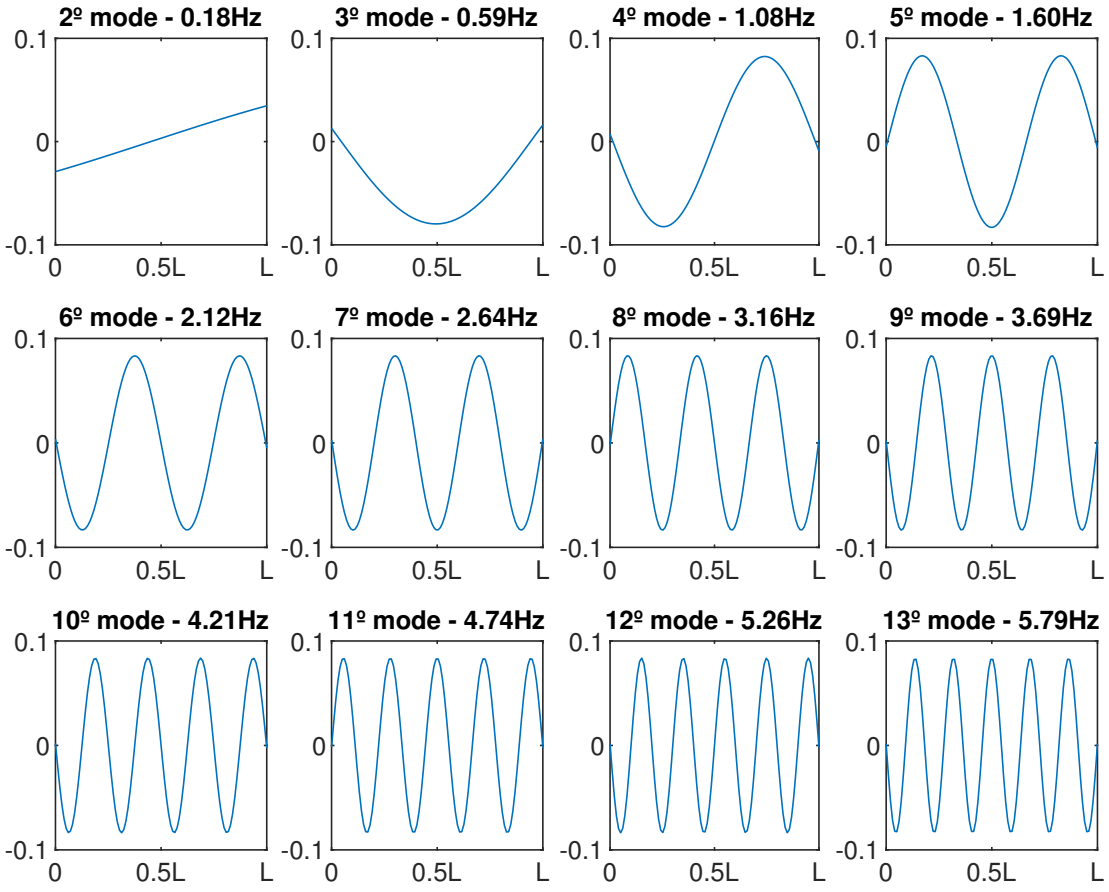

Figure 5 – Flexible modes shapes and natural frequencies.

$$\ddot{\boldsymbol{\eta}} + \mathbf{D}\dot{\boldsymbol{\eta}} + \boldsymbol{\Lambda}\boldsymbol{\eta} = \boldsymbol{\phi}(0)T_t - \boldsymbol{\phi}(L)T_b, \tag{2.4}$$

in which $\boldsymbol{\eta} \in \mathbb{R}^n$ is the vector of modal displacements, $\boldsymbol{\Lambda} \in \mathbb{R}^{n\times n}$ is a diagonal matrix of system eigenvalues or natural frequencies squared, $\mathbf{D} \in \mathbb{R}^{n\times n}$ is a diagonal matrix of damping, whose elements of the diagonal are $2\zeta_i\omega_{ni}$, in which $\zeta_i = 0.01$ is the damping factor and ω_{ni} is the natural frequency of the i-th mode, and $\boldsymbol{\phi}\colon \mathbb{R} \to \mathbb{R}^n$ represents the approximated eigenfunctions. Note that since the natural frequency associated with the rigid body mode is null, neither the rigid body displacement nor its derivative appears

in Eq. (2.4). Thus, when transforming Eq. (2.4) to differential equations of first order – for controller design, dynamic analysis and numerical integration – it is not necessary to define the rigid body displacement as a state. Indeed, adding the rigid body displacement as a state makes the state space representation of the desired operating configuration a function of time, precluding the design of the control techniques proposed in chapter 4. These observations motivate the definition of a state without the rigid body displacement:

$$\mathbf{x} = \begin{bmatrix} \eta_2 & \dots & \eta_n & \dot{\eta}_1 & \dots & \dot{\eta}_n \end{bmatrix}^\intercal = \begin{bmatrix} \bar{\boldsymbol{\eta}}^\intercal & \dot{\bar{\boldsymbol{\eta}}}^\intercal \end{bmatrix}^\intercal. \tag{2.5}$$

This definition leads to the following equations of motion using a state space representation:

$$\begin{aligned} &\dot{\mathbf{x}} = \mathbf{A}\mathbf{x} + \mathbf{B}_t T_t + \mathbf{B}_b T_b(\mathbf{x}) = \mathbf{f}(\mathbf{x}, T_t) \\ &\mathbf{A} = \begin{bmatrix} \mathbf{0} & \bar{\mathbf{I}} \\ -\bar{\mathbf{\Lambda}} & -\mathbf{D} \end{bmatrix}, \quad \mathbf{B}_t = \begin{bmatrix} \mathbf{0} \\ \boldsymbol{\phi}(0) \end{bmatrix}, \quad \mathbf{B}_b = \begin{bmatrix} \mathbf{0} \\ -\boldsymbol{\phi}(L) \end{bmatrix}. \end{aligned} \tag{2.6}$$

In Eqs. (2.5) and (2.6), a bar over a letter is used to distinguish between variables with and without components associated with the rigid body mode, i.e., $\bar{\mathbf{\Lambda}}$ is the matrix $\mathbf{\Lambda}$ without the first column, $\bar{\boldsymbol{I}}$ is the identity matrix without the first row and $\bar{\boldsymbol{\eta}}$ is the vector $\boldsymbol{\eta}$ without the first element.

Although the system with only the first two terms on the right-hand side of Eq. (2.6) is linear, the frictional force T_b described by Eq. (2.3) makes Eq. (2.6) nonlinear and nonsmooth. Moreover, since the frictional force used in the model is set-valued (AUBIN; CELLINA, 2012), i.e., $\forall\, \omega_0 \in [-\delta, \delta]$, $T_b(\omega_0) \in [-a_2 N_b, a_2 N_b] \subset \mathbb{R}$, the system (2.6) can be regarded as a differential inclusion. This fact may raise questions that are not usually dealt with in engineering problems, such as the existence and uniqueness of solutions. As demonstrated in some nonsmooth mechanics references, there are mechanical problems described by differential inclusions that are not well-posed (solutions do not exist or are not unique), see for example the Painlevé paradox (LEINE; NIJMEIJER, 2013; BROGLIATO, 2016). Fortunately, the frictional force (2.3) satisfies all conditions (LEINE; NIJMEIJER, 2013) to guarantee the existence and uniqueness of solutions (a different conclusion would be reached if the stiction friction model was adopted (LEINE; NIJMEIJER, 2013)). Since existence and uniqueness are ensured, the other question for the problem (2.6) is about the numerical integration methods to approximate its solution. Despite not being the most recommended, usual ODE integrators can provide reasonable approximations for the exact solutions of nonsmooth problems, especially if the algorithm is equipped with a variable step size. The Karnopp's friction model also provides a numerical advantage, because it introduces an interval for the static friction, which makes the differential equations non-stiff within the stick mode (LEINE; NIJMEIJER, 2013). Based

on these arguments, we chose to apply the explicit Runge-Kutta (4,5) formula, available in Matlab ode45 function.

Other important questions about the model developed are related to the series discretization method and modal reduction or, more precisely, how the number of finite elements and modes considered affects the system response. To investigate these questions, simulations of some typical drilling conditions were performed and the system response was compared for different numbers of modes and elements. Three cases were evaluated: a modal reduction considering two modes (corresponding to the frequently employed 2 DOF model), thirteen modes (the model adopted in this thesis, with a frequency bandwidth of 6 Hz) and thirty modes (a reference model, with frequency bandwidth of 15 Hz). In each case, the number of elements was selected to obtain convergence for the natural frequency of every mode in the frequency range considered, which resulted in one element, thirty elements and eighty elements, with obvious correspondence with the number of modes. The selected WOB was 120 kN and the initial condition was given by the entire drill string rotating undeformed with an angular velocity of 70 rpm. Since the open-loop system is unstable, the feedback torque

$$T_t = k_p\,(\omega_r - \omega_t) + k_i \int_0^t (\omega_r - \omega_t)\,\mathrm{d}\tau \tag{2.7}$$

was considered for a better comparison between the given scenarios, in which $\omega_r = 100$ rpm is the target angular velocity, and k_p and k_i are control gains. Chapters 3 and 4 present a deeper discussion on feedback control laws, at this point it is only necessary to understand that the applied torque T_t in Eq. (2.6) was replaced by the expression given in Eq. (2.7).

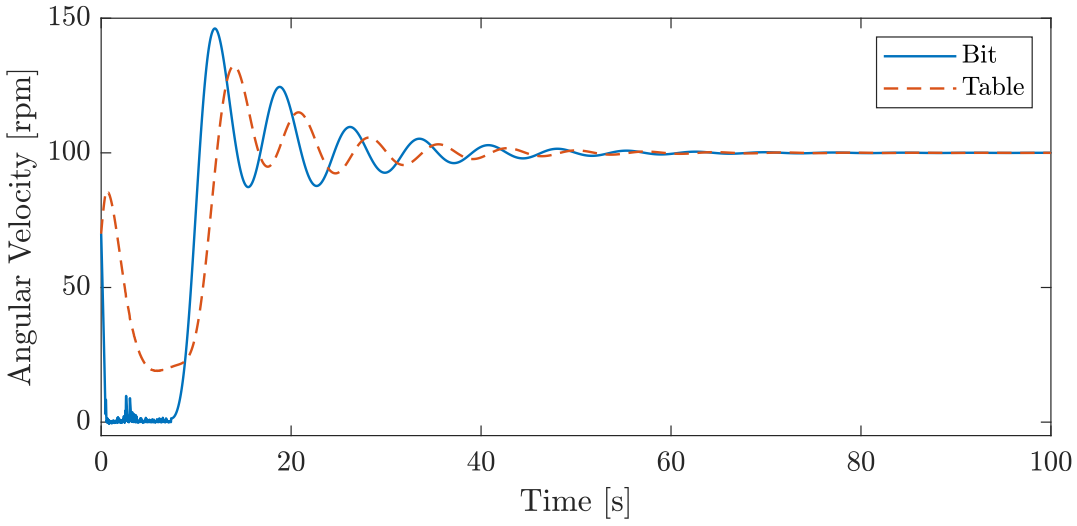

Figure 6 – Bit and rotary table velocities for the case with 2 modes, $(k_p, k_i) = (650,90)$.

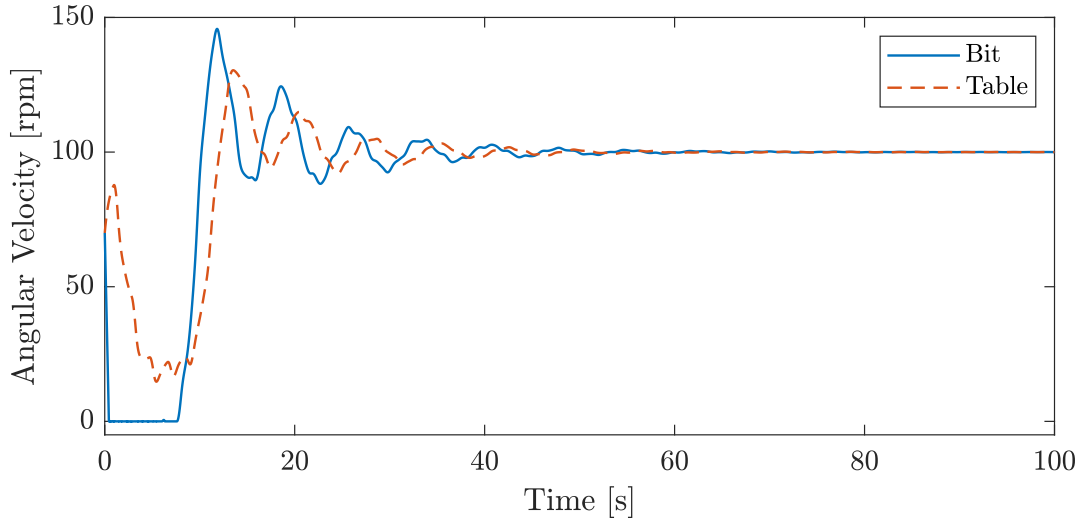

Figure 7 – Bit and rotary table velocities for the case with 13 modes, $(k_p, k_i) = (650,90)$.

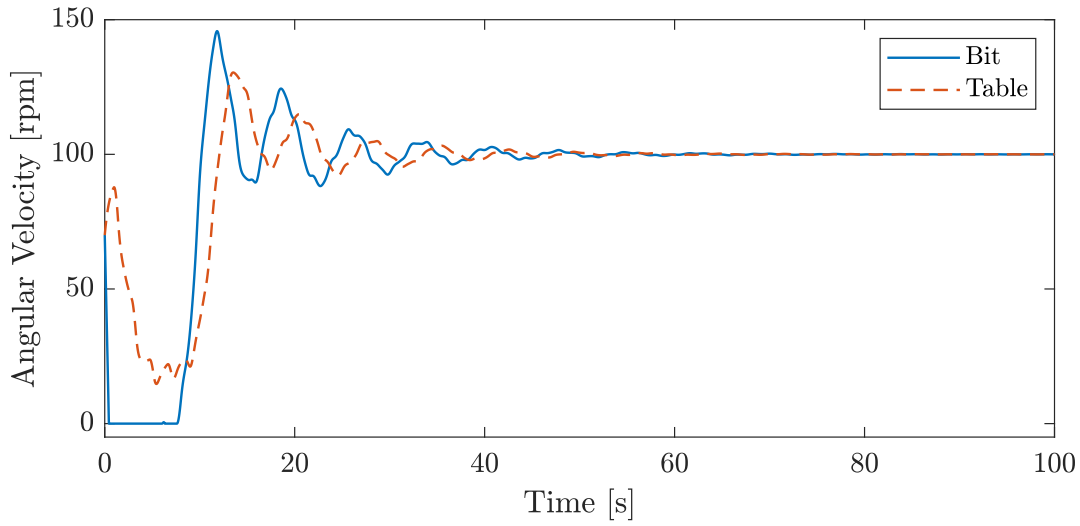

Figure 8 – Bit and rotary table velocities for the case with 30 modes, $(k_p, k_i) = (650,90)$.

Figures (6)-(8) illustrate the system response for the control gains (k_p, k_i) =(650,90). For these control gains, the curve shapes are similar in all cases, and the system with only two modes could be employed for a general assessment of the response. Still, oscillations with higher frequency and small amplitudes do not appear for the case with two modes, for which the stick phase is also misrepresented, since the drill bit reaches a speed of up to 10 rpm while for the other cases the drill bit is effectively at rest. To highlight the difference between the responses, the errors between the cases with the least number of modes and the reference model (thirty modes) were depicted in Figure 9. In this figure, e_2 is given by the absolute value of the difference between the bit angular velocity for the cases with two and thirty modes, and e_{13} is defined similarly. While the maximum error $e_2 = 11.27$ rpm shows that the model with only two modes may not be enough for an accurate evaluation of the response, the maximum error $e_{13} = 0.09$ rpm indicates that, for

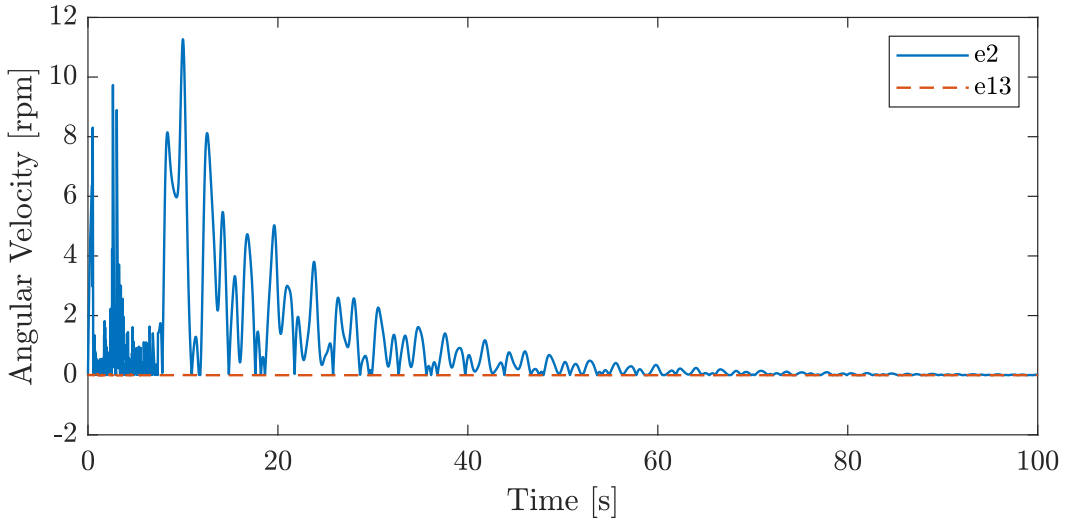

Figure 9 – Error between the cases with the least number of modes and the reference model, $(k_p, k_i) = (650,90)$.

the simulated operating condition, it is not necessary to use more than thirteen modes.

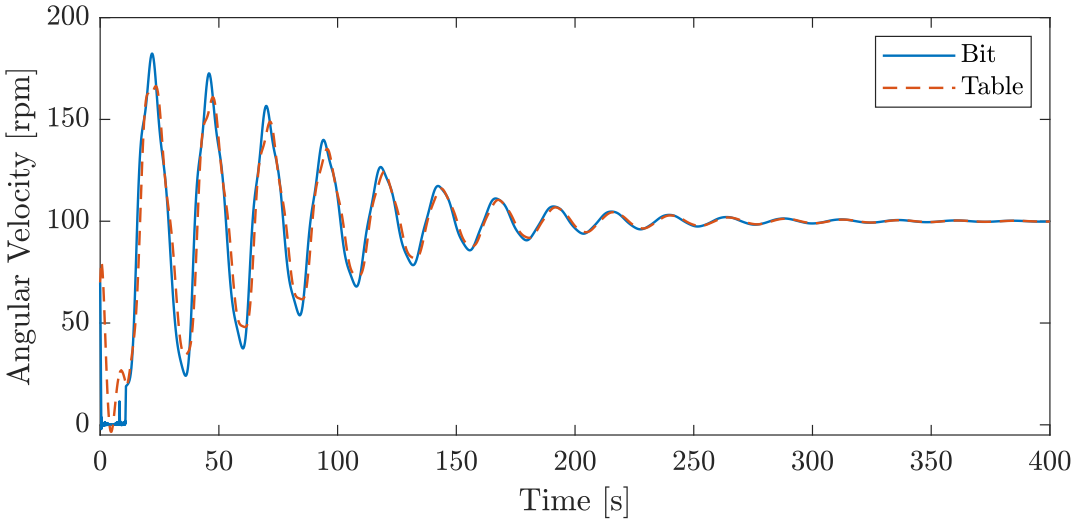

Figure 10 – Bit and rotary table velocities for the case with 2 modes, $(k_p, k_i) = (296,70)$.

A critical scenario can be observed when using control gains that lead to stick-slip oscillations. This scenario is depicted in Figures (10)-(12), that show the system response for the control gains $(k_p, k_i) = (296,70)$. These results show that the model with two modes was not sufficient even to obtain qualitative information about the response, since in Figure 10 the response converges to the operating point, whereas in the other two cases the system exhibits stick-slip oscillations. Hence, higher frequency modes can influence system instability and should be considered in the response analysis, especially in cases where information on stability margins is desired. Furthermore, an analysis of the error shows that even in the presence of stick-slip, the system with thirteen modes was sufficient to obtain an accurate response, with yet a maximum error of $e_{13} = 0.09$

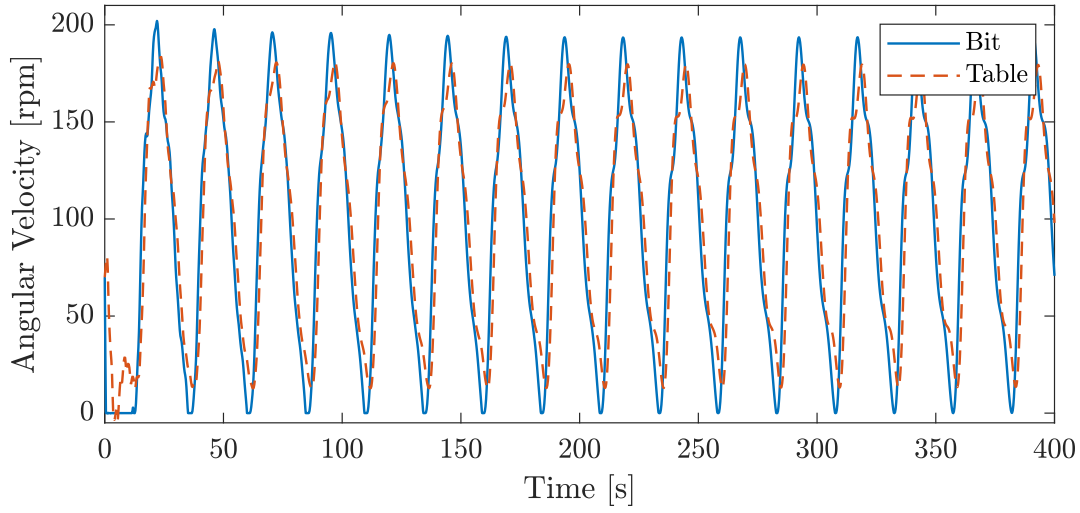

Figure 11 – Bit and rotary table velocities for the case with 13 modes, $(k_p, k_i) = (296{,}70)$.

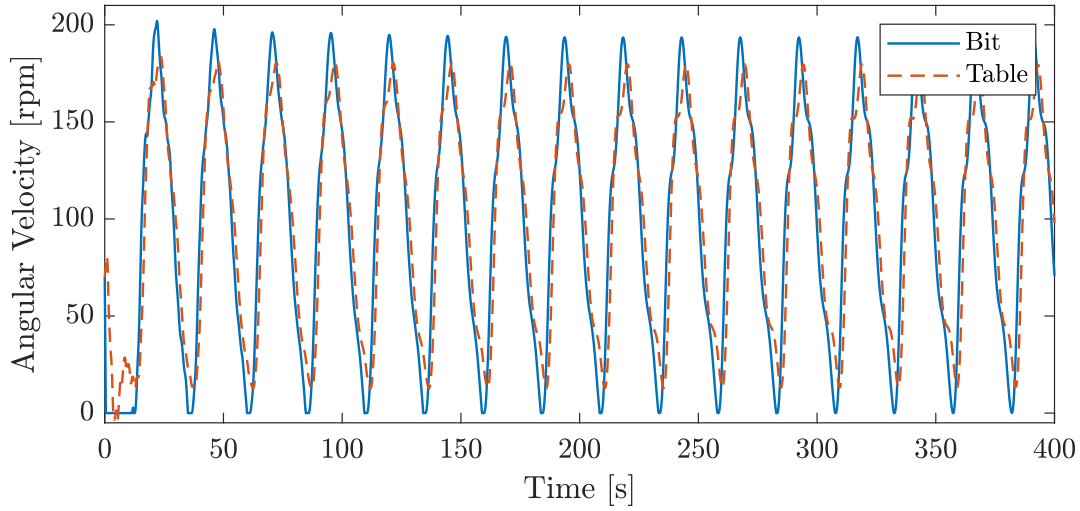

Figure 12 – Bit and rotary table velocities for the case with 30 modes, $(k_p, k_i) = (296{,}70)$.

rpm, as shown in Figure 13. Therefore, the comparison between models with thirteen and thirty modes reveals that the former reliably represents the system behavior in different operating conditions.

2.2 Model reformulation

Some of the analyses developed in sections 3 and 4 are more conveniently done if the operating point is at the origin of the coordinate system. Since the desired operating configuration is characterized by the entire drill string rotating deformed with a constant velocity, its representation using the state defined in Eq. (2.5) is already constant, but not zero (with the rigid body displacement, the desired state would be a function of time, and a further step would be necessary to remove it). Thus, the first steps in reformulating

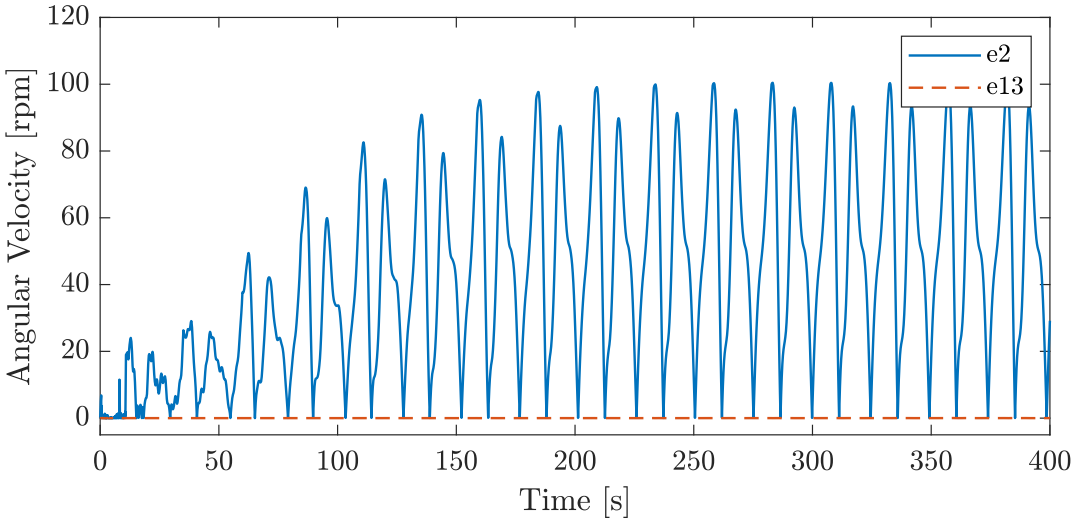

Figure 13 – Error between the cases with the least number of modes and the reference model, $(k_p, k_i) = (296{,}70)$.

the system equations aim to shift the operating point to the origin of a new coordinate system. For that, let the configuration corresponding to the drill string rotating at the desired angular velocity (ω_r) in terms of system states be

$$\mathbf{x}_{eq} = \begin{bmatrix} \bar{\boldsymbol{\eta}}_{eq} \\ \dot{\boldsymbol{\eta}}_{eq} \end{bmatrix}. \tag{2.8}$$

Then, the applied control torque T_t is decomposed into a feedback component u, to suppress vibrations, and a constant feedforward component $\tilde{u}$, inducing $\mathbf{x}_{eq}$, such that

$$T_t = \tilde{u} + u. \tag{2.9}$$

The constant parameters $\mathbf{x}_{eq}$ and $\tilde{u}$ are given by the relation $\omega_r = \boldsymbol{\phi}^{\intercal}(L)\dot{\boldsymbol{\eta}}_{eq}$ combined with the equilibrium condition of Eq. (2.6), $\mathbf{f}(\mathbf{x}_{eq}, \tilde{u}) = \mathbf{0}$:

$$\mathbf{A}\mathbf{x}_{eq} + \mathbf{B}_t\tilde{u} + \mathbf{B}_b T_b(\omega_r) = \mathbf{0}. \tag{2.10}$$

Next, define the new coordinate system $\boldsymbol{\xi}$ by the translation:

$$\boldsymbol{\xi} = \begin{bmatrix} \boldsymbol{\xi}_d \\ \boldsymbol{\xi}_v \end{bmatrix} = \begin{bmatrix} \bar{\boldsymbol{\eta}} - \bar{\boldsymbol{\eta}}_{eq} \\ \dot{\boldsymbol{\eta}} - \dot{\boldsymbol{\eta}}_{eq} \end{bmatrix} = \mathbf{x} - \mathbf{x}_{eq}. \tag{2.11}$$

Finally, the substitution of Eqs. (2.9) and (2.11) into Eq. (2.6) leads to the equations of motion in coordinate $\boldsymbol{\xi}$

$$\dot{\boldsymbol{\xi}} = \mathbf{A}\boldsymbol{\xi} + \mathbf{B}_t u + \mathbf{B}_b q(\omega_d) = \mathbf{g}\left(\boldsymbol{\xi}, u\right), \tag{2.12}$$

in which the desired operating point has been shifted to the origin. In Eq. (2.12), $q(\omega_d)$ is a translated reaction torque

$$q\left(\omega_d\right) = T_b\left(\omega_d + \omega_r\right) - T_b\left(\omega_r\right) = T_b\left(\boldsymbol{\phi}^{\intercal}(L)\boldsymbol{\xi}_v + \omega_r\right) - T_b\left(\omega_r\right), \tag{2.13}$$

such that $q(0) = 0$, and ω_d is the difference between the drill bit and target velocities

$$\omega_d = \omega_b - \omega_r = \boldsymbol{\phi}^{\intercal}(L)\boldsymbol{\xi}_v. \tag{2.14}$$

Equation (2.12) was obtained on the assumption that Eq. (2.10) holds, and consequently, $\tilde{u} = T_b(\omega_r)$. However, as the bit-rock interaction variables are rarely know and subject to changes according to the drill bit condition and the rock formation lithology, there is the possibility that $\tilde{u} \neq T_b(\omega_r)$, and the feedforward torque $\tilde{u}$ may yield a steady-state error. To ensure that at the equilibrium the drill string rotates with the desired angular velocity, Eq. (2.12) is augmented with the error integral

$$\dot{\sigma} = e = \omega_t - \omega_r = \boldsymbol{\phi}^{\intercal}(0)\boldsymbol{\xi}_v \tag{2.15}$$

yielding the augmented system

$$\dot{\boldsymbol{\zeta}} = \begin{bmatrix} \dot{\sigma} \\ \dot{\boldsymbol{\xi}} \end{bmatrix} = \begin{bmatrix} \boldsymbol{\phi}^{\intercal}(0)\boldsymbol{\xi}_v \\ \mathbf{A}\boldsymbol{\xi} + \mathbf{B}_t u + \mathbf{B}_b q(\omega_d) \end{bmatrix} = \mathbf{A}_n\boldsymbol{\zeta} + \mathbf{B}_{tn}u + \mathbf{B}_{bn}q(\omega_d) = \mathbf{h}\left(\boldsymbol{\zeta}, u\right). \tag{2.16}$$

At first, it may seem artificial to augment the system with the error integral since the dynamics of $\boldsymbol{\xi}$ do not depend on σ. However, the idea of adding σ as a state is to measure this variable and use it for feedback, such that u, and consequently $\boldsymbol{\xi}$, become a function of σ. This is a standard procedure in control theory known as integral action that guarantees regulation in the presence of uncertainties if the closed-loop system is structurally stable (KHALIL, 2002).

3 Dynamic analysis

This chapter aims to describe the behavior of the drill string in open- and closed-loop configurations. The determination of the limit sets and equilibrium points, as well as a stability analysis of the desired operating point, are carried out to obtain some insight into the drill string dynamics. The knowledge acquired from these analyses is used in chapter 4 for the controller design.

3.1 Open-loop

Although the drill string model adopts the hypotheses of small deformations and linear stress-strain relationships, Karnopp's friction model with an exponential decaying term makes the whole system nonlinear and nonsmooth. The interaction between these components provides interesting nonlinear behavior for the system, one of which is the existence of multiple equilibrium points. The standard procedure of evaluating the zeros of the vector field gives these equilibria, albeit they can also be determined using a physically oriented approach, by analyzing the diagram shown in Figure 3. For a given constant value of the applied torque $T_t = \tilde{u}$ and considering the balance between the external torques applied to the system ($T_t = T_b$), by Newton's first law, we conclude that the drill string is either stationary or moving as a rigid body with constant speed. Without loss of generality, let $\delta = 0$ in Eq. (2.3) in order to associate the stationary condition with a single equilibrium point. The angular velocities ω corresponding to each equilibrium can be determined by Eq. (2.3), and are illustrated in Figure 14 for a given value of the applied torque $T_t = \tilde{u}$, with $\tilde{u} \in (a_1 N_b, a_2 N_b)$. In terms of the states $\mathbf{x}$ and $\boldsymbol{\xi}$, defined in Eqs. (2.5) and (2.11), respectively, the equilibrium points are

$$\mathbf{x}_{eq} = \begin{bmatrix} \bar{\boldsymbol{\eta}}_{eq} \\ \omega_r/\phi_1(0) \\ \mathbf{0}_{n-1} \end{bmatrix}, \qquad \mathbf{x}_{eq2} = \begin{bmatrix} \bar{\boldsymbol{\eta}}_{eq} \\ 0 \\ \mathbf{0}_{n-1} \end{bmatrix}, \tag{3.1a}$$

$$\boldsymbol{\xi}_{eq} = \begin{bmatrix} \mathbf{0}_{n-1} \\ 0 \\ \mathbf{0}_{n-1} \end{bmatrix}, \qquad \boldsymbol{\xi}_{eq2} = \begin{bmatrix} \mathbf{0}_{n-1} \\ -\omega_r/\phi_1(0) \\ \mathbf{0}_{n-1} \end{bmatrix}, \tag{3.1b}$$

in which ω_r is the angular velocity corresponding to desired operating configuration, $\bar{\boldsymbol{\eta}}_{eq}$ is the drill string deformation due to the balance between applied torques, ϕ_1 (the function ϕ_1 was evaluated at zero, but it could have been evaluated at any other point since it is associated with the rigid body mode and, therefore, is constant) is the first component of

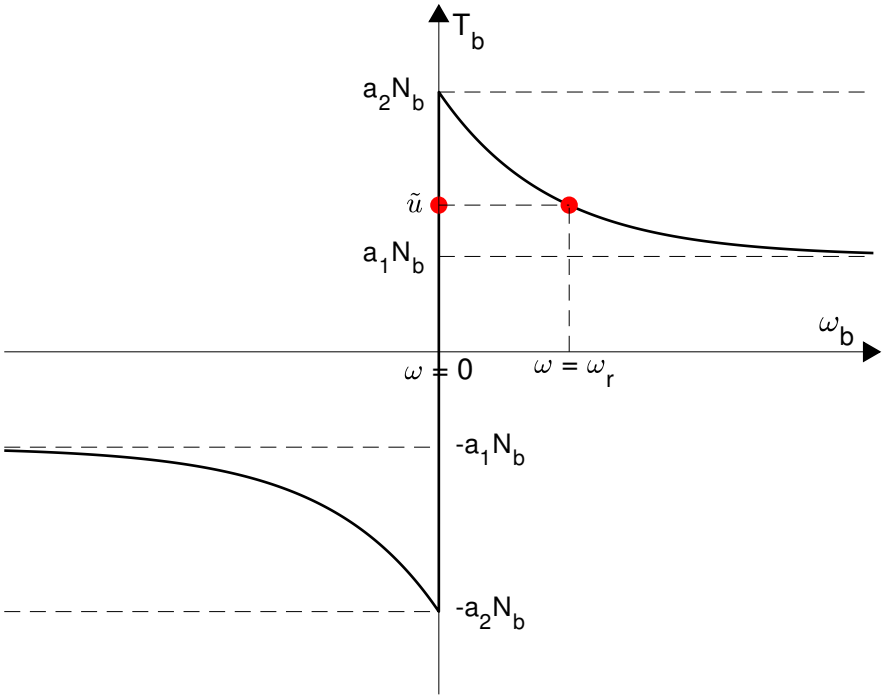

Figure 14 – Angular velocities ω corresponding to each equilibrium point for an applied torque $T_t = \tilde{u}$.

the vector of eigenfunctions and the subscript $n-1$ is the dimension of the zero vector. The equilibria $\mathbf{x}_{eq}$ and $\boldsymbol{\xi}_{eq}$ correspond to the desired operating configuration, while $\mathbf{x}_{eq2}$ and $\boldsymbol{\xi}_{eq2}$ are associated with a stuck drill bit. Note that the only difference between these configurations is the value of the rigid body velocity. In the sequence, the stability of the operating point is investigated considering the open-loop system described by Eq. (2.12).

For a target angular velocity ω_r sufficiently greater than zero, q is a smooth function of ω_d, and the qualitative behavior of the solutions of equation (2.12) in a neighborhood of the origin can be determined by a linear approximation at this point (assuming $\boldsymbol{\xi}_{eq}$ is hyperbolic). Linearization of Eq. (2.12) at the origin leads to the associated linear system

$$\dot{\boldsymbol{\xi}} = \mathbf{A}_l \boldsymbol{\xi}, \tag{3.2}$$

in which, by abuse of notation, $\boldsymbol{\xi}$ is also used to represent the dynamics of the linearized system and $\mathbf{A}_l$ is the matrix of first order partial derivatives of $\mathbf{g}$ with respect to $\boldsymbol{\xi}$, evaluated at the origin

$$\mathbf{A}_l = \left.\frac{\partial \mathbf{g}}{\partial \boldsymbol{\xi}}\right|_{\boldsymbol{\xi}=\mathbf{0}} = \begin{bmatrix} \mathbf{0} & \bar{\mathbf{I}} \\ -\bar{\boldsymbol{\Lambda}} & -[\mathbf{D} + n_d \boldsymbol{\phi}(L)\boldsymbol{\phi}^{\intercal}(L)] \end{bmatrix}, \tag{3.3}$$

where n_d is the derivative of q (Eq. (2.13)) at zero

$$n_d = \left.\frac{\mathrm{d}q}{\mathrm{d}\omega_d}\right|_{\omega_d=0} = -\beta(a_2 - a_1)e^{-\beta\omega_r}WOB. \tag{3.4}$$

Matrix $\mathbf{A}_l$, which represents the linearized system dynamics, is a combination of matrix $\mathbf{A}$, which characterizes the dynamics of the drill string itself, and matrix $n_d\boldsymbol{\phi}(L)\boldsymbol{\phi}^\intercal(L)$, which is the local contribution of the bit-rock interaction. This contribution appears in matrix $\mathbf{A}_l$ together with the term $\mathbf{D}$, which represents system dissipation factors. However, as the matrix $\boldsymbol{\phi}(L)\boldsymbol{\phi}^\intercal(L)$ is positive semi-definite and the coefficient n_d is negative, this contribution produces the opposite effect of the energy dissipation term $\mathbf{D}$. Thus, the reaction torque applied to the bit is locally equivalent to a viscous damper with a negative damping coefficient n_d, yielding the observed instability in field operations.

The apparent negative damping effect has already been described in classical nonlinear oscillations texts and is regarded as a source of instability of equilibrium points and the existence of limit cycles, see for example the Van der Pol oscillator and Froude's pendulum (ANDRONOV; VITT; KHAIKIN, 1966; GUCKENHEIMER; HOLMES, 1983). Several works (BRETT, 1992; MIHAJLOVIĆ et al., 2004; SALDIVAR et al., 2013) also mention negative damping as one of the causes of instability and occurrence of stick-slip oscillations for the drilling problem in oil wells. The expression derived in Eq. (3.4) based on the friction model adopted in Eq. (2.3) not only corroborates these statements, but introduces the concept of the negative damping coefficient based on the linear approximation and indicates how the drilling parameters affect its magnitude. Therefore, field observations (BRETT, 1992) indicating that increasing the WOB or decreasing the angular velocity may lead to unstable drilling operations can be explained using the negative damping coefficient, since both of the described operations increase its magnitude. Likewise, higher values of the difference between static and dynamic friction coefficients produce the same effect on n_d and can also induce instability. Such direct relationships cannot be drawn for the decay rate β, as n_d is not a monotonic function of β; nevertheless, simple calculations show that the magnitude of n_d increases for $\beta \in (0, 1/\omega_r)$ and decreases otherwise.

To validate the previous discussion, we proceed with a numerical stability analysis of the linearized system (3.2). For that, consider first the following definitions: let $\mathbf{x}^* \in \mathbb{R}^n$ be an equilibrium of an autonomous system represented by the differential equation $\dot{\mathbf{x}} = \mathbf{f}(\mathbf{x})$, and $\mathbf{M}$ be the linear approximation of $\mathbf{f}$ at $\mathbf{x}^*$:

$$\mathbf{M} = \left.\frac{\partial \mathbf{f}}{\partial \mathbf{x}}\right|_{\mathbf{x}=\mathbf{x}^*}. \tag{3.5}$$

Let also $\upsilon(\mathbf{M})$ denote the spectral abscissa of $\mathbf{M}$, i.e., $\upsilon(\mathbf{M})$ is the real part of the rightmost eigenvalue of matrix $\mathbf{M}$. Then, the point $\mathbf{x}^*$ is:

- stable, if for any neighborhood U of $\mathbf{x}^*$, there exists a neighborhood $V \subset U$ such that any trajectory $\mathbf{x}(t)$ starting in V ($\mathbf{x}(0) \in V$) remains in U for all $t \geq 0$;
- asymptotically stable, if in addition to being stable, there exists a neighborhood W of $\mathbf{x}^*$, such that $\mathbf{x}(t) \to \mathbf{x}^*$ as $t \to \infty$ for every $\mathbf{x}(0) \in W$. $\mathbf{x}^*$ is said to be globally asymptotically stable if $W = \mathbb{R}^n$;
- spectrally stable, if $\upsilon(\mathbf{M}) < 0$;
- unstable, if it is not stable.

Another important result, known as Lyapunov's indirect method (KHALIL, 2002), is that spectral stability implies asymptotic stability and $\upsilon(\mathbf{M}) > 0$ implies instability of the equilibrium point.

Hence, the effects of the negative damping coefficient on the stability of $\boldsymbol{\xi}_{eq}$ can be assessed by evaluating $\upsilon(\mathbf{A}_l)$ for different values of n_d. The results of this analysis are illustrated in Figure 15, which shows that $\upsilon(\mathbf{A}_l)$ is always positive for $n_d < 0$ and moves further away from the imaginary axis as n_d decreases. These results attest the previous discussion, as they show an unstable operating point for negative values of the negative damping coefficient. As discussed in chapter 2, the absence of damping for the rigid body mode implies a null eigenvalue for $n_d = 0$. If damping were added to the rigid body mode, the effects of the negative damping coefficient would be countervailed, and $\boldsymbol{\xi}_{eq}$ would be asymptotically stable for small values of $|n_d|$. Since an accurate model for the dissipation sources may be hard to derive and requires update according to the drilling operating conditions, it was preferred to keep the system without damping for the rigid body mode, and deal with a critical case for controller design, where the operating point of the open-loop system is unstable for any value of $n_d < 0$.

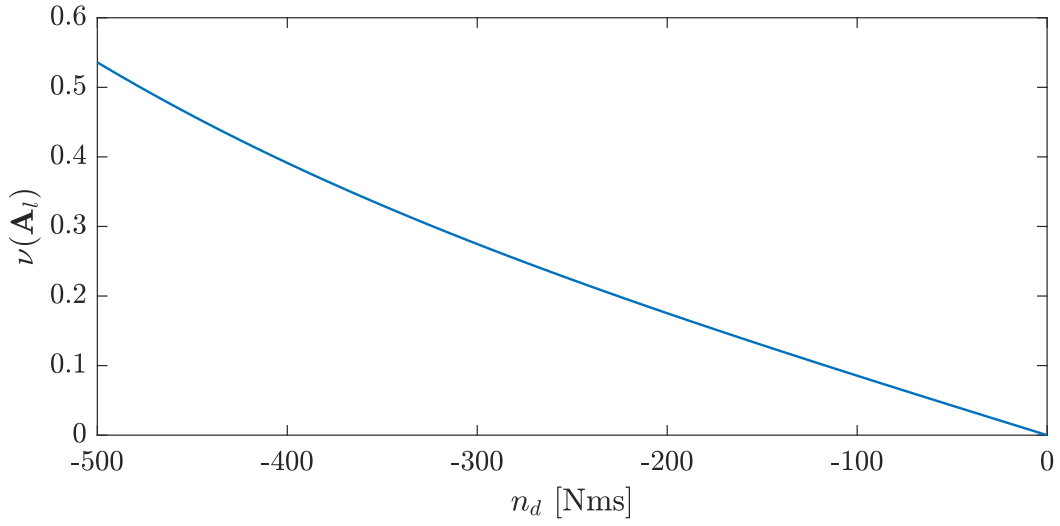

Figure 15 – Spectral abscissa of the matrix $\mathbf{A}_l$ as a function of n_d.

The stability of the operating point $\boldsymbol{\xi}_{eq}$ is further analyzed by simulating the nonlinear system given in Eq. (2.12). The WOB of 120 kN and the target velocity $\omega_r = 100$ rpm were once more selected for demonstration of the results. Figures 16 and 17 depict the system response for initial conditions given by small perturbations around the equilibrium point. The scenario in which the system response goes from the vicinity of the unstable equilibrium $\boldsymbol{\xi}_{eq}$ to the stable equilibrium $\boldsymbol{\xi}_{eq2}$ is shown in Figure 16. When the drill bit initial velocity is slightly less than ω_r, expression (2.3) indicates that the initial reaction torque is greater than the applied torque $\tilde{u}$ (see Figure 14). Since the torque on bit increases for decreasing angular velocities and the applied torque $\tilde{u}$ is constant, the drill bit angular speed undergoes a progressive reduction until it gets stuck. The opposite behavior occurs for an initial drill bit velocity slightly above ω_r, as shown in Figure 17. In this circumstance, the initial reaction torque is lower than the applied torque, and due to the negative slope relationship between the drill bit velocity and the reaction torque, the drill bit velocity progressively increases, and the system response diverges.

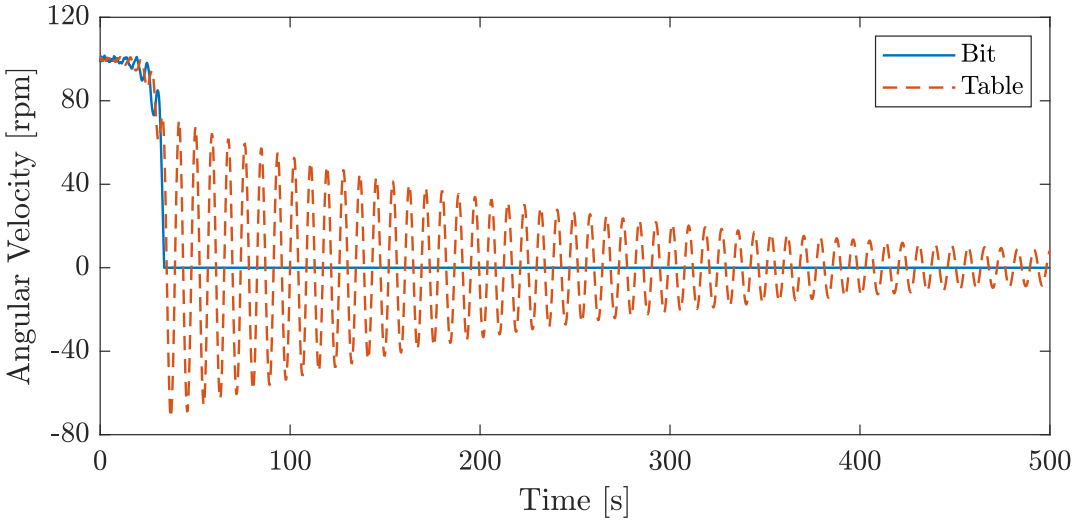

Figure 16 – Bit and rotary table velocities for an initial condition given by a negative perturbation in the rigid body velocity of the equilibrium $\boldsymbol{\xi}_{eq}$.

Other types of dynamic behavior, such as stick-slip oscillations, can be observed for initial conditions that are not in the neighborhood of the equilibrium point or when a control action is applied. These types of responses are investigated in the next section, which shows the typical behavior of the closed-loop system for a given class of control laws.

3.2 Closed-loop

The previous section showed that the open-loop drilling system has two equilibria and that the point of interest is unstable due to the apparent negative damping effect.

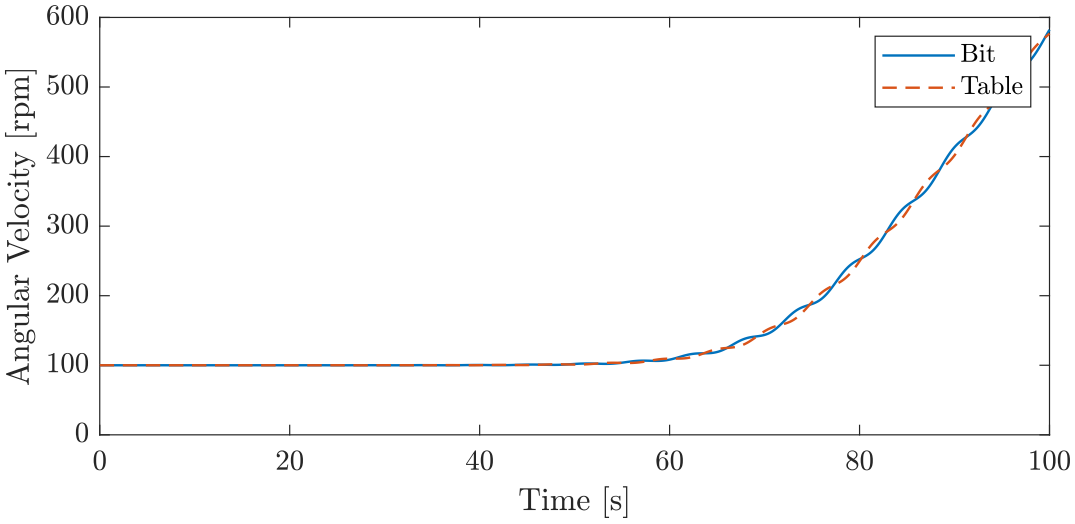

Figure 17 – Bit and rotary table velocities for an initial condition given by a positive perturbation in the rigid body velocity of the equilibrium $\boldsymbol{\xi}_{eq}$.

The primary goal of employing a controller for this system is to reverse this situation, i.e., rendering the operating point asymptotically stable. As discussed in subsection 1.2.2, several control techniques can be employed for this purpose, the main differences between them being which signals are used for feedback and how they are manipulated to yield an effective control action. To illustrate the types of responses that the closed-loop system may exhibit, we initially consider the elementary PI controller. The PI control law is defined as a sum of a term proportional to the error and another proportional to the integral of the error. Since the desired configuration is characterized by the whole drill string rotating with a constant speed, and surface measurements are generally more accessible, the error is usually defined as the difference between the rotary table and target velocities, $e = \omega_t - \omega_r$. This definition leads to the control action given in Eq. (2.7), which, in terms of the states defined in Eq. (2.16), can be rewritten as

$$u = -k_p \boldsymbol{\phi}^{\intercal}(0)\boldsymbol{\xi}_v - k_i \sigma. \tag{3.6}$$

This control law couples equations (2.12) and (2.15), making the state $\boldsymbol{\xi}$ a function of σ. Due to this coupling, the equilibrium condition ($h(\boldsymbol{\zeta}, u) = \mathbf{0}$) of the closed-loop system represented by Eq. (2.16) implies $\omega_t = \omega_r$. Therefore, unlike the open-loop system, the closed-loop system with PI control has a single equilibrium point, which corresponds to the desired operating configuration (the whole drill string rotating with the angular velocity ω_r), and the permanent stuck bit situation illustrated in Figure 16, which is related to the equilibrium $\boldsymbol{\xi}_{eq2}$, is eliminated. Since the frictional force (2.13) is bounded and the control action is opposite to the error and its derivative, the case in which the operating point is unstable does not yield an unbounded response, and the situation where the system response diverges (Figure 17) is also eliminated.

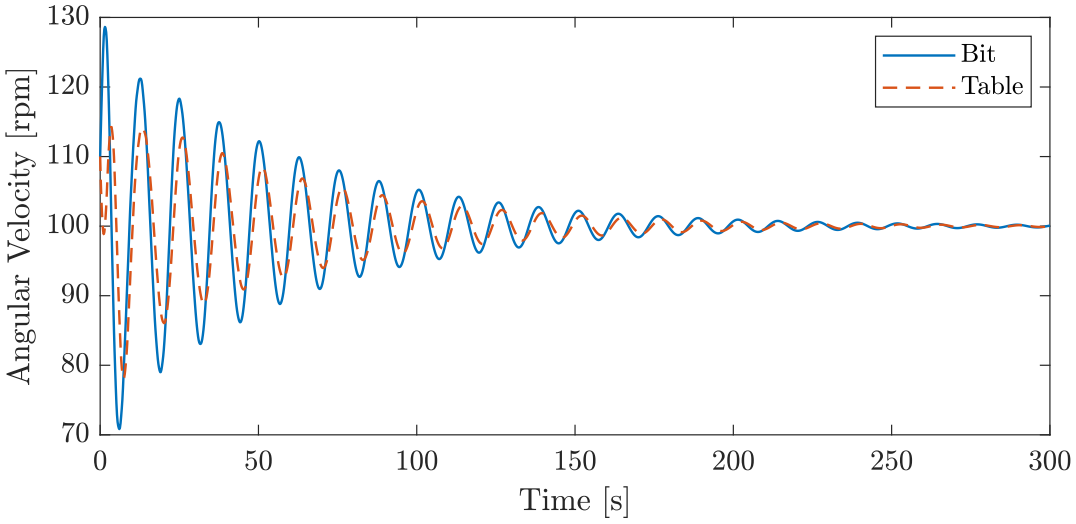

Figure 18 – Bit and rotary table velocities for a small perturbation at the equilibrium using control gains $(k_p, k_i) = (500, 250)$.

To illustrate the above statements, simulations are performed for the WOB of 120 kN and a target velocity of 100 rpm using distinct PI control gains. In the first scenario, a pair of control gains $(k_p, k_i) = (500, 250)$ is selected to render the operating point of the closed-loop system asymptotically stable. Figure 18 depicts the closed-loop system response using these control gains for an initial condition in the neighborhood of the operating point, $\boldsymbol{\zeta}(0) = \begin{bmatrix} 0 & 0.1\mathbf{x}_{eq}^{\intercal} \end{bmatrix}^{\intercal}$. Since the control gains were selected to guarantee asymptotic stability, the system response converges to the operating point, as expected. However, a different behavior is observed for initial conditions that are not in the vicinity of the operating point. Figure 19 shows the system response using the same control gains when the drill string starts undeformed with an angular velocity of 70 rpm. In this case, instead of converging to the operating point, the system response approaches and stays in a limit cycle. Focusing on the drill bit response, Figure 19 shows, at the beginning of the simulation, the drill bit speed decreasing until reaching a complete standstill (stick phase). At this stage, the positive error increases the applied torque due to the integral action and, when the applied torque overcomes the reaction frictional torque, the drill bit starts rotating again (slip phase). As the drill string may be twisted several times during the stick phase, after the drill bit is released its angular velocity reaches a value much higher than the target velocity, sharply reducing the applied torque due the integration of the negative error. In this circumstance, the applied torque is considerably less than the necessary to keep the bit rotating at the target speed, and the bit speed is reduced until it re-enters the stick phase. This phenomenon occurs in a periodic fashion, producing the so-called drill bit stick-slip oscillations. The control effort and the necessary constant torque $\tilde{u}$ to maintain the drill bit rotating at the target velocity are displayed in Figure 20.

The limit behavior discussed previously is also observed when the operating point

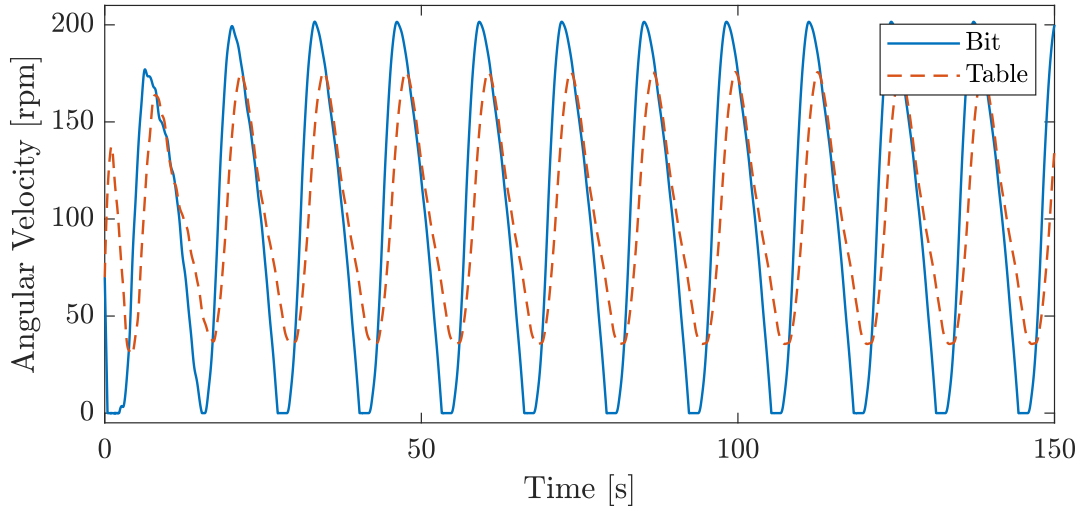

Figure 19 – Bit and rotary table velocities when the drill string starts undeformed with an angular velocity of 70 rpm using control gains $(k_p, k_i) = (500, 250)$.

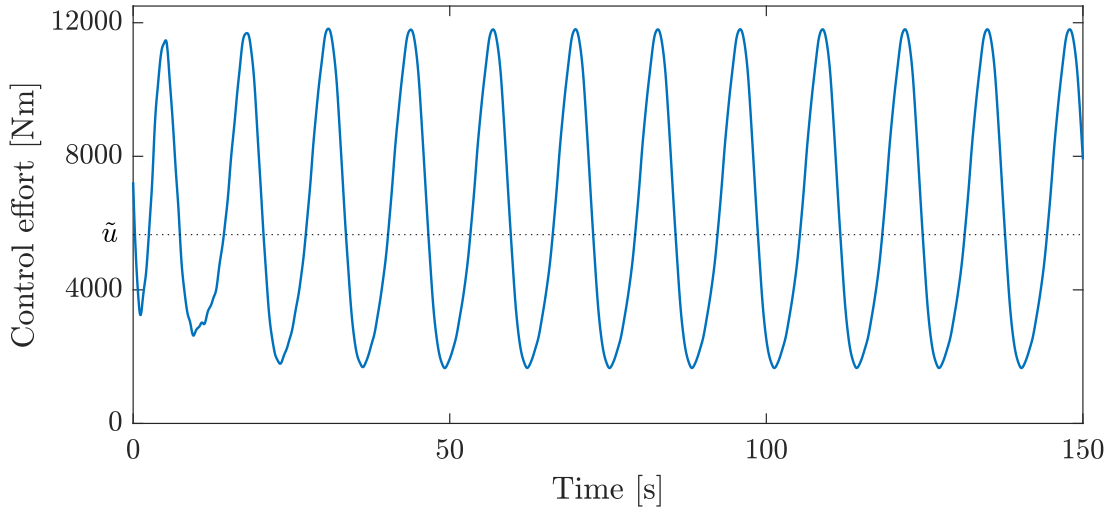

Figure 20 – Applied torque when the drill string starts undeformed with an angular velocity of 70 rpm using control gains $(k_p, k_i) = (500, 250)$.

is not asymptotically stable. For instance, Figure 21 shows the system response for a pair of control gains $(k_p, k_i) = (100, 600)$ that leads to an unstable operating point. Despite the operating point being unstable as in the open-loop system, the response of the closed-loop system does not diverge or tend to the second equilibrium point ($\boldsymbol{\xi}_{eq2}$), but rather reaches again the limit cycle. The initial condition for this simulation is a random small perturbation at the equilibrium.

These results identify the two basic stable limit sets that the closed-loop system possesses using a PI-type controller: an equilibrium and a limit cycle. As shown in the case where the operating point is asymptotically stable, care must be taken because the region of attraction may be limited, and some perturbations in the equilibrium may lead to the appearance of stable and persistent stick-slip oscillations. Therefore, if the designed

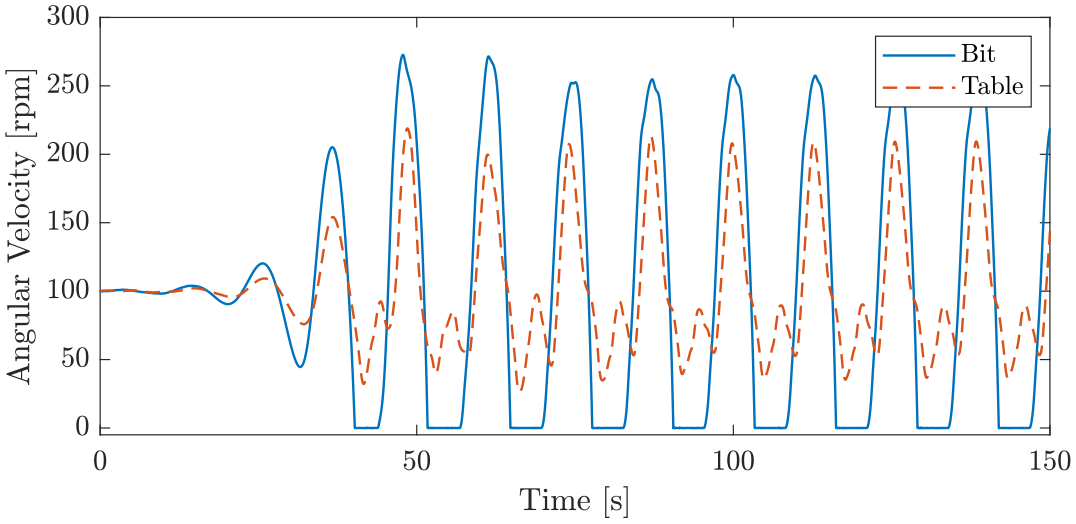

Figure 21 – Bit and rotary table velocities for a random small perturbation at the equilibrium using control gains $(k_p, k_i) = (100, 600)$.

controller guarantees only asymptotic stability, it is important to carry out simulations with the occurrence of at least one stick phase to guarantee that the operating point has a large region of attraction, minimizing the chances of stick-slip occurrence. The two limit sets determined previously are the same for the linear controllers designed in chapter 4, and will serve as a guide for evaluating the performance of the designed controllers in sections 5 and 6.

4 Controller design

This chapter proposes two distinct linear control techniques relying exclusively on sensors measurements for mitigating drill string torsional vibrations. The chapter starts with an investigation of which signals might be relevant for feedback and proceeds to establish the structure of the output matrix. The next two sections deal with the controller gain design. The first technique presented was developed and applied to the vibration control of linear systems in a previous work (CRUZ NETO; TRINDADE, 2019), and consists of determining the control gain of an output feedback controller (OSOF) such that its performance is as close as possible to that of a full state feedback controller (LQR). The second technique is based on the negative damping coefficient concept introduced in section 3.1, and aims to enlarge the limits of drill string safe operation by finding the control gains that maximize the value of the negative damping coefficient for which the operating point is asymptotically stable. These techniques are tested in chapters 5 and 6 via numerical simulations of the model developed in chapter 2.

4.1 Output matrix

In control theory, and particularly in vibration control of flexible structures, the types and locations of sensors are as meaningful as the control gains. For the control of drill string torsional vibrations, a variety of measurements have been considered for feedback: the angular velocity and displacement of the rotary table (TRINDADE, 2020), the WOB (MONTEIRO; TRINDADE, 2017), the torque at the rotary table (HALSEY; KYLLINGSTAD; KYLLING, 1988), the torque on bit (ABDULGALIL; SIGUERDIDJANE, 2004), the shear strain at the top of the drill string (TUCKER; WANG, 2003), the drill bit velocity (NAVARRO-LOPEZ; LICEAGA-CASTRO, 2009) and the difference between the drill bit and rotary table displacements (YIGIT; CHRISTOFOROU, 2006). Since the goal of the control techniques developed in the following sections is to guarantee asymptotic stability, this work considers that the signals used for feedback are related to the system's states defined in Eq. (2.16). Furthermore, these signals must be either directly measured or obtained via a simple manipulation, such as integration. Rather than limiting the signals used for feedback to just measurements on the rotary table, a broader scenario is analyzed, where measurements can be obtained along the drill string. However, since sensors placement in field operations is restricted and real-time large distance data transmission is not available at the majority of oil wells, the focus of the analyzes are on cases where the additional sensors are close to the rotary table, with a maximum placement range of 10% of the total drill string length. As this is a narrow set, a large

number of sensors may give redundant information, so it was decided to use only two sensors. Indeed, it was found in simulations that increasing the number of sensors while maintaining the placement restriction did not improve performance. Although emphasis is placed on the scenario with restricted positioning, few simulations in chapter 5 study the effects of placing the additional sensor along the entire drill string to assess how much it is possible to improve the controller performance.

The effects of the measured signals on the closed-loop system are analyzed according to their influence on the entries of the linearized closed-loop state matrix. To this end, it is initially necessary to establish the control law. The general expression of a single-input controller with linear static output feedback is

$$u = -\mathbf{K}\mathbf{y}, \tag{4.1}$$

in which $\mathbf{K} \in \mathbb{R}^{1\times s}$, with s representing the number of sensors, is a constant control gain and $\mathbf{y}$ represents the measured signals, which can be written as a function of system's states:

$$\mathbf{y} = \mathbf{C}\boldsymbol{\zeta}. \tag{4.2}$$

in which $\mathbf{C} \in \mathbb{R}^{s\times 2n}$ is the output matrix. The substitution of Eqs. (4.1) and (4.2) in Eq. (2.16) gives

$$\dot{\boldsymbol{\zeta}} = (\mathbf{A}_n - \mathbf{B}_{tn}\mathbf{K}\mathbf{C})\,\boldsymbol{\zeta} + \mathbf{B}_{bn}q(\omega_d), \tag{4.3}$$

such that the linearized closed-loop state matrix is

$$\mathbf{A}_{cl} = \mathbf{A}_l - \mathbf{B}_{tn}\mathbf{K}\mathbf{C}, \tag{4.4}$$

in which $\mathbf{A}_l$ is the linear approximation of the augmented open-loop system (2.16) at the operating point ($\mathbf{A}_l$ is also used for the linear approximation of the augmented system, an admitted abuse of notation):

$$\mathbf{A}_l = \left.\frac{\partial \mathbf{h}}{\partial \boldsymbol{\zeta}}\right|_{\boldsymbol{\zeta}=\mathbf{0}} = \begin{bmatrix} 0 & \mathbf{0} & \boldsymbol{\phi}^{\intercal}(0) \\ \mathbf{0} & \mathbf{0} & \bar{\mathbf{I}} \\ \mathbf{0} & -\bar{\boldsymbol{\Lambda}} & -[\mathbf{D} + n_d\boldsymbol{\phi}(L)\boldsymbol{\phi}^{\intercal}(L)] \end{bmatrix}. \tag{4.5}$$

To analyze the effects of feedback on $\mathbf{A}_{cl}$, start with the scenario of a single sensor at the rotary table using the PI control law, which considers velocity and displacement for feedback. The output matrix for the PI controller is

$$\mathbf{C} = \begin{bmatrix} 1 & \mathbf{0} & \mathbf{0} \\ \mathbf{0} & \mathbf{0} & \boldsymbol{\phi}^{\intercal}(0) \end{bmatrix} \tag{4.6}$$

which leads to the following linearized closed-loop state matrix

$$\mathbf{A}_{cl} = \begin{bmatrix} 0 & \mathbf{0} & \boldsymbol{\phi}^{\intercal}(0) \\ \mathbf{0} & \mathbf{0} & \bar{\mathbf{I}} \\ -k_i\boldsymbol{\phi}(0) & -\bar{\boldsymbol{\Lambda}} & -\left[\mathbf{D} + n_d\boldsymbol{\phi}(L)\boldsymbol{\phi}^{\intercal}(L) + k_p\boldsymbol{\phi}(0)\boldsymbol{\phi}^{\intercal}(0)\right] \end{bmatrix}. \tag{4.7}$$

In this case, the proportional gain acts on the damping term, while the integral gain is mainly a component that guarantees regulation. Note that, due to the rigid body mode, feeding back the displacement does not affect the entries corresponding to the natural frequencies (differently from systems without a rigid body mode). An alternative to acting on the natural frequencies would be to feed back the displacement without the component associated with the rigid body mode. This approach is studied in a paper that was published recently (CRUZ NETO; TRINDADE, 2023). However, as a straightforward method to obtain this signal has not yet been determined, this work proposes another approach to modify the natural frequencies, which consists in using a second sensor and feeding back the difference between the measured displacements of both sensors. The output matrix for this approach is

$$\mathbf{C} = \begin{bmatrix} 1 & 0 & 0 & 0 \\ \mathbf{0} & \bar{\boldsymbol{\phi}}(\alpha_1) - \bar{\boldsymbol{\phi}}(\alpha_2) & \mathbf{0} & \mathbf{0} \\ \mathbf{0} & \mathbf{0} & \boldsymbol{\phi}(\alpha_1) & \boldsymbol{\phi}(\alpha_2) \end{bmatrix}^{\intercal} \tag{4.8}$$

in which α_1 and α_2 are the locations of the first and second sensors, respectively. Due to the need for an integrator at the rotary table, because the error derivative was defined as the difference between the rotary table and target velocities, the first sensor location is $\alpha_1 = 0$. Different locations for the second sensor are examined in chapter 5. The first column of matrix $\mathbf{C}^{\intercal}$ corresponds to the error integral, the second is associated with the difference between the measured displacements, the third corresponds to the velocity measured at the rotary table and the fourth to the velocity measured at α_2. The first element of the vector $\bar{\boldsymbol{\phi}}(\alpha_1) - \bar{\boldsymbol{\phi}}(\alpha_2)$ was removed to make the dimensions of $\mathbf{C}$ and $\boldsymbol{\zeta}$ compatible. This elimination can be done without loss of generality, since the presence of the rigid body mode implies

$$\left[\boldsymbol{\phi}(\alpha_1) - \boldsymbol{\phi}(\alpha_2)\right]^{\intercal}\boldsymbol{\eta} = \left[\bar{\boldsymbol{\phi}}(\alpha_1) - \bar{\boldsymbol{\phi}}(\alpha_2)\right]^{\intercal}\bar{\boldsymbol{\eta}}. \tag{4.9}$$

Feeding back the signals specified in Eq. (4.8) yields the following closed-loop state matrix

$$\mathbf{A}_{cl} = \begin{bmatrix} 0 & \mathbf{0} & -K_1\boldsymbol{\phi}^\intercal(0) \\ \mathbf{0} & \mathbf{0} & -\left[\bar{\boldsymbol{\Lambda}} + K_2\boldsymbol{\phi}(0)\left(\bar{\boldsymbol{\phi}}^\intercal(\alpha_1) - \bar{\boldsymbol{\phi}}^\intercal(\alpha_2)\right)\right]^\intercal \\ \boldsymbol{\phi}(0) & \bar{\mathbf{I}}^\intercal & -\left[\mathbf{D} + n_d\boldsymbol{\phi}(L)\boldsymbol{\phi}^\intercal(L) + \boldsymbol{\phi}(0)\left(K_3\boldsymbol{\phi}^\intercal(\alpha_1) + K_4\boldsymbol{\phi}^\intercal(\alpha_2)\right)\right]^\intercal \end{bmatrix}^\intercal . \quad (4.10)$$

The addition of the second sensor makes the controller more versatile, making it capable of modifying the flexible components of the drill string and increasing its ability to act on the damping terms. Chapter 5 will show that the addition of the second sensor considerably extends the limits of safe drilling operation. Another interesting remark derived from Eq. (4.10) is that feeding back the displacement measured by the first sensor is useful for output regulation, but there is no point in feeding back uniquely the displacement measured by the second sensor, since it does not affect any element of $\mathbf{A}_{cl}$. Indeed, adding a new state to represent the displacement of another point on the drill string would yield a null eigenvalue for the closed-loop linearized matrix, which could preclude the design of some control techniques. Therefore, the output matrix general structure is given in Eq. (4.8) and the effects of varying the position of the second sensor are analyzed in chapter 5. Two distinct methods for determination of the control gains are developed in the following sections. Since the OSOF formulation was originally developed to also design the sensors locations, it was decided to keep this framework in the subsequent presentation. As the results obtained with the OSOF give a clear indication of what is the optimal positioning of the second sensor, this information is used in the development of the negative damping based controller, so that it only considers the controller gain design.

4.2 Optimal static output feedback (OSOF) controller

This section presents the general formulation of the optimal static output feedback (OSOF) controller for a linear system, which derives from the linear quadratic regulator (LQR). An obstacle in applying the LQR control to practical problems is the requirement of measuring all states for feedback. Although the linear quadratic gaussian (LQG) control solves this issue by using an observer to estimate unmeasured states, it does not possess some important structural properties of the LQR, such as low sensitivity to uncertainties and high frequency margins. Indeed, LQG control does not ensure the existence of stability margins (DOYLE, 1978), and the loop transfer recovery techniques are restricted to minimum phase plants and tends to generate high gains (SKOGESTAD; POSTLETHWAITE, 2005). The optimal static output feedback control, initially proposed in (LEVINE; ATHANS, 1970), suggests a simple alternative to the LQR and LQG controllers, using the same quadratic cost function of the LQR but with the constraint of using only the signals specified by the output matrix for feedback. Briefly, the OSOF formulation can be described as follows.

Given a linear dynamical system

$$\dot{\mathbf{x}} = \mathbf{A}\mathbf{x} + \mathbf{B}\mathbf{u} \tag{4.11a}$$

$$\mathbf{y} = \mathbf{C}\mathbf{x} \tag{4.11b}$$

$$\mathbf{u} = -\mathbf{K}\mathbf{y} \tag{4.11c}$$

in which $\mathbf{y}$ describes the measured states, a control law of the type (4.11c) is sought such that the system (4.11a) is stable and the following quadratic cost function is minimized

$$J_Q = \int_0^\infty \mathbf{x}^\intercal \mathbf{Q}\mathbf{x} + \mathbf{u}^\intercal \mathbf{R}\mathbf{u} \, \mathrm{d}t \tag{4.12}$$

The cost function (4.12) describes a trade-off between performance and control effort, which should be balanced according to controlled system specifications by choosing the weighting matrices $\mathbf{Q}$ and $\mathbf{R}$. For the well-posedness of the problem, $\mathbf{Q}$ must be at least positive semi-definite and $\mathbf{R}$ must be positive definite. Assuming that (4.11a) is stabilizable using output feedback, the problem of minimizing (4.12) subject to the constraints (4.11) can be rewritten in a more convenient form (CRUZ NETO, 2018) as

$$\min_{\mathbf{K}} \quad \mathrm{tr}\{\mathbf{P}\mathbf{x}_0\mathbf{x}_0^\intercal\} \tag{4.13a}$$

$$\text{subject to} \quad \mathbf{A}_c^\intercal\mathbf{P} + \mathbf{P}\mathbf{A}_c + \mathbf{Q} + (\mathbf{K}\mathbf{C})^\intercal\mathbf{R}\mathbf{K}\mathbf{C} = \mathbf{0}, \tag{4.13b}$$

in which $\mathbf{x}_0$ is the vector of system initial conditions, tr is the trace operator and $\mathbf{A}_c$ is the closed loop state matrix ($\mathbf{A}_c = \mathbf{A} - \mathbf{B}\mathbf{K}\mathbf{C}$). The constraint given in equation (4.13b) is a Lyapunov equation that has a unique solution $\mathbf{P}$ for every $\mathbf{A}_c$ that is Hurwitz. Therefore, for every control gain $\mathbf{K}$ that makes the closed-loop system stable, equation (4.13b) can be solved to determine a matrix $\mathbf{P}$ that will be used to evaluate the cost function (4.13a) for a given initial condition.

To determine the first order necessary conditions for optimality, we first convert this constrained problem into an unconstrained problem using a matrix $\mathbf{S}$ of Lagrange multipliers, such that the Lagrangian is

$$L = \mathrm{tr}\{\mathbf{P}\mathbf{x}_0\mathbf{x}_0^\intercal\} + \mathrm{tr}\{\mathbf{S}(\mathbf{A}_c^\intercal\mathbf{P} + \mathbf{P}\mathbf{A}_c + \mathbf{Q} + (\mathbf{K}\mathbf{C})^\intercal\mathbf{R}\mathbf{K}\mathbf{C})\} \tag{4.14}$$

then, the necessary conditions to obtain a stationary point for this cost function are given by

$$\frac{\partial L}{\partial \mathbf{S}} = \mathbf{A}_c^\intercal \mathbf{P} + \mathbf{P}\mathbf{A}_c + \mathbf{Q} + (\mathbf{K}\mathbf{C})^\intercal \mathbf{R}\mathbf{K}\mathbf{C} = 0 \tag{4.15a}$$

$$\frac{\partial L}{\partial \mathbf{P}} = \mathbf{A}_c \mathbf{S} + \mathbf{S}\mathbf{A}_c^\intercal + \mathbf{x}_0 \mathbf{x}_0^\intercal = \mathbf{0} \tag{4.15b}$$

$$\frac{1}{2}\frac{\partial L}{\partial \mathbf{K}} = \mathbf{R}\mathbf{K}\mathbf{C}\mathbf{S}\mathbf{C}^\intercal - \mathbf{B}^\intercal \mathbf{P}\mathbf{S}\mathbf{C}^\intercal = \mathbf{0} \tag{4.15c}$$

Methods for solving equations (4.15) are given by (CRUZ NETO, 2018). Henceforth, the focus is placed on the dependence of the solution on initial conditions. Since there is no way to decouple equations (4.15) and equation (4.15b) has a dependence on system initial condition, so do the optimal output control gain $\mathbf{K}$. The first approach to deal with this dependence was proposed by (LEVINE; ATHANS, 1970). Their suggestion consisted in optimizing the expected value of the cost function (4.13a) given a linearly independent set of initial states, which was equivalent to assuming that the initial condition $\mathbf{x}_0$ is a random variable uniformly distributed on the surface of a unit hyper-sphere. This approach was intended to provide a mathematical simplification, so it was only necessary to replace matrix $\mathbf{x}_0\mathbf{x}_0^\intercal$ by the identity matrix in the optimization problem (4.13).

Recently, some contributions to the OSOF control have been proposed in (CRUZ NETO; TRINDADE, 2019). Initially, aiming to apply the OSOF control to distributed parameter systems, sensors locations were included as optimization variables in order to improve the performance of the output feedback controller. Moreover, a new approach to deal with the dependence on system initial conditions was suggested. Since any output controller has a performance criterion below that of the full state feedback controller, it would be desirable that the values of the cost functions for both controllers would be as close as possible for any initial condition. Based on this statement, the optimization problem (4.13) was replaced by

$$\min_{(\mathbf{K},\boldsymbol{\alpha})} \max_{\mathbf{x}_0} \quad \frac{\mathbf{x}_0^\intercal \mathbf{P}_o(\mathbf{K},\boldsymbol{\alpha})\mathbf{x}_0}{\mathbf{x}_0^\intercal \mathbf{P}_l \mathbf{x}_0} \tag{4.16a}$$

$$\text{subject to} \quad \mathbf{A}_c^\intercal \mathbf{P}_o + \mathbf{P}_o \mathbf{A}_c + \mathbf{Q} + (\mathbf{K}\mathbf{C}(\boldsymbol{\alpha}))^\intercal \mathbf{R}\mathbf{K}\mathbf{C}(\boldsymbol{\alpha}) = \mathbf{0}, \tag{4.16b}$$

in which $\mathbf{x}_0^\intercal \mathbf{P}_o(\mathbf{K},\boldsymbol{\alpha})\mathbf{x}_0$ is the cost function of the output feedback controller, $\mathbf{x}_0^\intercal \mathbf{P}_l \mathbf{x}_0$ is the cost function of the LQR controller and $\boldsymbol{\alpha}$ represents sensors locations. Simply put, this optimization attempts to find an output feedback controller whose performance is as close as possible to the LQR controller for any initial condition. Given the weighting matrices $(\mathbf{Q},\mathbf{R})$, the matrix $\mathbf{P}_l$ is a constant, and can be calculated by solving the corresponding algebraic Riccati equation (ARE).

The proposed criterion is a ratio of the OSOF and LQR cost functions, and has the advantage of being independent of excitation and measurement locations. Moreover,

this ratio is always greater than or equal to one, since the cost function of the LQR is minimal for any initial condition, and it also can be interpreted as a metric that measures how close the performance of output feedback controller is to that of the state feedback controller.

The problem given in equation (4.16) requires more elaborated algorithms, since, a priori, it is necessary to solve two optimization problems. However, it was proved (CRUZ NETO, 2018) that the problem of determining the initial condition that maximizes the ratio given in (4.16a) has an analytical solution. The proof is similar to that of showing that natural frequencies are stationary points in Rayleigh's quotient (a reader familiar with Rayleigh's quotient will notice that both this quotient and the one given in equation (4.16a) are characterized by the ratio of two quadratic forms). The initial condition that maximizes this ratio is given by the largest eigenvalue (λ_m) of the following generalized eigenvalue problem:

$$\mathbf{P}_o\mathbf{v} = \lambda\mathbf{P}_l\mathbf{v}. \tag{4.17}$$

Using this result, the optimization (4.16) can be finally rewritten as

$$\min_{(\mathbf{K},\boldsymbol{\alpha})} \quad \lambda_m\left(\mathbf{P}_o(\mathbf{K},\boldsymbol{\alpha}),\mathbf{P}_l\right) \tag{4.18a}$$

$$\text{subject to} \quad \mathbf{A}_c^\intercal\mathbf{P}_o + \mathbf{P}_o\mathbf{A}_c + \mathbf{Q} + (\mathbf{KC}(\boldsymbol{\alpha}))^\intercal\mathbf{RKC}(\boldsymbol{\alpha}) = \mathbf{0}, \tag{4.18b}$$

A schematic representation of OSOF controller design using a generic optimization algorithm is depicted in Figure 22.

Some last remarks regarding the application of the OSOF formulation for the drill string problem are in order. Since the OSOF formulation is developed for linear systems, the linear closed-loop state matrix (4.10) and the output matrix (4.8) are used in optimization (4.18). As the linearized closed-loop matrix depends on the negative damping coefficient, the OSOF control design depends on the specified operating conditions (WOB and target velocity) and the properties of the bit-rock interaction. Therefore, due to the uncertainties involved in the process, a sensitivity analysis, which is carried out in chapter 6, is mandatory. Another important aspect to emphasize is that the system output matrix depends entirely on which sensors are available, so it is possible to use another matrix $\mathbf{C}$ while maintaining the OSOF formulation to design the control gains and sensors locations. For example, to design a PI controller based on the OSOF formulation, one should use the output matrix (4.6) and apply optimization (4.18) to determine only the control gains.

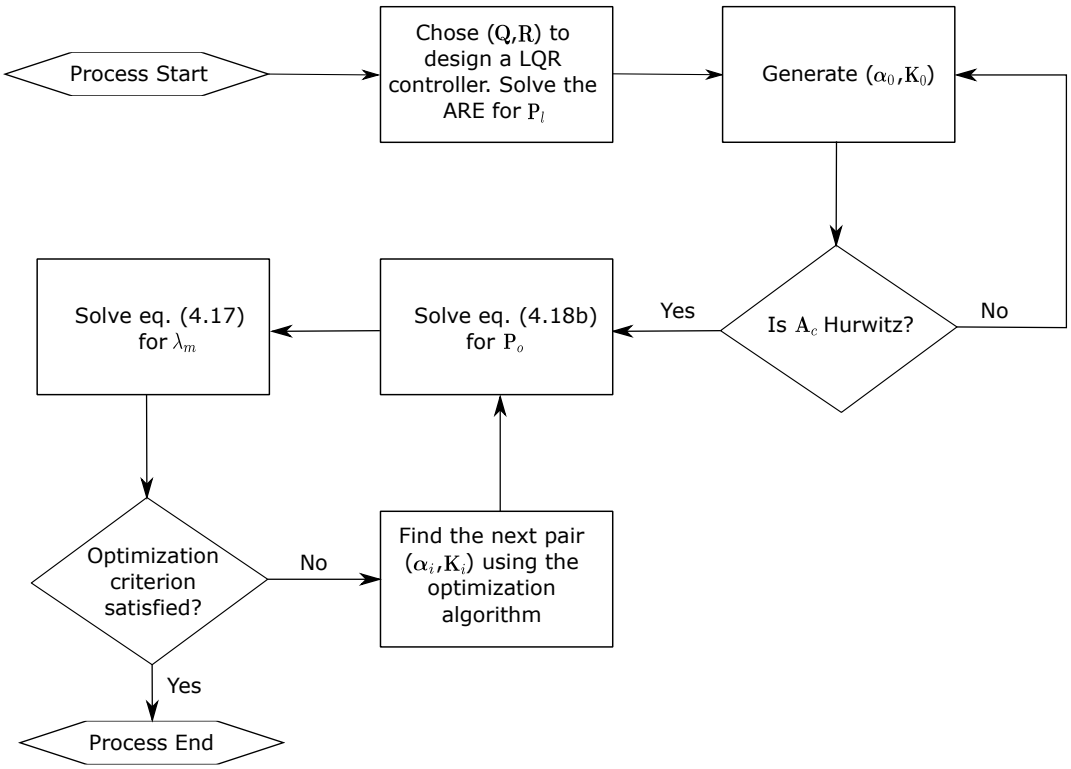

Figure 22 – Flowchart of the OSOF controller design.

4.3 Negative damping based controller (NDBC)

This section proposes a controller that aims to maximize the robustness of the closed-loop system. The underlying principle of the proposed control technique is the negative damping coefficient and its influence on the local stability of the drilling system. As discussed in section 3.1, the apparent negative damping effect resulting from the bit-rock interaction is the main factor causing instability of the operating point. Due to the dependence of the negative damping coefficient on the drilling parameters indicated in Eq. (3.4), a controller that guarantees stability for a wide range of values of this coefficient will consequently allow stable drilling for a wide range of operating conditions (WOB and target angular velocity) and uncertainties in the friction parameters. To enlarge the region of safe drilling as much as possible, the proposed control technique aims to maximize the range of values of the negative damping coefficient for which the operating point is asymptotically stable. This idea can be formalized in the following manner.

Suppose the parameters of the friction function (2.3) are unknown and let $n_d \in \mathbb{R}_-$ represent a possible value that the negative damping coefficient may assume. Thus, the linearized closed-loop state matrix (4.4) can be written as a function of the control gain $\mathbf{K}$ and n_d as

$$\mathbf{A}_{cl}(\mathbf{K}, n_d) = \mathbf{A}_l(n_d) - \mathbf{B}_{tn}\mathbf{K}\mathbf{C}. \tag{4.19}$$

Next, for a given $\mathbf{K}$, define Z as the set of values of n_d for which the spectral abscissa is positive

$$Z = \{n_d \in \mathbb{R}_- \,|\, \nu\left(\mathbf{A}_{cl}(\mathbf{K}, n_d)\right) > 0\} \tag{4.20}$$

and γ as the supremum of this set

$$\gamma = \sup\, Z. \tag{4.21}$$

Then, the control gain is given by the optimization

$$\min_{\mathbf{K}}\ \gamma, \tag{4.22}$$

which aims to find the controller that guarantees asymptotic stability for the largest possible connected set of values of the negative damping coefficient. To understand the motivation behind the optimization formulation and some nuances on the evaluation of the cost function, a few examples are examined.

Figure 23 depicts $\nu\left(\mathbf{A}_{cl}(\mathbf{K}, n_d)\right)$ as a function of n_d for three distinct control gains: $\mathbf{K}_1 = [15\ \ 180\ \ -280\ \ 520]$, $\mathbf{K}_2 = [45\ \ 70\ \ 1670\ \ -1180]$ and $\mathbf{K}_3 = [68\ \ 0\ \ 549\ \ 0]$. For the first control gain, $\nu\left(\mathbf{A}_{cl}(\mathbf{K}_1, n_d)\right)$ is positive for any value of the negative damping coefficient. Therefore, the set Z for the control gain $\mathbf{K}_1$ is simply $\mathbb{R}_-$, and its supremum assumes the largest possible value $\gamma = 0$, reflecting the worst scenario in which the operating point is unstable for any value of the negative damping coefficient. For the second control gain, $\nu\left(\mathbf{A}_{cl}(\mathbf{K}_2, n_d)\right)$ has a single zero at approximately $n_d = -407.1$, such that Z is the interval $(-\infty, -407.1)$ and its supremum is $\gamma = -407.1$. A different situation is observed for the third control gain, for which $\nu\left(\mathbf{A}_{cl}(\mathbf{K}_3, n_d)\right)$ has three zeros. For this control gain, Z is the union of intervals $(-\infty, -447.5) \cup (-436.7, -378.7)$, and its supremum is $\gamma = -378.7$. In this case, even though $n_d = -447.5$ is the lowest value for which the operating point is asymptotically stable, there are larger values of the negative damping coefficient – $n_d \in (-436.7, -378.7)$ – corresponding to an unstable operating point. This last example reveals the motivation of minimizing the supremum of Z, as the optimization goal is to find a controller that ensures asymptotic stability for all negative damping coefficient values in a specified range or, using the terms defined in the optimization, for all $n_d > \gamma$. Although situations where $\nu\left(\mathbf{A}_{cl}(\mathbf{K}, n_d)\right)$ has more than one zero were rarely observed for most of the control gains analyzed, they represent a scenario that may occur during the optimization, and highlight the importance of optimizing γ.

The examples discussed above also suggest a simple way of computing the cost function γ. Initially, to determine whether the control gain lies in a similar situation as $\mathbf{K}_1$,

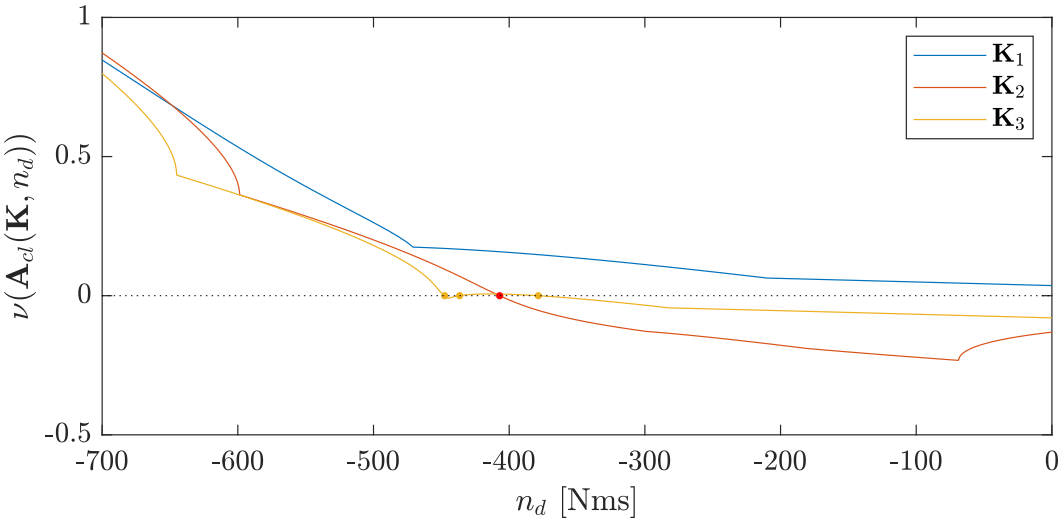

Figure 23 – Spectral abscissa of the linearized closed-loop state matrix as a function of the negative damping coefficient for three different control gains.

one only needs to check if $\nu\left(\mathbf{A}_{cl}(\mathbf{K}, 0)\right) > 0$. If this inequality holds, then $\gamma = 0$, otherwise γ is the largest value of n_d for which $\nu\left(\mathbf{A}_{cl}(\mathbf{K}, n_d)\right) = 0$, which can be determined using several different numerical methods for finding zeros of functions (STOER; BULIRSCH, 2002).

Another interesting remark about the proposed optimization concerns the relationship between the negative damping coefficient and the drilling parameters. Since the negative damping coefficient is a monotonic function of several drilling parameters (WOB, ω_r, a_2, a_1), optimization (4.22) together with Eq. (3.4) can be used to establish drilling parameters ranges for which the operating point is asymptotically stable. For example, assuming the other parameters are constant, the operating point is asymptotically stable for any target angular velocity greater than

$$\omega_r = \ln\left(\frac{\beta(a_1 - a_2)WOB}{\gamma}\right)^{\frac{1}{\beta}}, \tag{4.23}$$

provided $\omega_r > \delta$. Further relationships can be derived similarly for the other drilling parameters that are monotonic functions of the negative damping coefficient: WOB, a_2 and a_1.

Since some friction parameters may have an interdependence, another useful way to assess system robustness is through the highest combined admissible variation in drilling parameters relative to a nominal operating condition. For prescribed target angular velocity and WOB values, the latter associated with the friction parameters identified in Table 2, it is possible to compute a nominal value of the negative damping coefficient n_{d_0}. Given n_{d_0} and γ corresponding to a control gain $\mathbf{K}$, the largest admissible variation in the drilling parameters relative to a nominal operating condition can be expressed by the

ratio

$$\epsilon = \frac{\gamma}{n_{d_0}}. \tag{4.24}$$

As as example, consider the control gain $\mathbf{K}_2$ studied previously. Assume the selected operating condition consists of an WOB of 140 kN and a target angular velocity ω_r of 100 rpm. Using the corresponding friction parameters in Table 2, the negative damping coefficient associated with this condition is $n_{d_0} = -290.1$ Nms. Therefore, given that $\gamma = -407.1$ for $\mathbf{K}_2$, the substitution of both values in Eq. (4.24) gives $\epsilon = 1.40$. Thus, the closed-loop system with the control gain $\mathbf{K}_2$ tolerates changes in the drilling parameters that combined would allow a variation of 40% in the negative damping coefficient relative to the prescribed operating condition.

Another interpretation for optimization (4.22) is that it may be employed to establish limits for the robustness of a given controller. For example, suppose the controller selected for the drilling system is a PI-type. Then, if one succeeds in finding the global optimum (or at least a good approximation of it) of optimization (4.22) using the output matrix (4.6) of the PI controller, the result obtained for the cost function γ will establish the upper bound of the negative damping coefficient (maximum WOB values, minimum angular speed values, and so forth) for any PI-type controller. Therefore, the operating limits obtained using other control design strategies, for example SoftSpeed, or Stiff PI (KYLLINGSTAD, 2017), must always be lower than the limits obtained using optimization (4.22). It is important to emphasize that optimization (4.22) ensures only local asymptotic stability, such that the operating limits obtained refer to local robustness properties of the closed-loop system. Simulations performed in chapters 5 and 6 investigate to what extent the results obtained for the linear system can be expanded to the nonlinear system.

5 Numerical simulations for the controlled drill string - Deterministic model

In this chapter, the control techniques developed in chapter 4 are applied to the drill string model presented in chapter 2. The chapter starts by establishing the conditions considered in the simulations and the criteria for evaluating the controller's performance. The next two sections presents and discusses the numerical results for the NDBC and OSOF controllers, respectively.

5.1 Simulation conditions and performance criteria

Initially, it is important to restate some of the model properties to clarify the conditions considered in simulations. All geometric and physical properties of the drill string are constant, according to Table 1. Although the WOB value is considered constant throughout a simulation, different WOB values are analyzed to investigate the effectiveness of the controllers for distinct operating conditions. The values chosen for the WOB are 120 and 140 kN, which imply the use of the corresponding friction coefficients given in Table 2. The case with higher WOB (140 kN) presents a harsher environment (more prone to stick-slip oscillations), and was selected to examine the proposed methodology for a more challenging condition from a vibration control perspective. The target angular velocity, established as $\omega_r = 100$ rpm, corresponds to the operating condition identified in (TUCKER; WANG, 2003) and belongs to the typical range $85 \leq \omega_r \leq 135$ rpm of angular velocities for drilling systems (NAVARRO-LOPEZ; LICEAGA-CASTRO, 2009). Other operating conditions and variations in the drilling parameters are analyzed in chapter 6. Lastly, unless otherwise stated, it was considered as an initial condition the entire system rotating undeformed at a constant speed of 70 rpm, which is henceforth referred to as the standard initial condition. This initial condition emulates a severe drilling environment, and the purposes of adopting this condition are to obtain information about the stability of the operating point when the system response undergoes the stick phase and to assess the controller's performance in a harsh situation. The differential equations were integrated using the MATLAB® built-in integrator ode45.

The criteria adopted for assessing the controller's effectiveness comprise two factors: the time response (drill bit and rotary table velocities) and control effort. One of the metrics for evaluating the closed-loop response is the average deviation from the drill bit target angular velocity

$$J = \frac{1}{\Delta t} \int_0^{\Delta t} \frac{|\omega_b - \omega_r|}{\omega_r} \, \mathrm{d}t, \tag{5.1}$$

in which the timespan was set to $\Delta t = 100$ s. As this metric combines several characteristics of the system response, other specific criteria are also evaluated: the duration of the stick phase, and the drill bit angular velocity maximum overshoot and settling time (5% of the steady-state value) . The criterion adopted for evaluating the closed-loop system performance in terms of the control effort is the highest applied torque.

5.2 OSOF controller

The first step in designing the OSOF controller, heeding Figure 22, is to select weighting matrices $(\mathbf{Q}, \mathbf{R})$ that produce a LQR controller with reasonable compromise between performance and control effort. The matrix $\mathbf{Q}$ is chosen such that weighted inner product of the system state represents the system total energy augmented with a factor q_i that multiplies the error integral:

$$\mathbf{Q} = \begin{bmatrix} q_i & \mathbf{0} & \mathbf{0} \\ 0 & \bar{\mathbf{\Lambda}} & \mathbf{0} \\ 0 & \mathbf{0} & \mathbf{I} \end{bmatrix}. \tag{5.2}$$

The constant q_i affects the magnitude of the integral gain (gain associated with the error integral). For $q_i \approx 0$ (for $q_i = 0$ the ARE has no solution), the closed-loop system has no integral gain and the time response is benefited by the absence of overshoot. However, without integral gain there is a steady-state error in the presence of uncertainties, so the q_i value must be chosen to guarantee a compromise between performance and robustness. The value of $\mathbf{R}$ (which is a scalar for this problem) needs to be adjusted according to the actuator's limitation. In the present case, to make a comparison with a PI controller, the value of $\mathbf{R}$ was tuned to guarantee similar levels of control effort between the OSOF and PI controllers.

Having determined the weighting matrices, we proceed to the optimization defined in equation (4.18). This optimization is nonconvex and, although heuristic optimization methods are generally preferred in this occasion, the sequential quadratic programming (SQP) method was successfully applied in a previous work (CRUZ NETO; TRINDADE, 2019). For the problem at study in this thesis, the SQP algorithm with random initial guesses still provided good results with low computational effort. Therefore, the optimal gains and sensors locations were determined using the SQP algorithm with several initial guesses, and the best local optima were selected. The values of the parameters q_i, $\mathbf{R}$, the optimal control gains and the optimal second sensor location are summarized in Table 3. The units of each component of the control gain vector are Nm for K_1 and K_2, and Nms for

K_3 and K_4. The largest ratio between the cost functions of the OSOF and LQR controllers is also indicated in Table 3, and is expressed in percentage by $\lambda_m^* = (\lambda_m - 1) \times 100$.

Table 3 – OSOF control parameters.

WOB	Gain	Position	$\mathbf{R}$	q_i	λ_m^*
120 kN	$\mathbf{K} = [54.5 \quad -2113.4 \quad 829.7 \quad -44.1]$	$\alpha_2 = 0.1L$	0.0042	29	42.29%
140 kN	$\mathbf{K} = [32.6 \quad -1600.8 \quad 674.6 \quad 0.3]$	$\alpha_2 = 0.1L$	0.0131	41	86.80%

Some remarks can already be derived from the results presented in Table 3. Initially, it is noted that the second sensor optimal location was at the limit of the specified range for both WOB values. Since for small distances between the sensors the difference in velocities and displacements signals is reduced, the optimization attempts to keep the sensors as far apart as possible. This observation is also reflected in the magnitude of the control gains. As the difference between the displacements at the rotary table and at position $\alpha_2 = 0.1L$ is small, the optimization increases the magnitude of the control gain corresponding to this measurement (the second element of $\mathbf{K}$) to increase its influence on the system response, yielding the large control gains obtained for both WOB values. Figure 24 and Figure 25 illustrate this claim by comparing the feedback signal corresponding to the second control gain and the one corresponding to the third control gain. Note that the amplitude of the signal corresponding to the third control gain is around five times greater than that of the signal corresponding to the second control gain. The operating condition for these simulations is a WOB of 120 kN and a target angular velocity of 100 rpm, and the starting scenario is given by the standard initial condition.

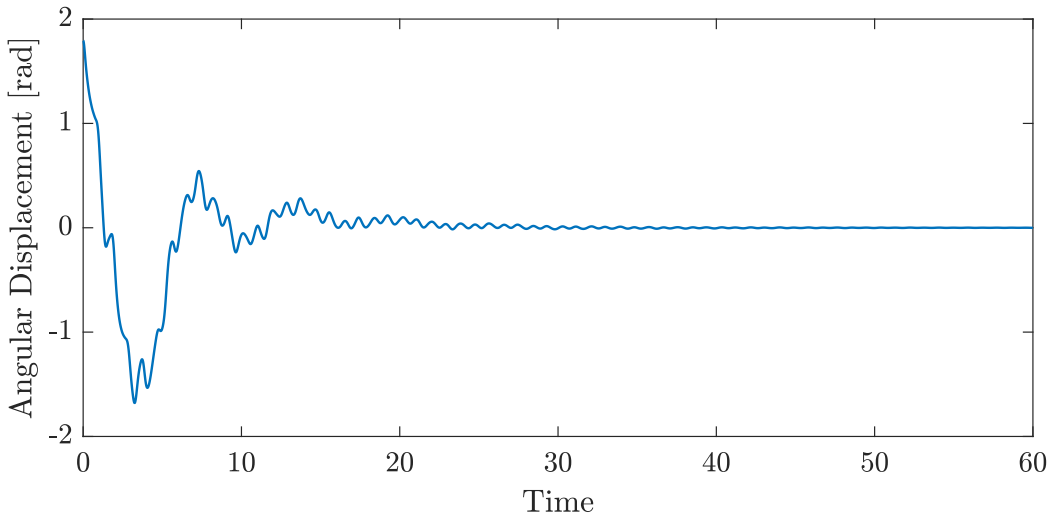

Figure 24 – Feedback signal associated with the second control gain.

Another aspect indicated in Table 3 is the difference in performance between the OSOF and the LQR in terms of the quadratic cost function (4.12), which is characterized by the variable λ_m^*. For instance, the λ_m^* value obtained for the OSOF controller

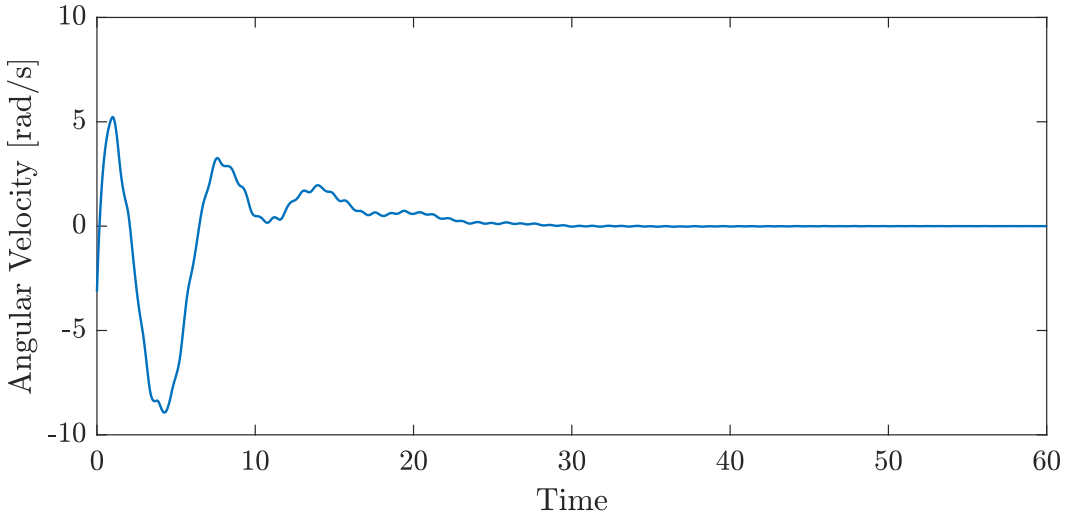

Figure 25 – Feedback signal associated with the third control gain.

corresponding to the WOB of 120 kN indicates that the difference between the cost functions of the OSOF and LQR considering a linear approximation at the operating point is 42.3% in the worst scenario (for the initial condition that maximizes the ratio between the cost functions of both controllers). The performance indexes obtained for both WOB values are well above the λ_m^* =4.05% obtained by (CRUZ NETO; TRINDADE, 2019), who also designed an OSOF with two sensors, but for a linear system without sensor placement constraints. An investigation at the end of this section without the placement restriction indicates that this is indeed the major factor explaining the higher difference in the cost functions of both controllers. Still, despite the higher λ_m value, an evaluation of the nonlinear system response shows a remarkable performance of the output feedback controller.

Figures 26-28 compare OSOF and LQR considering the drill bit and rotary table angular velocities and the applied control effort for the WOB of 120 kN. The first interesting aspect to be highlighted is the ability of both controllers, whose design relies on a linear approximation, to keep the operating point asymptotically stable despite the system's trajectory going far from the linearization point, even when the drill bit passes through the stick phase. In addition to providing stability, both controllers also achieved remarkable results in terms of performance, which will become apparent afterwards in a comparison with an optimized PI controller. In general, the LQR excelled in every criterion concerning the drill bit velocity, although the control effort to achieve this level of performance was much higher than that applied by the OSOF controller. Considering all performance criteria, the highest relative difference in favor of LQR was the stick time, which was 52% higher for the OSOF controller, while the maximum control effort applied by the LQR controller was 74% higher than that required by the OSOF. The performance metrics corresponding to these results are compiled in Table 4, together with the

other main results of this section. Overall, in view of the resembling shapes of the response curves with significantly less required torque, the OSOF formulation provided a controller with good trade-off between performance and control effort.

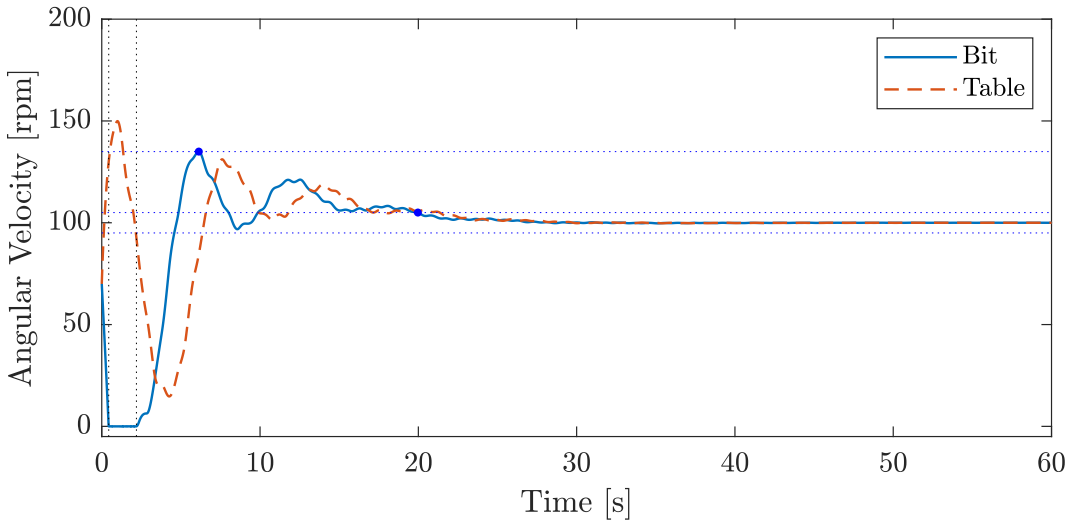

Figure 26 – Bit and rotary table velocities using OSOF controller with WOB = 120 kN.

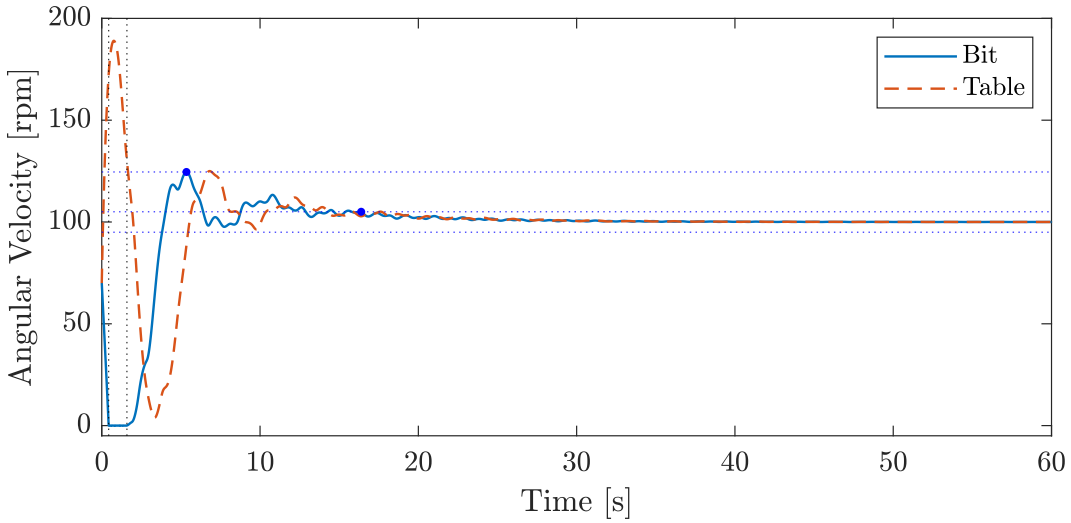

Figure 27 – Bit and rotary table velocities using LQR controller with WOB = 120 kN.

The time responses and control efforts for the WOB of 140 kN are depicted in figures 29-31. Results of the simulations and the performance metrics presented in Table 4 corroborate the experimental observations (BRETT, 1992) indicating that a higher WOB represents a more critical environment, and consequently more challenging from the vibration control standpoint. These results are also in agreement with the negative damping coefficient concept, since the coefficient associated with the 120 kN WOB, $n_d = -210.75$ Nms, is higher than that associated with the 140 kN WOB, $n_d = -290.08$ Nms. Similarly to the results obtained for the WOB of 120 kN, all results associated with the drill bit

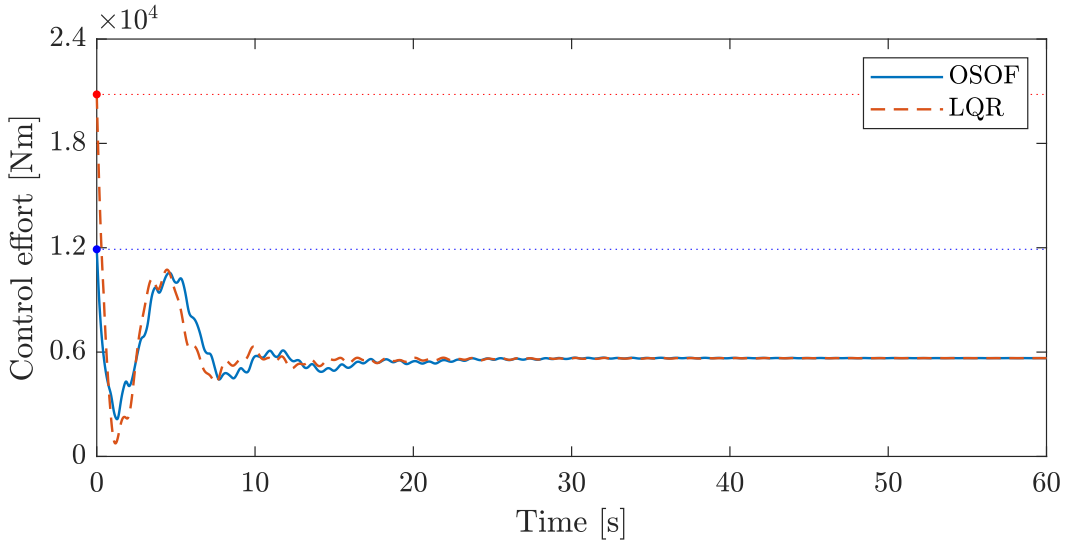

Figure 28 – Applied torque using OSOF and LQR controllers with WOB = 120 kN.

velocity response favored the LQR, while the difference in control effort for the 140 kN WOB was even higher than that obtained for the lower WOB. The highest relative difference in favor of LQR was once more the stick time, which was 64% higher for the OSOF controller, while the maximum control effort for the LQR controller was 93% higher than that applied by the OSOF controller. Therefore, although the OSOF controller was not able to reproduce the LQR, it still achieved a good trade-off between control effort and performance.

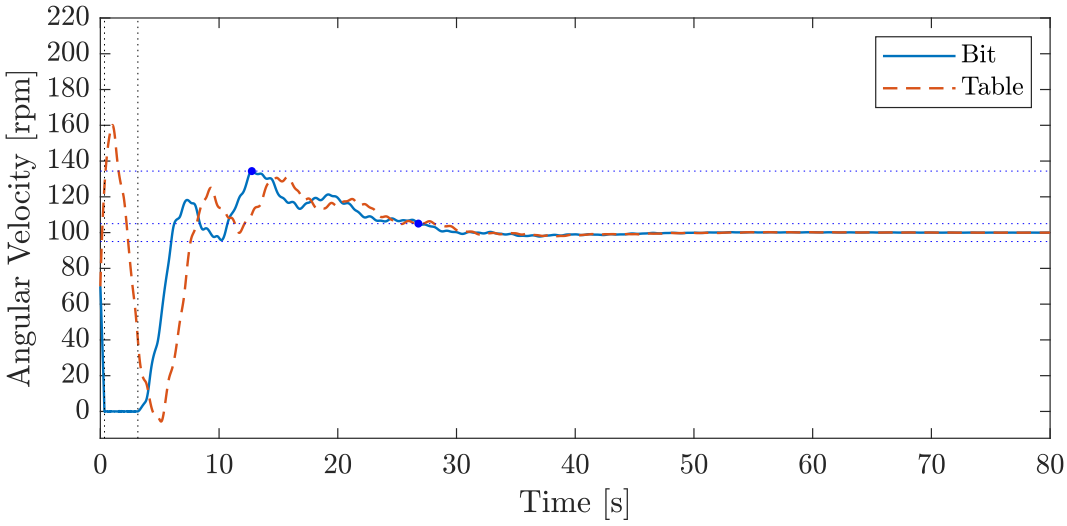

Figure 29 – Bit and rotary table velocities using OSOF controller with WOB = 140 kN.

Since the large number of sensors required by the LQR control makes its implementation unfeasible, the main objective of simulating the drill string with this controller is to provide a performance reference. To obtain more information on the effectiveness of the proposed control strategy, the OSOF control is compared to the PI control, a

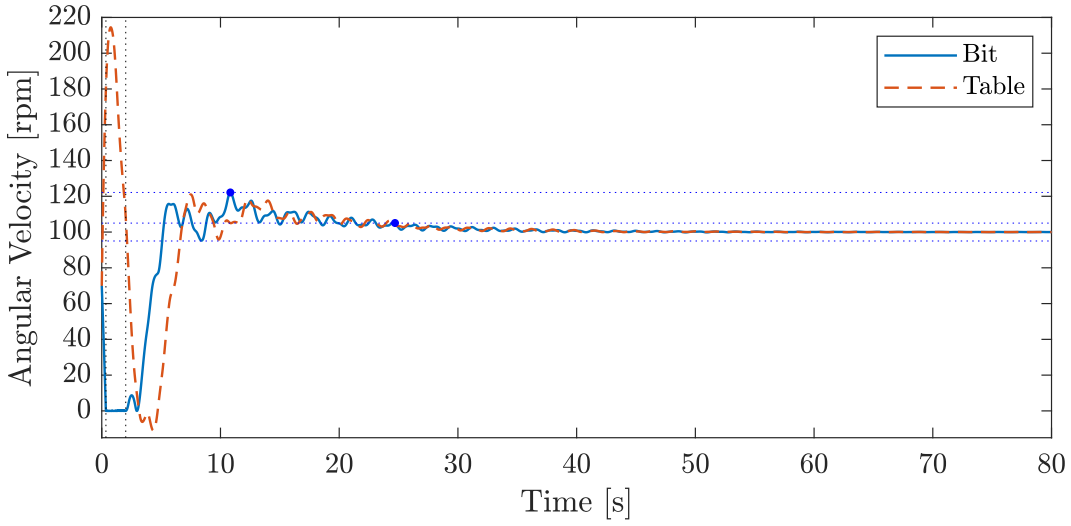

Figure 30 – Bit and rotary table velocities using LQR controller with WOB = 140 kN.

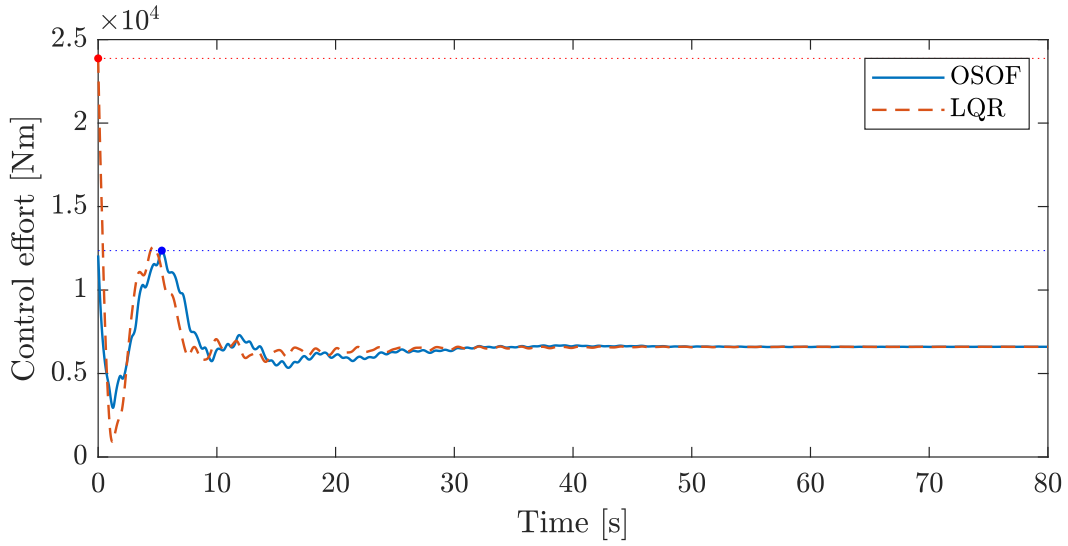

Figure 31 – Applied torque using OSOF and LQR controllers with WOB = 140 kN.

technique employed in several drilling rigs. A successful application of the PI control depends primarily on how the proportional (k_p) and integral (k_i) gains are determined. Many approaches can be used to determine the gains of a PI controller, such as tuning techniques based on time and frequency responses, fuzzy logic, subspace identification, and so forth (JOHNSON; MORADI, 2005). In this thesis, similar to the approach suggest by (MONTEIRO; TRINDADE, 2017), the PI control gains are taken as optimization variables that minimize the average deviation from the drill bit target angular velocity (5.1). Although the shape of this cost function apparently indicates a smooth behavior, a local analysis reveals several irregularities. Figure 32 shows the performance index as a function of k_i for a constant value of $k_p = 500$. The second graph is just a zoom-in of the first one to highlight the irregularities. Due to these discontinuities, classical optimization

algorithms struggled to find the optimal control gains, such that our choice was turned towards heuristic algorithms. An optimization using the particle swarm method yielded the control gains $(k_p, k_i) = (633.4,166.7)$ for the 120 kN WOB and $(k_p, k_i) = (640.7,158.7)$ for the 140 kN WOB.

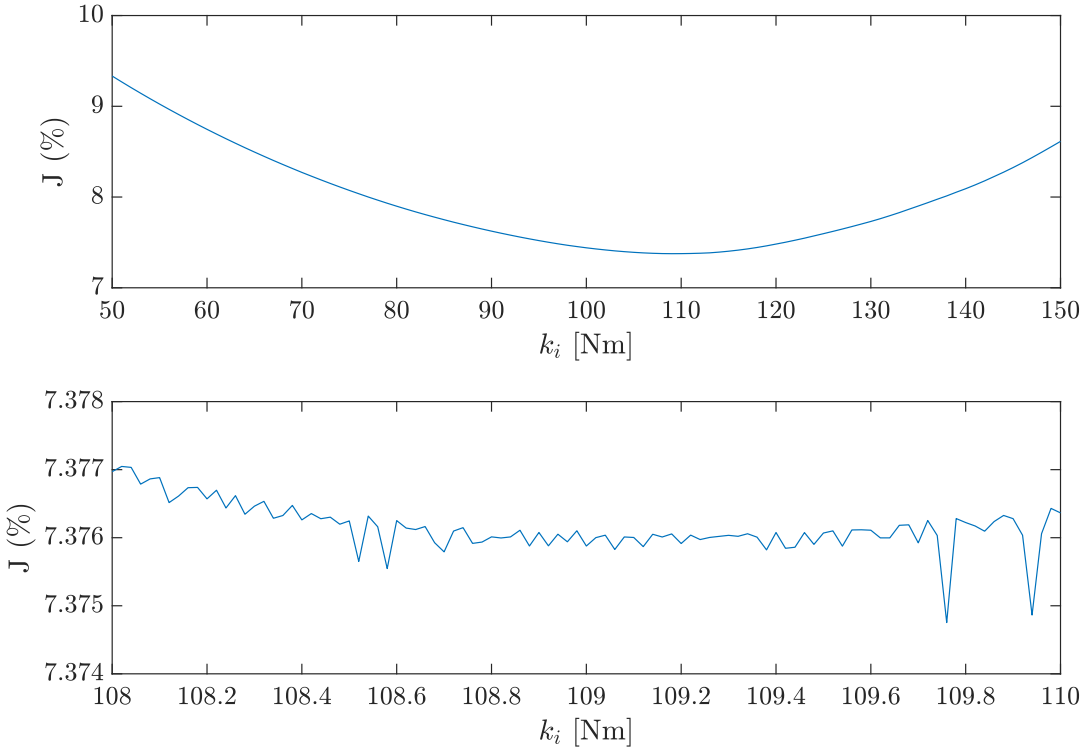

Figure 32 – Angular velocity average deviation J as a function of k_i for $k_p = 500$.

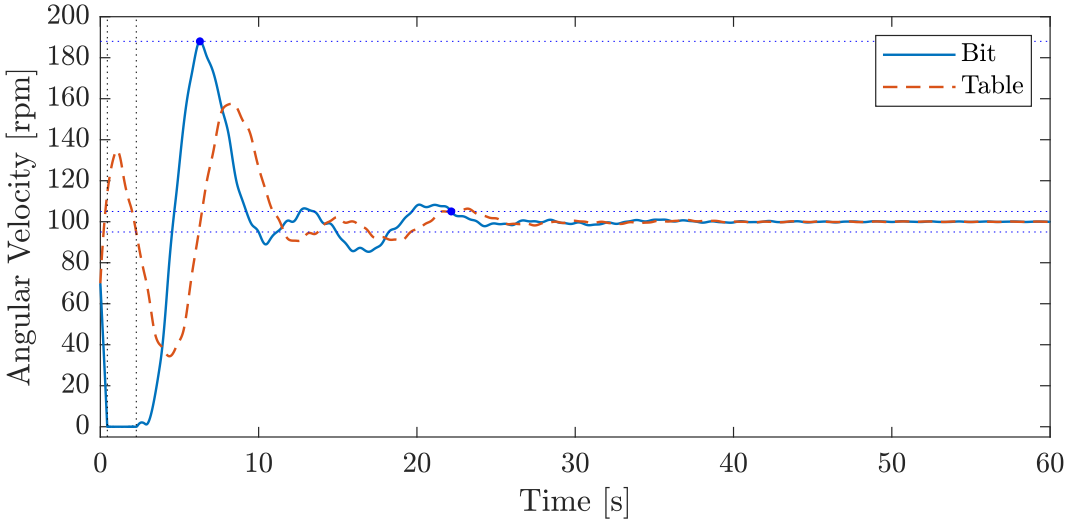

Figure 33 – Bit and rotary table velocities using PI controller with WOB = 120 kN.

Simulation results using the PI control gains found in the optimization are presented in Figures 33-36. The control effort displayed by the OSOF control was again superimposed on Figures 34 and 36 to elucidate the comparison. Analyses of the time

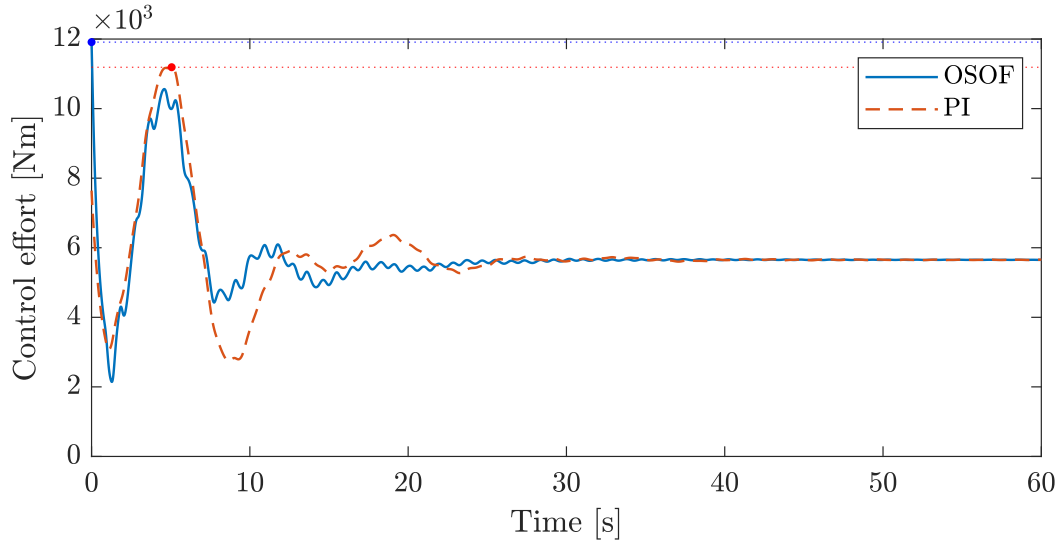

Figure 34 – Applied torque using OSOF and PI controllers with WOB = 120 kN.

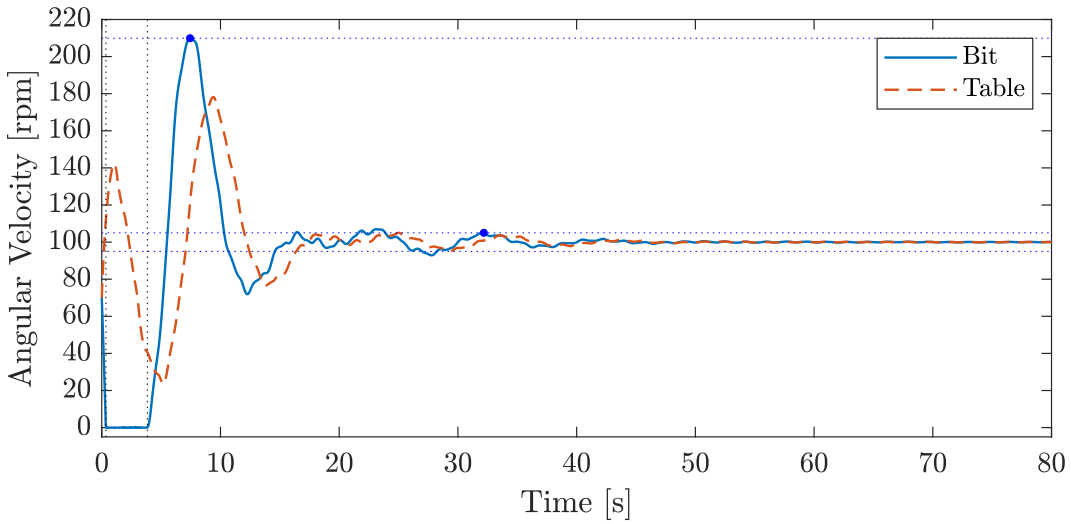

Figure 35 – Bit and rotary table velocities using PI controller with WOB = 140 kN.

responses with the OSOF and PI controls show an advantage in favor of the former for every aspect related to the drill bit response, especially the overshoot reduction. Considering the WOB of 120 kN, the PI controller overshoot was 152% higher, while for the 140 kN WOB the overshoot was 220% higher than the obtained for the OSOF. These results indicate a critical advantage for OSOF control, as higher variations in the angular velocity can favor fatigue and damage to drill string components. Another relevant aspect is that these favorable results were achieved without increasing the applied control effort, as the difference in the maximum applied torque between both controllers was always less than 9% (the OSOF maximum applied torque was even lower for the WOB of 140 kN). Lastly, the OSOF formulation provides another advantage in terms of computational effort. While the evaluation of the index J requires a simulation of the nonlinear and nonsmooth system, the determination of λ_m only requires the solution of an eigenvalue problem. To put

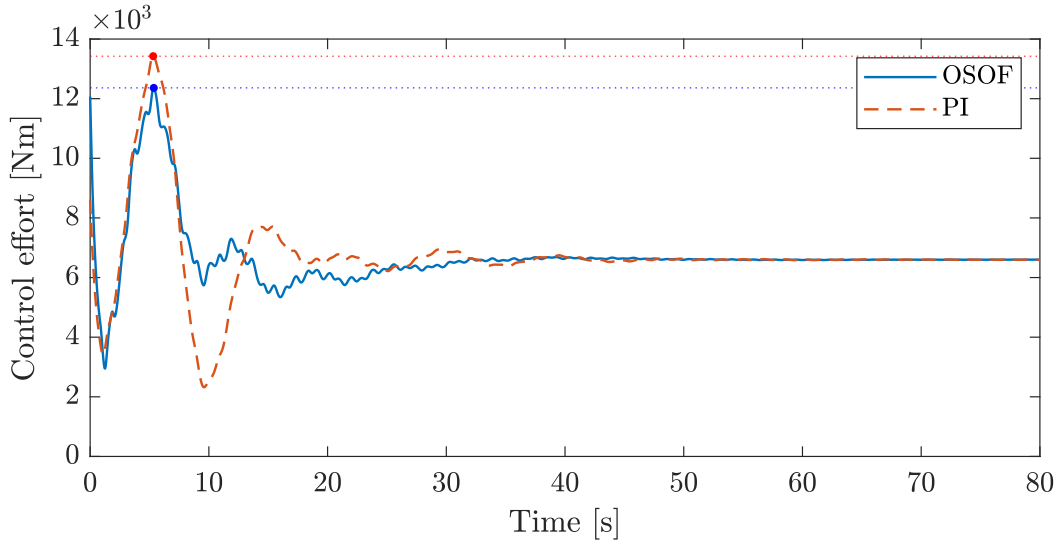

Figure 36 – Applied torque using OSOF and PI controllers with WOB = 140 kN.

into perspective, the entire process of finding an initial guess such that $\mathbf{A}_c$ is Hurwitz and optimizing for this guess takes in average half a second. Under the same hardware and software configurations, for some cases where stick-slip oscillations were observed, only the evaluation of J took around 15 seconds. If we take into account statistical analyses or optimizations, in which several simulations are required, these values may become major issues.

To summarize, the main results of this section are compiled in Table 4. To provide a better comparison of the results, the time responses considering only the drill bit angular velocity for each controller and for each WOB configuration are also depicted in Figures 37 and 38.

Table 4 – Main results for OSOF, LQR and PI controllers considering the standard initial condition.

WOB	120 kN			140 kN		
Controller	OSOF	LQR	PI	OSOF	LQR	PI
J (%)	5.58	4.11	7.16	8.06	5.74	9.49
Stick Time (s)	1.75	1.15	1.83	2.81	1.71	3.49
Settling Time (s)	19.96	16.39	22.17	26.79	24.71	32.17
Overshoot (%)	34.95	24.56	87.99	34.39	22.14	109.91
Max. Applied Torque (kNm)	11.91	20.82	11.19	12.36	23.87	13.43

As a final analysis for the nominal system, we removed the sensor placement constraint in the optimization to assess how much is possible to improve the controller performance. Additionally, instead of keeping the second sensor location as an optimization variable, its position was fixed at some locations along the drill string, and only the control gains were optimized. This analysis provides an overview of the approximation between

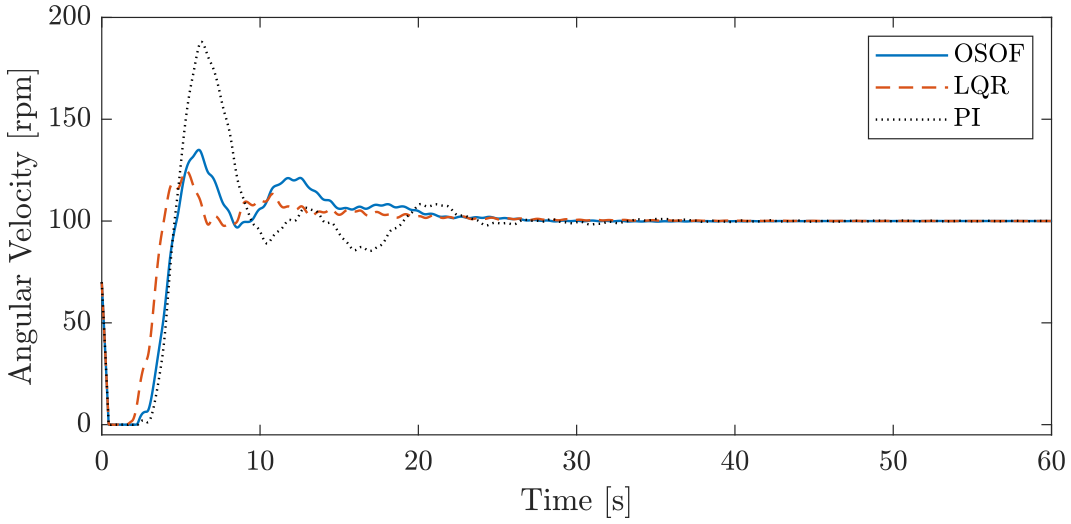

Figure 37 – Bit velocity for OSOF, LQR and PI controllers with WOB = 120 kN.

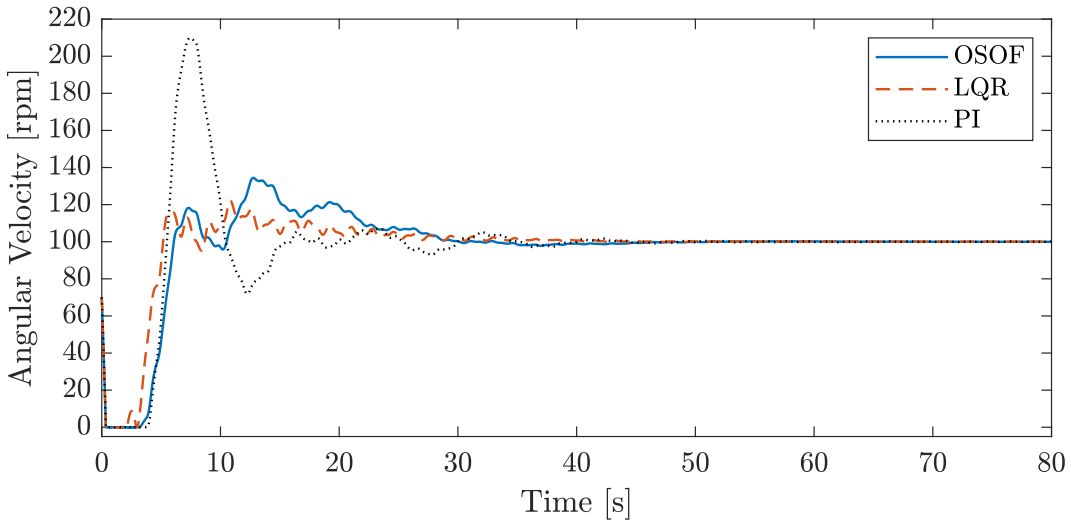

Figure 38 – Bit velocity for OSOF, LQR and PI controllers with WOB = 140 kN.

OSOF and LQR controllers as the position of the second sensor gradually increases. Since the performance improvement of the OSOF controller was negligible when limiting the control effort to comparable values as those employed using the PI controller, the weighting factors $\mathbf{R}$ and q_i were adjusted to allow higher limits for the applied torque. It is worth mentioning that as the J optimization did not consider any restriction on the control effort, it is not possible to improve the performance of the PI controllers obtained earlier, even when applying higher torque values. The optimal control gains corresponding to each location of the second sensor are given in Table 5 for the 120 kN WOB. Although the λ_m values obtained for the 140 kN WOB were higher, they displayed the same tendency observed in Table 5.

Table 5 already reveals some patterns in the variation of control gains. As the second sensor moves towards the drill bit, the magnitude of the signal related to the

Table 5 – Control gains and λ_m^* as a function of the second sensor location for the 120 kN WOB and weighting parameters $R = 0.0049$ and $q_i = 51$.

Position (m)	Gain	λ_m^* (%)
200	$\mathbf{K} = [64.9 \quad -2731.2 \quad 776.5 \quad -19.8]$	47.88
400	$\mathbf{K} = [63.0 \quad -1597.5 \quad 833.6 \quad -39.8]$	40.58
600	$\mathbf{K} = [62.2 \quad -1233.3 \quad 881.4 \quad -48.2]$	35.11
800	$\mathbf{K} = [62.9 \quad -1079.4 \quad 919.1 \quad -34.0]$	30.94
1000	$\mathbf{K} = [63.5 \quad -942.7 \quad 937.5 \quad -19.6]$	28.55
1200	$\mathbf{K} = [63.6 \quad -818.5 \quad 937.5 \quad -4.8]$	26.84
1400	$\mathbf{K} = [64.1 \quad -734.3 \quad 940.4 \quad 10.4]$	25.14
1600	$\mathbf{K} = [64.8 \quad -676.0 \quad 946.7 \quad 26.5]$	23.37
1800	$\mathbf{K} = [65.9 \quad -635.2 \quad 956.3 \quad 44.2]$	21.54
2000	$\mathbf{K} = [67.1 \quad -595.1 \quad 959.5 \quad 63.3]$	19.73
2200	$\mathbf{K} = [66.4 \quad -513.8 \quad 924.0 \quad 71.8]$	18.41
2400	$\mathbf{K} = [66.2 \quad -474.6 \quad 919.0 \quad 78.2]$	17.14
2600	$\mathbf{K} = [65.9 \quad -441.6 \quad 918.0 \quad 78.7]$	16.54
2800	$\mathbf{K} = [66.0 \quad -418.2 \quad 926.5 \quad 76.6]$	16.66
2900	$\mathbf{K} = [69.4 \quad -432.9 \quad 955.6 \quad 89.4]$	16.09
2925	$\mathbf{K} = [73.3 \quad -450.8 \quad 969.5 \quad 107.9]$	15.30
2950	$\mathbf{K} = [85.4 \quad -444.9 \quad 942.0 \quad 149.9]$	14.02
2975	$\mathbf{K} = [96.0 \quad -410.0 \quad 846.3 \quad 265.1]$	10.51
3000	$\mathbf{K} = [112.2 \quad -413.9 \quad 886.9 \quad 312.0]$	10.13

angular displacement difference increases, consequently reducing the need to have a high control gain associated with this measure. The control gains corresponding to the integral action and the angular speed measured by the second sensor also increase when the second sensor moves away from the rotary table, predominantly in the 100 meters nearby the drill bit. Still, all integral gain values for the OSOF control are below those obtained for the PI controllers, explaining why the overshoots observed with the latter were higher.

Figures 39 and 40 compare the OSOF controller with the second sensor at the drill bit and the LQR. Note that, although $\lambda_m^* = 10.13$ represents an approximation involving the linearized system, simulations of the nonlinear system show very similar response curves for both controllers. Considering the performance metrics related to the drill bit response, the highest relative difference between both controllers was the stick phase duration, which was 29% higher for the OSOF controller, while the difference for all other criteria was below 12%. The average deviation from the drill bit target angular velocity bit was also very similar for both controllers: 4.06% for the LQR and 4.25% for the OSOF. These results corroborate the findings in (CRUZ NETO; TRINDADE, 2019) for linear systems that it is possible to reproduce an LQR controller with a very reduced number of sensors using OSOF formulation, especially when there are no sensor placement constraints. When this limitation is present, the proximity between the OSOF and LQR controls decreases, but it is still possible to obtain a controller with good trade-

off between performance and control effort. An investigation into the robustness of the OSOF controllers is conducted in chapter 6.

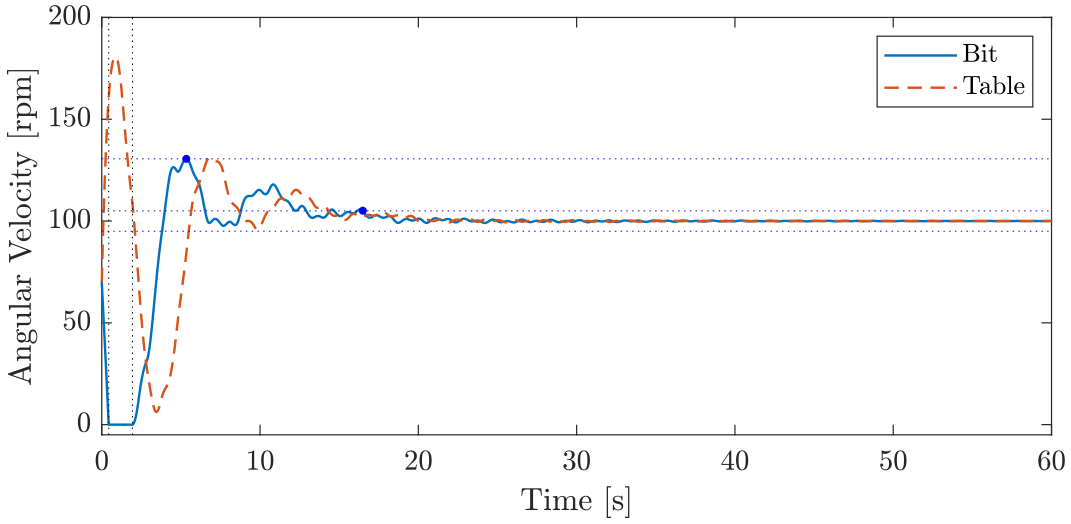

Figure 39 – Bit and rotary table velocities using OSOF with the second sensor at the drill bit.

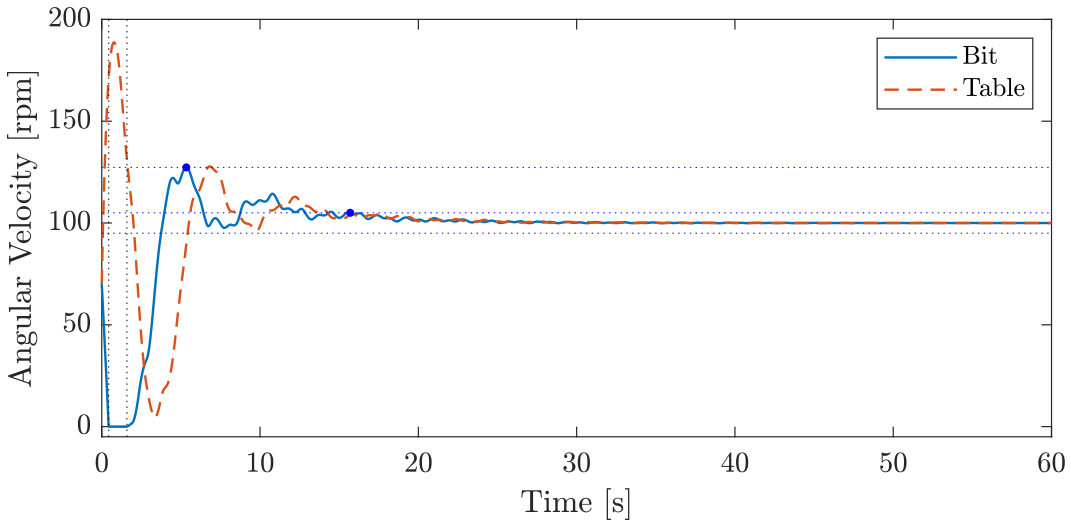

Figure 40 – Bit and rotary table velocities using LQR with $R = 0.0049$ and $q_i = 51$.

5.3 NDBC

The effectiveness of the NDBC strategy proposed in section 4.3 is examined in this section by applying it to the model developed in chapter 2. As thi methodology focuses on assuring asymptotic stability for the widest range of operating conditions, it is not necessary to specify the WOB or the target angular velocity, but only a linear state space model of the drill string itself and eventual dissipation sources that are not related to the negative damping coefficient (e.g., viscous damping). Using the results obtained

in section 5.2, the position of the second sensor was fixed at the limit of the specified range, $\alpha_2 = 0.1$L. Although the optimization for the determination of the control gain (4.22) is nonconvex and heuristic optimization methods are generally preferred in this occasion, the sequential quadratic programming (SQP) yielded satisfactory results. This method was applied for several initial guesses, and the best local optimum found was $\mathbf{K} = [0 \ \ -1976.3 \ \ 978.0 \ \ -92.4]$, corresponding to the cost function $\gamma = -544.25$ Nms. To understand what this γ value represents in terms of the closed-loop system robustness, the values of ϵ (4.24) were computed for each WOB considering the target velocity of 100 rpm. The negative damping coefficient associated with the lower WOB value (120 kN) is $n_{d_0} = -210.75$ Nms, which gives the ratio $\epsilon = 2.58$. Similarly, the negative damping coefficient corresponding to the 140 kN WOB is $n_{d_0} = -290.07$ Nms, which replacing in equation (4.24) gives $\epsilon = 1.88$. Therefore, the largest combined variation in the drilling parameters that the closed-loop system tolerates while still ensuring asymptotic stability is 158% for the lower WOB and 88% for the higher WOB.

Another important aspect of the optimal control gain is that its first component is null, meaning that the controller that ensures asymptotic stability for the widest possible range of values of n_d has no integral action. However, due to the uncertainties involved in the drilling process, a controller without integral gain would definitely generate a steady-state error. Thus, to understand the effects of the integral gain on stability and aiming to implement a controller with non-zero integral action, the influence of the integral gain on γ was analyzed by varying the first component of $\mathbf{K}$ while keeping the remaining control gains constant. The result of this analysis is indicated in Figure 41. These results attests that γ assumes the lowest possible value for $k_i = 0$, and indicates that the closed-loop system robustness decreases monotonically as k_i increases. Therefore, considering only the steady-state error and robustness, a sensible decision would be to select the smallest possible value of $k_i > 0$. However, the integral gain also plays a role in settling time, overshoot and stick phase duration.

To illustrate the influence of the integral gain on these aspects, simulations were performed using two values of this control gain: $k_i = 10$ and $k_i = 50$. The selected operating condition was a WOB of 160 kN and a target velocity of 100 rpm, and the starting scenario was represented by the standard initial condition. Figures 42 and 43 depict the bit and rotary table velocities for the two distinct values of the integral gain. The stick time duration corresponding to $k_i = 50$ is 8.62 s, whereas for $k_i = 10$ this interval is 19.75 s, more than twice that obtained for the higher control gain. The settling time also indicates a remarkable advantage for the higher integral gain: 30.24 s for $k_i = 50$ and 109.36 s for $k_i = 10$. The only aspect in favor of the lower integral gain is the overshoot, which reached 93.37% for $k_i = 10$ and 118.71% for $k_i = 50$. These general characteristics of the response are reflected by the J index, which is 18.15% for the higher integral gain and 40.36% for the lower integral gain. Therefore, to achieve a trade-off between these

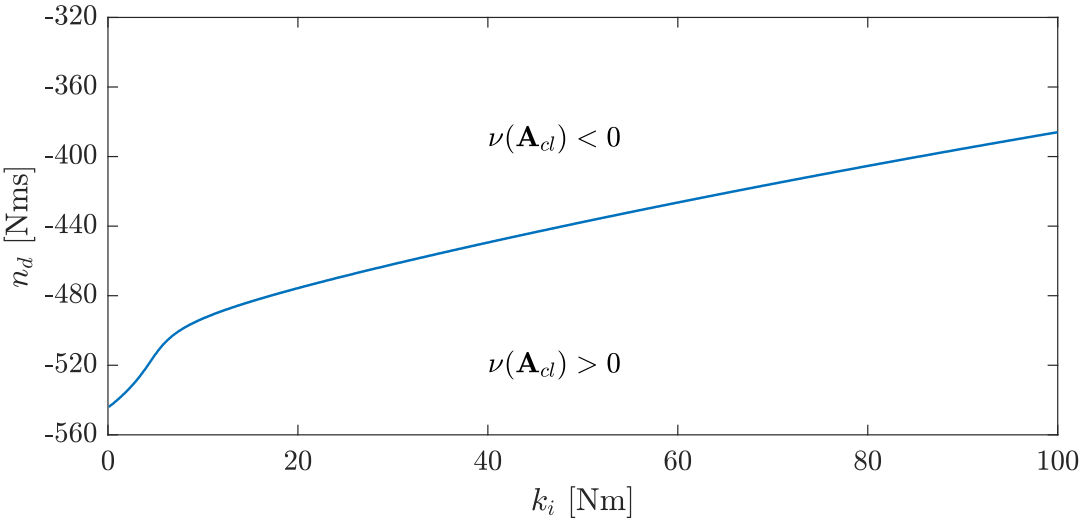

Figure 41 – Influence of the integral gain on γ.

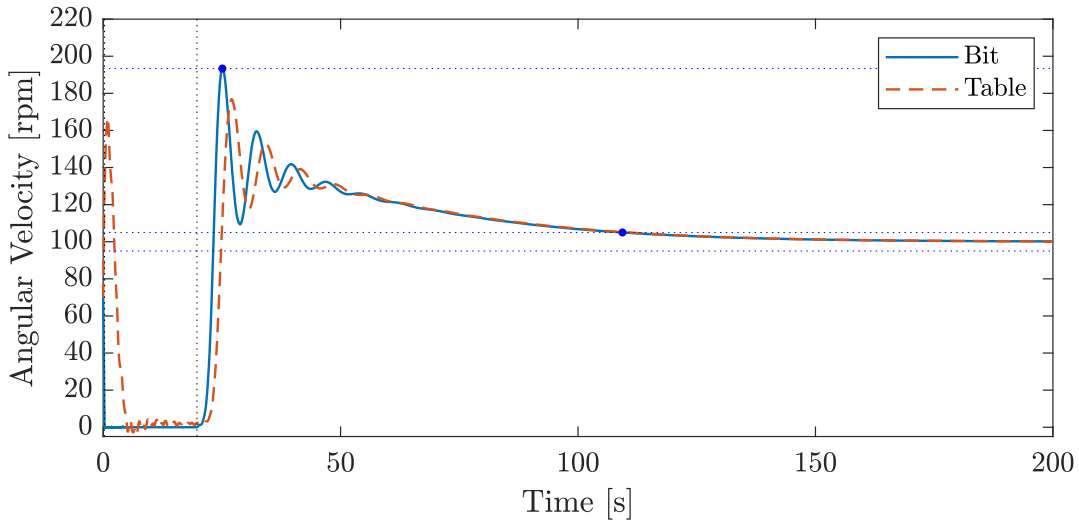

Figure 42 – Bit and rotary table velocities for $k_i = 10$ and WOB = 160 kN.

aspects, the integral gain for each WOB (120 and 140 kN) was determined in order to optimize the average deviation from the drill bit target angular velocity. The integral gains obtained via this optimization were $k_i = 75.8$ for the 120 kN WOB and $k_i = 48.7$ for the 140 kN WOB.

Although the control strategy developed provides maximum robustness for the closed-loop system regarding the negative damping coefficient, it gives no information about the nominal performance and applied control effort. To investigate how the proposed controller would perform in a nominal operating condition, its response is compared to that of the PI controllers obtained in section 5.2. Figures 44-47 depict the drill bit and rotary table velocities, in addition to the control effort applied by the NDBC and PI controllers for both WOB values. The main results concerning the performance metrics are grouped in Table 6. Despite not taking into account any aspect related to performance

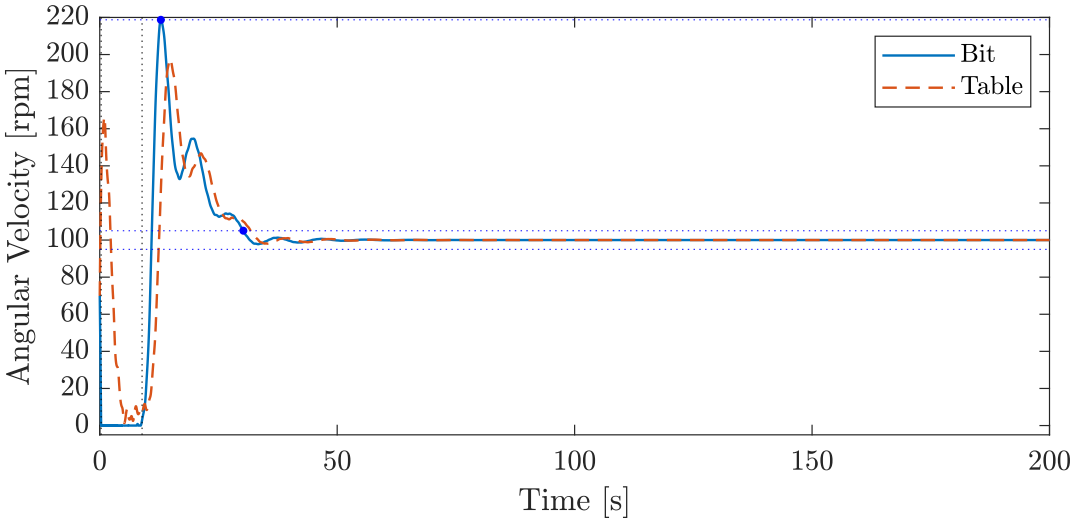

Figure 43 – Bit and rotary table velocities for $k_i = 50$ and WOB = 160 kN.

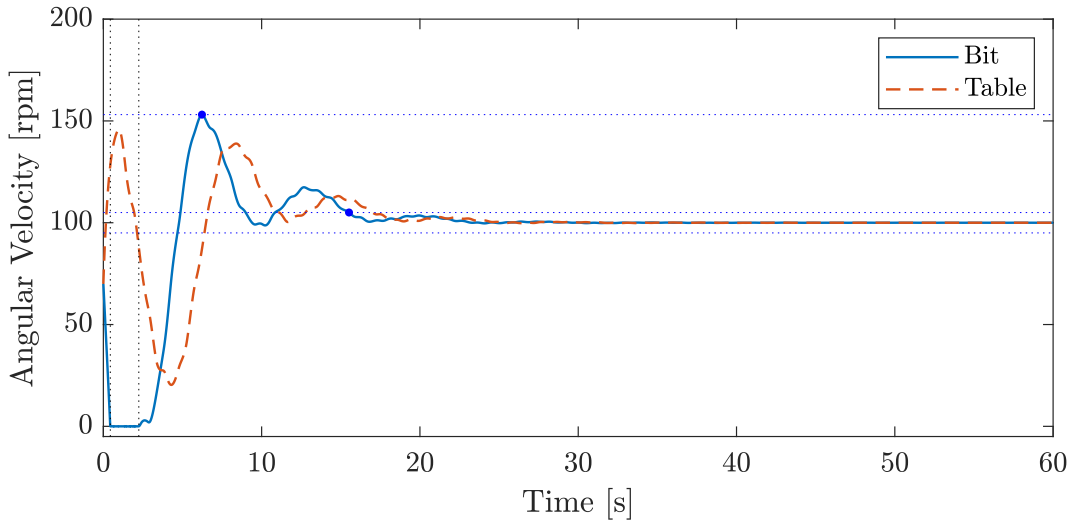

Figure 44 – Bit and rotary table velocities using NDBC with WOB = 120 kN.

or control effort (apart from k_i whose value is determined through an optimization of J), the NDBC had better results for every aspect related to the drill bit response, especially the overshoot reduction. Considering the WOB of 120 kN, the PI controller overshoot was 65.71% higher, while for the 140 kN WOB the overshoot was 78.74% higher than that obtained for the NDBC. These favorable results were achieved without significantly increasing the applied control effort, as the difference in the maximum applied torque between both controllers was always less than 8%. In addition to the satisfactory nominal results, the NDBC guarantees remarkably larger stability margins. The γ values corresponding to the PI controllers are $\gamma = -325.98$ Nms for the 120 kN WOB and $\gamma = -330.23$ Nms for the 140 kN WOB, whereas the values for the NDBC controllers are $\gamma = -409.56$ Nms and $\gamma = -439.02$ Nms for the lower and higher WOBs, respectively.

These results reveal a surprising feature of the proposed control strategy, since

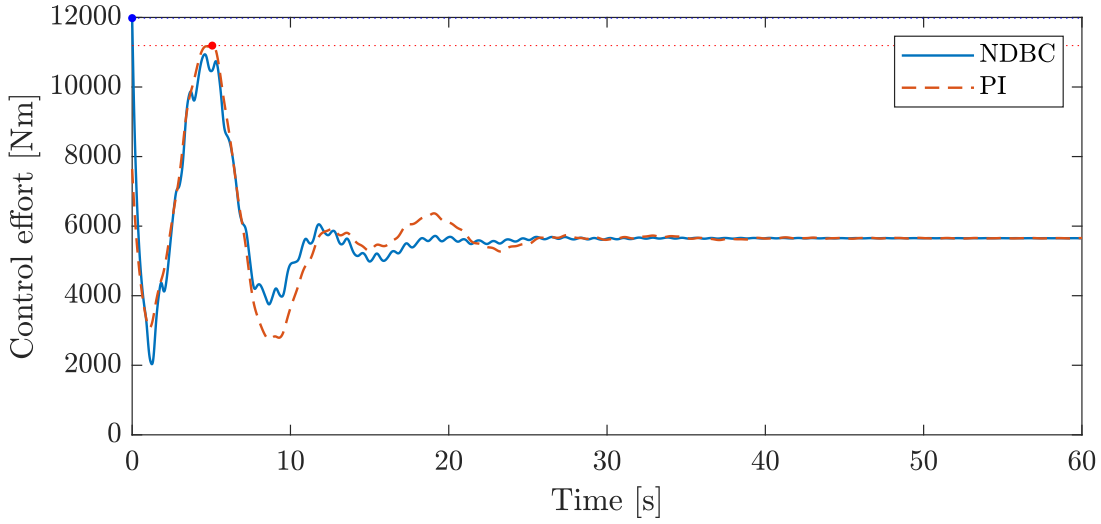

Figure 45 – Applied torque using NDBC and PI controllers with WOB = 120 kN.

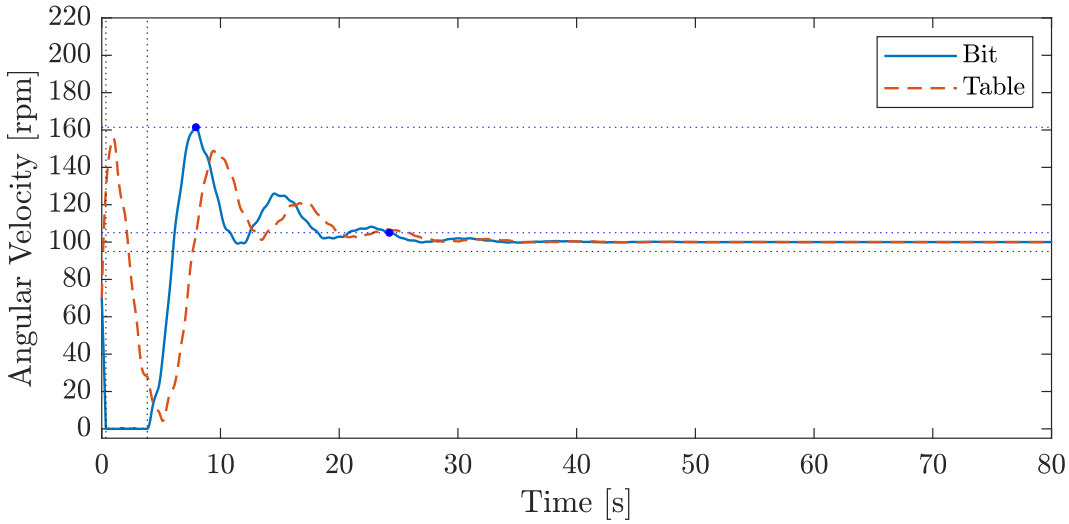

Figure 46 – Bit and rotary table velocities using NDBC with WOB = 140 kN.

the controller that guarantees maximum robustness in relation to the negative damping coefficient also provides a good trade-off between control effort and performance. As there are no performance specifications in the controller design, there is no theoretical assurance that equivalent results can be obtained for drill strings with different parameters or bit-rock interactions with distinct properties. Nonetheless, the good results obtained for both WOB configurations (different WOB, a_1, a_2 and β values) show potential for replicability, and motivate further investigations of the proposed control strategy for drilling systems with different parameters.

To access how much it is possible to improve the robustness of the controller and what is the influence of the position of the second sensor in this regard, the placement constraint was removed, and optimization (4.22) was carried out for fixed positions of the second sensor at some locations along the drill string. The optimal control gains associated

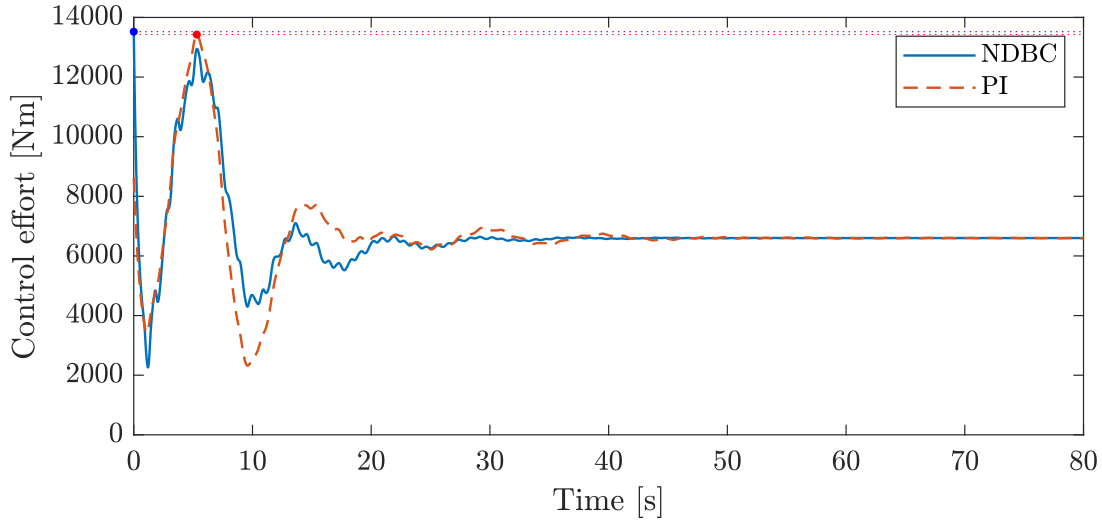

Figure 47 – Applied torque using NDBC and PI controllers with WOB = 140 kN.

Table 6 – Main results for NDBC and PI controllers considering the standard initial condition.

WOB	120 kN		140 kN	
Controller	NDBC	PI	NDBC	PI
J (%)	5.86	7.16	8.22	9.49
Stick Time (s)	1.78	1.83	3.15	3.49
Settling Time (s)	15.52	22.17	24.22	32.17
Overshoot (%)	53.10	87.99	61.49	109.91
Max. Applied Torque (kNm)	11.98	11.19	13.52	13.43

with each location of the second sensor and the corresponding γ values are presented in Table 7. To provide an idea of the relationship between the γ values obtained and the nominal operating conditions, the ϵ values associated with the 120 and 140 WOBs are also given in Table 7.

Unlike the results obtained for λ_m with the OSOF controller, γ does not show a monotonic dependence on the position of the second sensor. Although this dependence may indeed be non-monotonic, it may also be a consequence of the several local optima encountered during the optimization and the inability of the optimization algorithm to find the global optimum (results obtained with SQP were better than those obtained with the MATLAB built-in functions for the genetic algorithm, particle swarm and pattern search methods using default parameters). Nevertheless, the optimization conditions for each position of the second sensor were the same (SQP algorithm with random initial guesses), and they reveal an interesting pattern for γ. In the first 100 meters near the rotary table, there is a significant improvement in robustness in moving the second sensor from 50 to 100 meters, which is approximately 30% taking the 120 kN WOB as a reference (ϵ_{120}). In the next 300 meters (up to 400 m from the rotary table), there is still a small robustness

Table 7 – Control gains, γ and ϵ as a function of the second sensor location.

Position (m)	Gain	γ (Nms)	ϵ_{120}	ϵ_{140}
50	$\mathbf{K} = [0 \quad -2274.6 \quad 2818.0 \quad -2295.7]$	-466.56	2.21	1.61
100	$\mathbf{K} = [0 \quad -2760.4 \quad 2183.6 \quad -1499.4]$	-530.01	2.51	1.83
200	$\mathbf{K} = [0 \quad -1563.1 \quad 1895.2 \quad -1182.5]$	-535.60	2.54	1.85
300	$\mathbf{K} = [0 \quad -1976.3 \quad 978.0 \quad -92.4]$	-544.25	2.58	1.88
400	$\mathbf{K} = [0 \quad -1834.1 \quad 673.8 \quad 292.2]$	-543.99	2.58	1.88
600	$\mathbf{K} = [0 \quad -1142.0 \quad 719.6 \quad 229.2]$	-550.29	2.61	1.90
800	$\mathbf{K} = [0 \quad -1086.3 \quad 823.1 \quad 237.4]$	-552.66	2.62	1.91
1000	$\mathbf{K} = [0 \quad -767.4 \quad 875.8 \quad 117.4]$	-548.35	2.60	1.89
1200	$\mathbf{K} = [0 \quad -716.1 \quad 884.3 \quad 167.9]$	-551.37	2.62	1.90
1400	$\mathbf{K} = [0 \quad -481.4 \quad 848.5 \quad 94.1]$	-550.42	2.61	1.90
1600	$\mathbf{K} = [0 \quad -604.5 \quad 928.7 \quad 190.4]$	-549.26	2.61	1.89
1800	$\mathbf{K} = [0 \quad -613.6 \quad 982.4 \quad 211.4]$	-550.72	2.61	1.90
2000	$\mathbf{K} = [0 \quad -565.2 \quad 1000.7 \quad 217.1]$	-554.78	2.63	1.91
2200	$\mathbf{K} = [0 \quad -406.0 \quad 900.0 \quad 178.3]$	-554.64	2.63	1.91
2400	$\mathbf{K} = [0 \quad -585.0 \quad 1036.5 \quad 355.6]$	-560.33	2.66	1.93
2600	$\mathbf{K} = [0 \quad -580.4 \quad 999.1 \quad 540.8]$	-593.37	2.82	2.05
2800	$\mathbf{K} = [0 \quad -777.3 \quad 1132.3 \quad 886.6]$	-611.61	2.90	2.11
2900	$\mathbf{K} = [0 \quad -1356.5 \quad 1453.7 \quad 2071.1]$	-683.22	3.24	2.36
3000	$\mathbf{K} = [0 \quad -1457.1 \quad 1553.2 \quad 2585.6]$	-736.28	3.49	2.54

improvement of nearly 7% considering ϵ_{120}. However, from 600 to 2400 meters there is a gain of only 5% considering ϵ_{120}. Depending on the drilling rig, this small improvement may not be enough to justify the technology required to position the second sensor this far from the rotary table and transmit data in real time. On the other hand, in the 400 meters close to the drill bit, there is again a pronounced improved in robustness, with the closed-loop system tolerating a variation of the drilling parameters of 182% when the second sensor is at $\alpha_2 = 2600$ m and 249% when it is placed at the drill bit (taking the 120 kN WOB as a reference). Even when considering the largest WOB value in Table 2 as a reference (160 kN), the closed-loop system still ensures asymptotic stability for a variation of 104% in the drilling parameters. Therefore, taking into account only the robustness aspect, placing a sensor at the drill bit drastically improves drilling safety. However, the high values of the control gains suggest that the control effort in this case can be much higher and, as the integral gain in this case is null, the γ value for a controller with integral action should be smaller.

To illustrate the above statements, the closed-loop system using the controller with the second sensor at the drill bit was simulated for the WOB of 140 kN using an integral gain $k_i = 100$ Nm, which has a corresponding γ value of -663.64 Nms. Figures 48 and 49 show the time response and control effort for this controller. There are some remarkable results regarding the drill bit response: the stick phase duration is 0.82 seconds and the drill bit target velocity average deviation is 4.97% (even better than those obtained with

the LQR controller). However, the maximum applied control effort is the highest obtained so far, 50.10 kN, and the rotary table speed becomes negative and reaches almost -90 rpm. These observed phenomena represent a potentially hazardous situation, and may lead to damage to the motor and drill string components. Thus, although the model predicts asymptotic stability for large variations of parameters, simulations indicate the occurrence of some events that are perhaps not feasible in real drilling rigs, consequently reducing the estimates provided by the model. If there is the possibility of placing a sensor at the drill bit, an alternative for employing the NDBC could be to impose limits on the possible values of the control gains. Although this approach may reduce the required control effort, it will also reduce the stability margins, so further analyses are required to weigh the real benefits and costs of this scheme. Therefore, considering all results shown in this section, positioning the second sensor at 10% of the total drill string length seems to be a great practical solution.

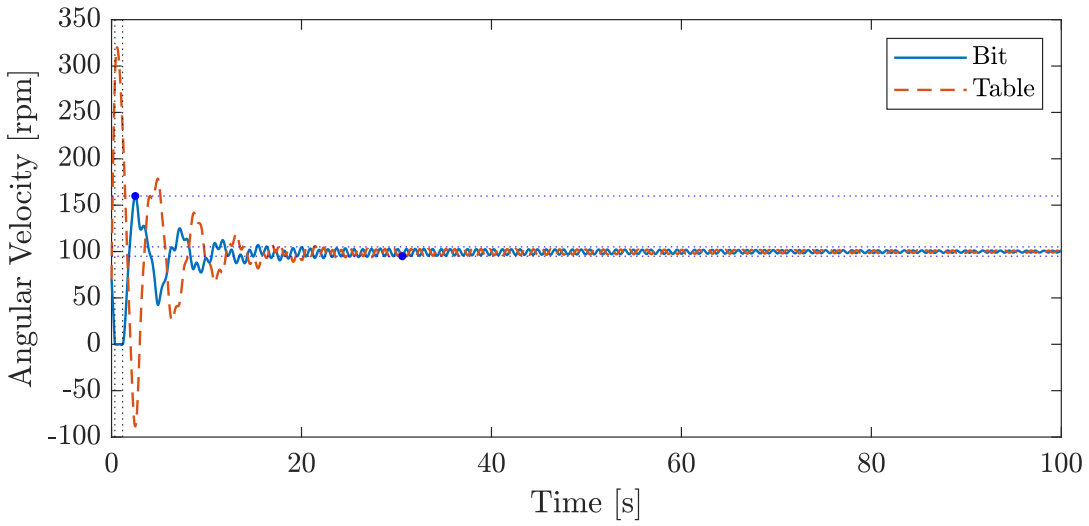

Figure 48 – Bit and rotary table velocities using NDBC with the second sensor at the drill bit for WOB = 140 kN.

A final comparison between NDBC, OSOF and PI controllers is presented in Figures 50 and 51, which contrast the drill bit velocity for all three controllers considering the 120 and 140 kN WOBs.

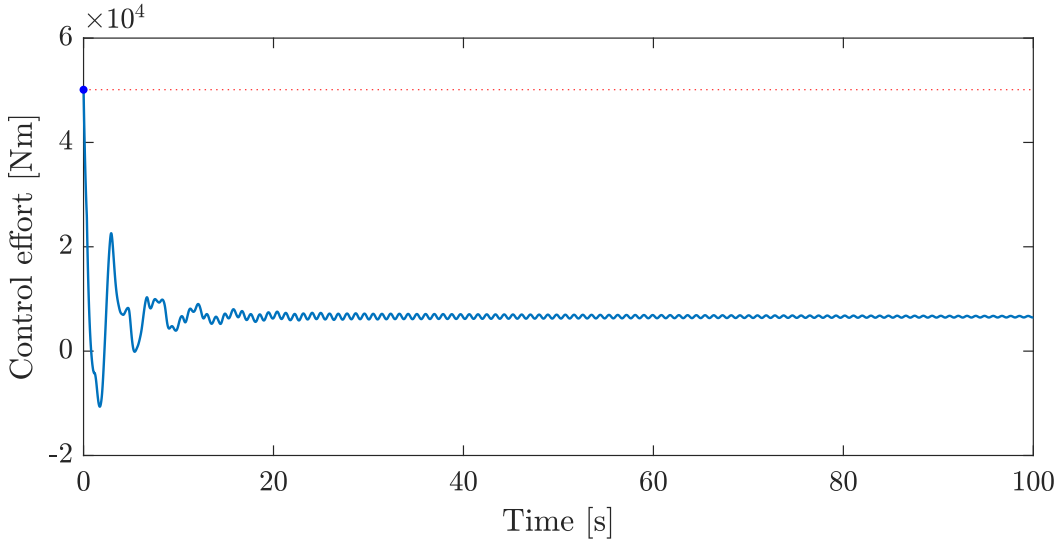

Figure 49 – Applied torque using NDBC with the second sensor at the drill bit for WOB = 140 kN.

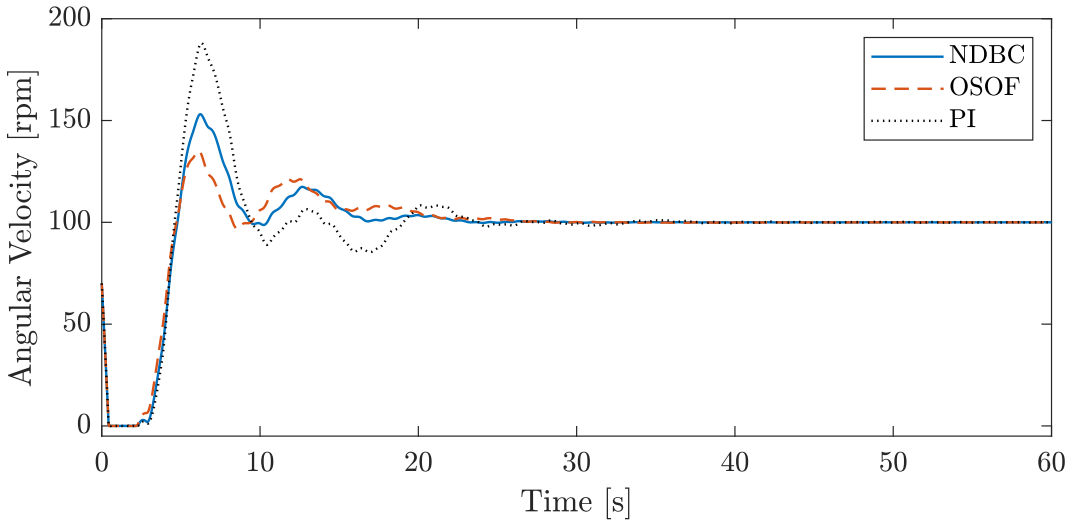

Figure 50 – Bit velocity for NDBC, OSOF and PI controllers with WOB = 120 kN.

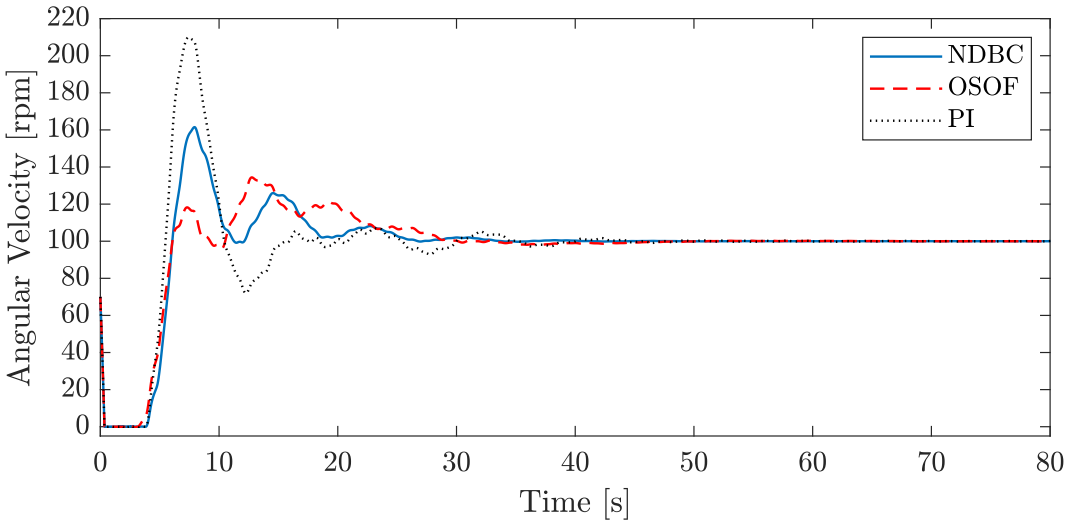

Figure 51 – Bit velocity for NDBC, OSOF and PI controllers with WOB = 140 kN.

6 Numerical simulations for the controlled drill string - Sensitivity Analysis

In the previous chapter, controllers were designed for the model developed in chapter 2 based on the strategies proposed in chapter 4, and their performances were evaluated assuming all system parameters were known. The current chapter intends to make a sensitivity analysis of the controllers determined in the previous chapter, verifying how the performance and stability of the system behave for variations in the system parameters and initial conditions. The first section investigates the stability of the operating point while the last one deals with performance.

6.1 Stability

As discussed in section 3.1, the main factor causing instability of the drilling system is the apparent negative damping effect. Using the concept of the negative damping coefficient introduced in the same section, it is possible to evaluate in a combined way how variations of several parameters locally affect the stability of the operating point. This concept serves as a starting point for the stability analyses in this section, which initially examine the limits of the negative damping coefficient for which the operating point is asymptotically stable for each controller determined in the previous chapter. As the results obtained for both WOB values show similar trends, we decided to focus on the more critical configuration of the 140 kN WOB. To clarify the properties of the controllers analyzed, the control gains for each controller are presented in Table 8, as well as some robustness results derived using the negative damping coefficient. Figure 52 also indicates the spectral abscissa of the linearized closed-loop system using each controller given in Table 8 as a function of n_d.

Table 8 – Main robustness results for NDBC, OSOF and PI controllers using the linear approximation.

Controller	Gain	γ (Nms)	WOB* (kN)	ω_r^* (rpm)	δa^* (%)
PI	$\mathbf{K} = [158.7 \;\; 640.7]$	-330.23	159.38	87.37	7.36
OSOF	$\mathbf{K} = [32.6 \;\; -1600.8 \;\; 674.6 \;\; 0.3]$	-411.64	198.67	65.89	22.28
NDBC	$\mathbf{K} = [48.7 \;\; -1976.3 \;\; 978.0 \;\; -92.4]$	-439.02	211.89	59.62	27.29

According to the results shown in Table 8 and Figure 52, the NDBC obtained larger stability margins (lower γ value) than the OSOF and PI controllers, as it could be expected from the NDBC formulation. Even using a non-zero integral gain, which does not correspond to the optimal solution of (4.22), the magnitude of γ associated with

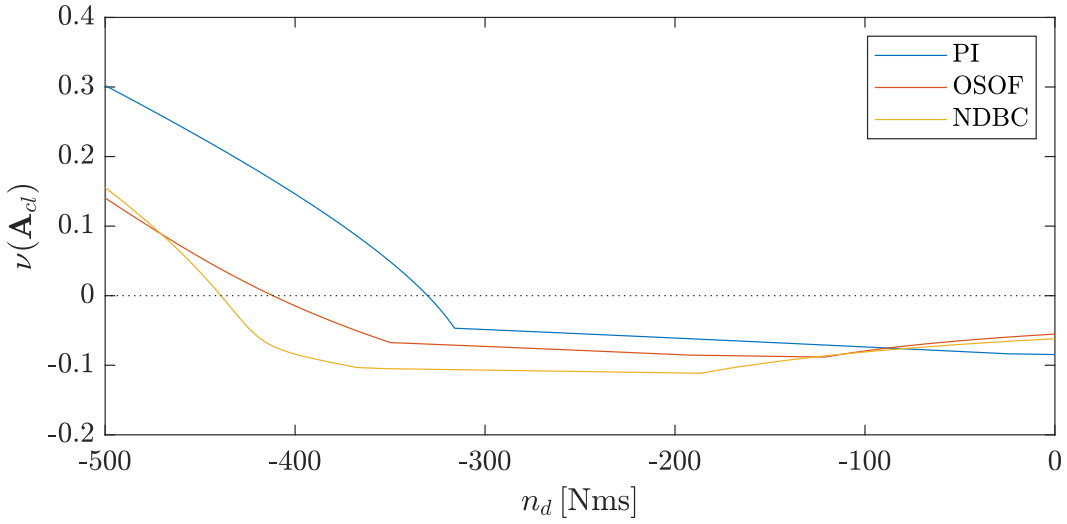

Figure 52 – Spectral abscissa as a function of n_d for the closed-loop system with NDBC, OSOF and PI controllers.

the NDBC was 32.94% and 6.65% higher than those obtained for the PI and OSOF controllers, respectively. Due to the one-to-one correspondence between the negative damping coefficient and several drilling parameters, the γ values can be used to provide bounds for the operating conditions (WOB and target velocity) and friction coefficients, which have a more concrete physical meaning. Using the γ values in Table 8 and Eq. (3.4), the limits for the angular velocity (ω_r^*), weight-on-bit (WOB*), and friction coefficients (WOB*) were determined, and are summarized in Table 8. Although some drilling parameters may have a correlation, for simplicity, each one of these limits was determined assuming constant all other parameters. In Table 8, δa is a positive value that represents a variation in percentage in both friction coefficients, such that the modified friction coefficients are $c_1 = a_1(1-\delta a)$ and $c_2 = a_2(1+\delta a)$. In addition to conveniently representing the variation in friction coefficients, this definition has the benefit of yielding a monotonic dependence between n_d and δa. It is important to emphasize that the calculated bounds rely on the linear approximation of the drilling system, so that these results hold, a priori, only for initial conditions in a neighborhood of the operating point. To illustrate these local stability properties, figures 53-55 depict the system response for small perturbations around the operating point. The convergence to the equilibrium is extremely slow because the eigenvalues are very close to the imaginary axis. Due to the slow convergence and only local stability properties, one should avoid operating the drilling system in these extreme conditions.

Since the γ value relies on the linear approximation at the operating point, it only provides local information on stability margins. Therefore, to obtain information about the global stability of the operating point it is important to investigate the system response to initial conditions far from the operating point. As discussed in section 3.2, the basic stable

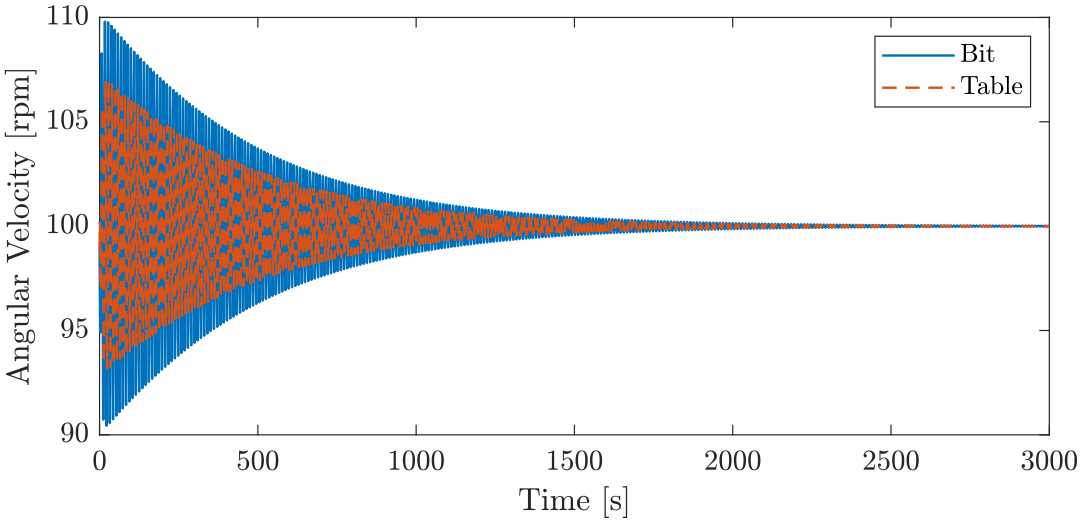

Figure 53 – Bit and rotary table velocities using PI controller with $\delta a = 7.22\%$.

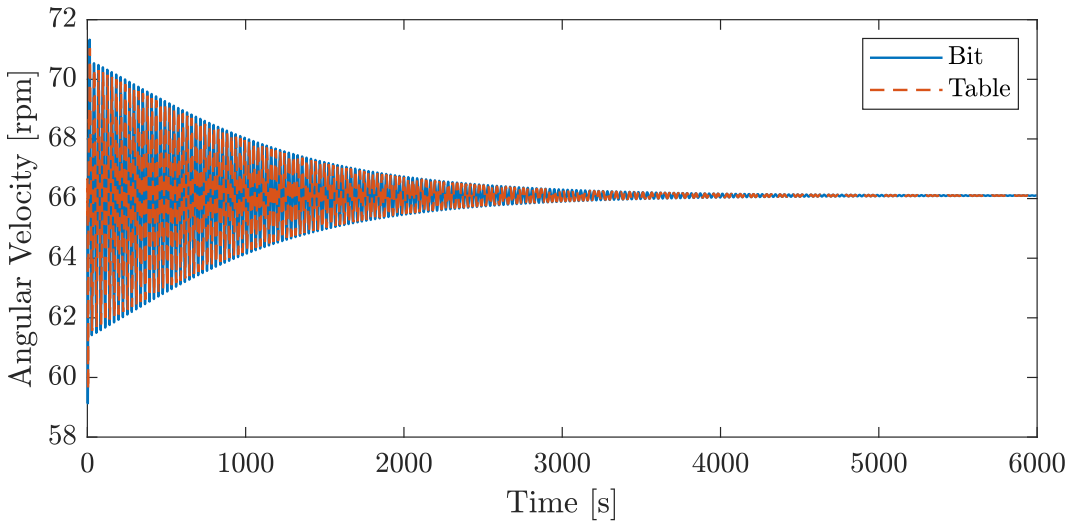

Figure 54 – Bit and rotary table velocities using OSOF controller with $\omega_r = 66.1$ rpm.

limit sets for the drilling system using a static output feedback controller with integral action are a limit cycle and an equilibrium. Additionally, the integral action also prevents the system response from diverging. Thus, a reasonable procedure to verify whether the system response converges to stick-slip oscillations is to simulate an initial condition for which the drill bit undergoes the stick phase. Although this type of simulation does not guarantee global stability, because the drill bit can enter the stick phase through many different initial conditions, it checks the critical scenario where the bit gets stuck and tests stability for regions far from the linearization point. Based on the results obtained in chapter 5, which show the drill bit always passing through the stick phase, the closed-loop system is simulated using the standard initial condition. Assuming this initial condition, the drilling parameters limits (ω_r^*, WOB* and WOB*) were determined as the extreme values for which the system response converged to the operating point. These results are

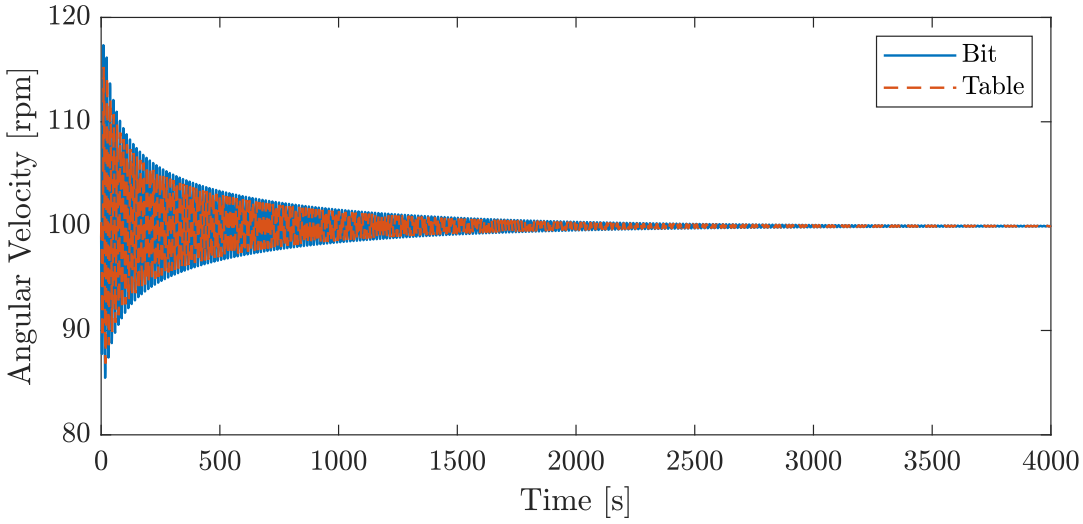

Figure 55 – Bit and rotary table velocities using NDBC with WOB = 211.7 kN.

presented in Table 9.

Table 9 – Robustness results for NDBC, OSOF and PI controllers using the standard initial condition.

Controller	Gain	WOB* (kN)	ω_r^* (rpm)	δa^* (%)
PI	$\mathbf{K} = [158.7 \;\; 640.7]$	157.71	88.42	6.72
OSOF	$\mathbf{K} = [32.6 \;\; -1600.8 \;\; 674.6 \;\; 0.3]$	183.75	72.74	16.59
NDBC	$\mathbf{K} = [48.7 \;\; -1976.3 \;\; 978.0 \;\; -92.4]$	211.89	60.86	27.29

A comparison between the bounds obtained using the linear approximation (Table 8) and the standard initial condition (Table 9) indicate some interesting differences. First, examining the OSOF controller results, the bounds derived from the standard initial condition are much tighter than those using the negative damping coefficient, showing a considerable difference between the nonlinear system and its approximation at the operating point. On the other hand, the limits obtained for the PI control in both scenarios are very similar, where the bounds for the case with initial conditions far from the equilibrium point are slightly more severe than those using the linear approximation. Despite the different results between the linear approximation and the standard initial condition for both controllers, the OSOF control still has larger stability margins in any scenario. Figures 56 and 57 illustrate the closed-loop system responses with PI and OSOF controllers using the corresponding δa^* values for each controller, while Figures 58 and 59 show the response for values just above δa^*.

Different stability margins for the nonlinear system and its linear approximation are somewhat expected since the linear approximation gives only partial information about the system behavior in the neighborhood of the operating point. However, the results obtained for the NDBC overcome this expectation, and show an impressive result in which

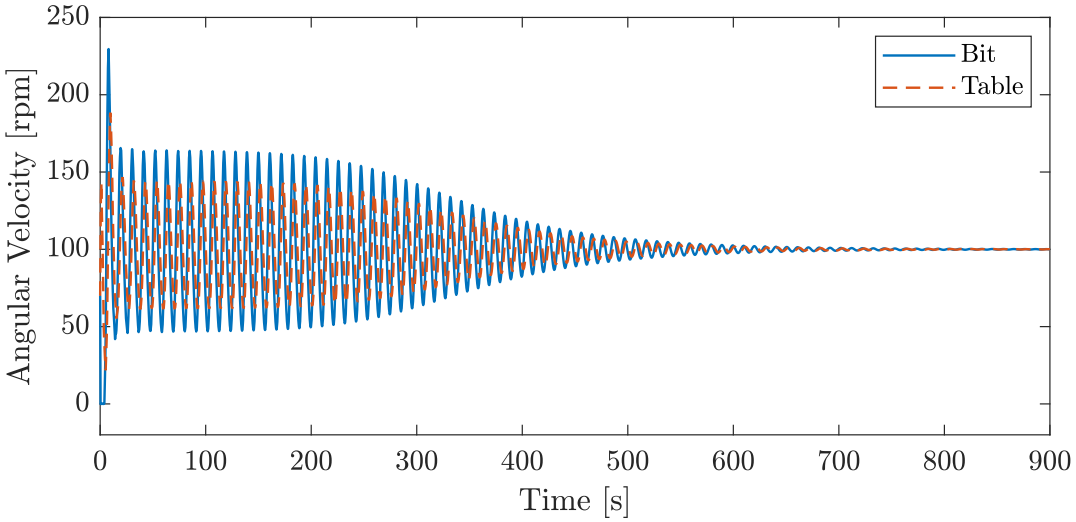

Figure 56 – Bit and rotary table velocities for the standard initial condition using PI controller with $\delta a = 6.72\%$.

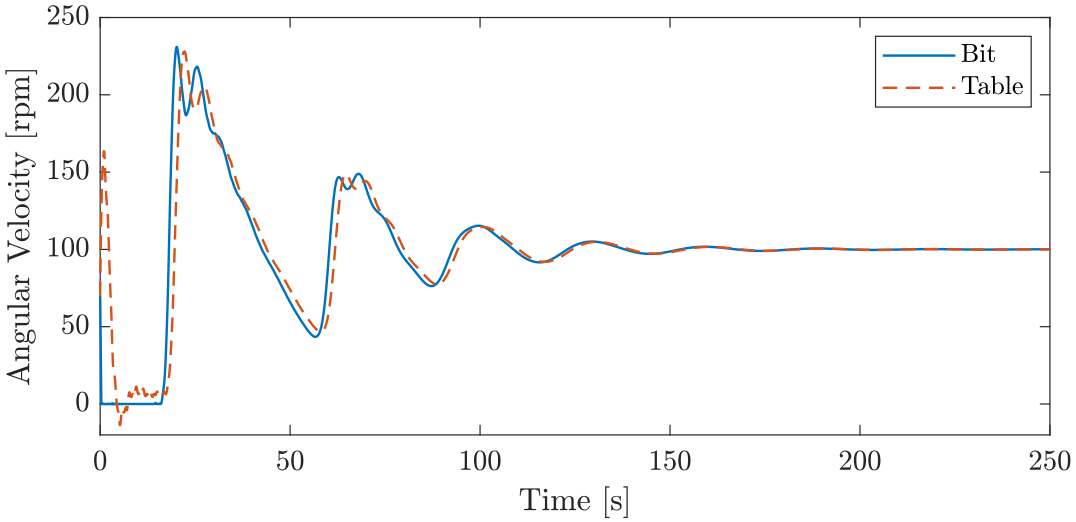

Figure 57 – Bit and rotary table velocities for the standard initial condition using OSOF controller with $\delta a = 16.59\%$.

the bounds (apart from the target velocity) for the nonlinear system and its approximation at the operating point are coincident. Of all drilling parameters, the target angular velocity is the one that concerns the least, as it is only reduced to avoid lateral vibrations in cases where its value is very high, which does not represent the case under study. Moreover, the bounds for the friction coefficients and WOB using the NDBC were the same not only for the standard initial condition, but for every initial condition simulated. For initial conditions where the drill string is undeformed, it was found that increasing the initial velocity yields larger periods of the stick phase in the critical scenarios (e.g., WOB = WOB*) and, for some controllers, this ends up reducing even more the stability bounds. For instance, considering an initial speed of 200 rpm, the PI controller bounds are reduced

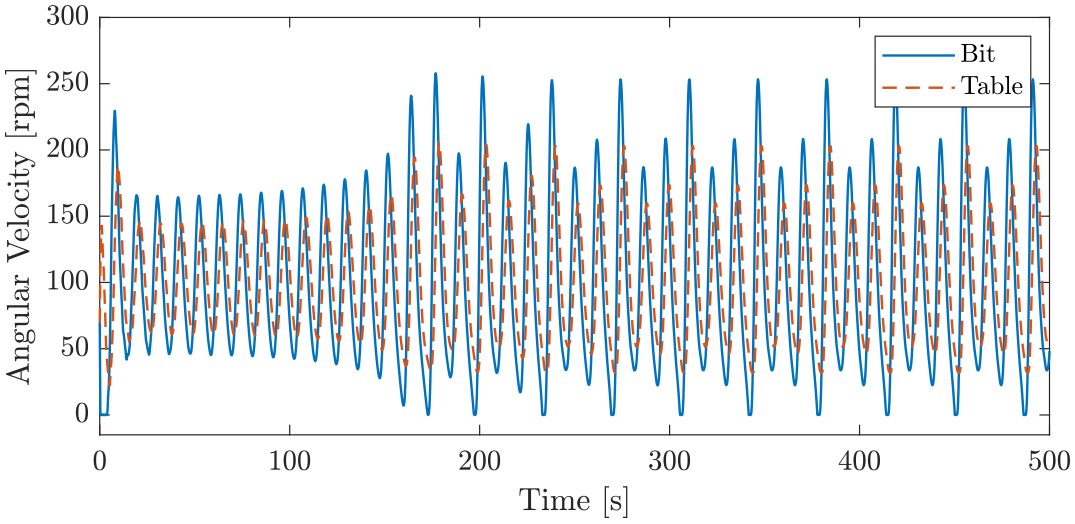

Figure 58 – Bit and rotary table velocities for the standard initial condition using PI controller with $\delta a = 6.73\%$.

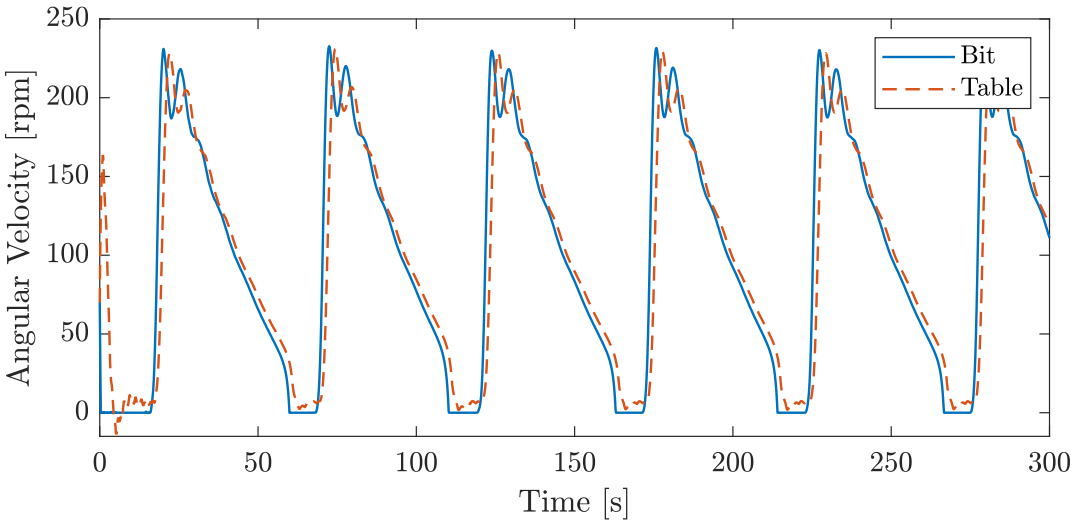

Figure 59 – Bit and rotary table velocities for the standard initial condition using OSOF controller with $\delta a = 16.60\%$.

to $\text{WOB}^* = 156.94$ kN and $\delta a^* = 6.44\%$, whereas the corresponding bounds of the NDBC remain the same. To illustrate these results, Figures 60 and 61 show the closed-loop system response using NDBC and PI controllers for δa slightly below δa^* and considering the higher initial angular speed. These results indicate a remarkable feature of the NDBC because, not only the stability margins obtained by the linear approximation are higher, but they hold even for initial conditions that are not in the neighborhood of the operating point.

As indicated in Figure 41, the stability margins derived using the linear approximation increase as the integral gain k_i decreases. According to this result, one way to reduce the probability of stick-slip oscillations is to decrease the integral gain. Similar

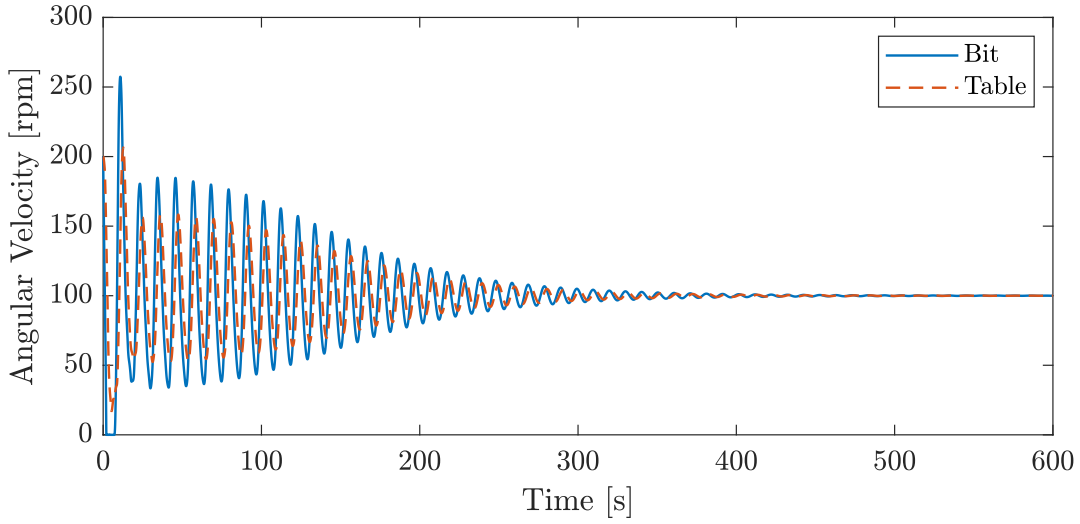

Figure 60 – Bit and rotary table velocities using PI controller with $\delta a = 6.43\%$ for an initial speed of 200 rpm.

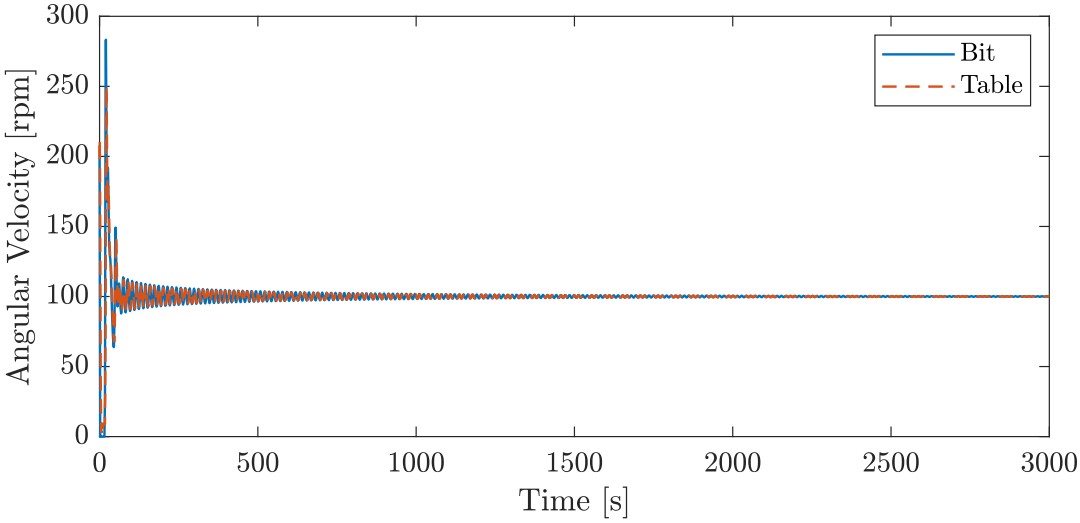

Figure 61 – Bit and rotary table velocities using NDBC with $\delta a = 27.23\%$ for an initial speed of 200 rpm.

to the analyses done previously, it was verified whether these conclusions were still valid for initial conditions far from the operating point. For each value of k_i, the closed-loop system was simulated in critical cases where the negative damping coefficient was equal to γ. The friction curves whose derivative corresponded to the γ value were selected by varying either the WOB or δa. The results of these simulations suggest that there is a continuous range of integral gain values $0 < k_i < \bar{k}_i$, with $\bar{k}_i = 70.2$ Nm, for which the operating point remains globally asymptotically stable. The region of the apparent global asymptotic stability of the operating point is highlighted in Figure 62. Thus, a difference between the nonlinear system and its approximation appears only for high values of k_i, and the apparent global stability of the closed-loop system with the NDBC is preserved

when the integral gain value is reduced.

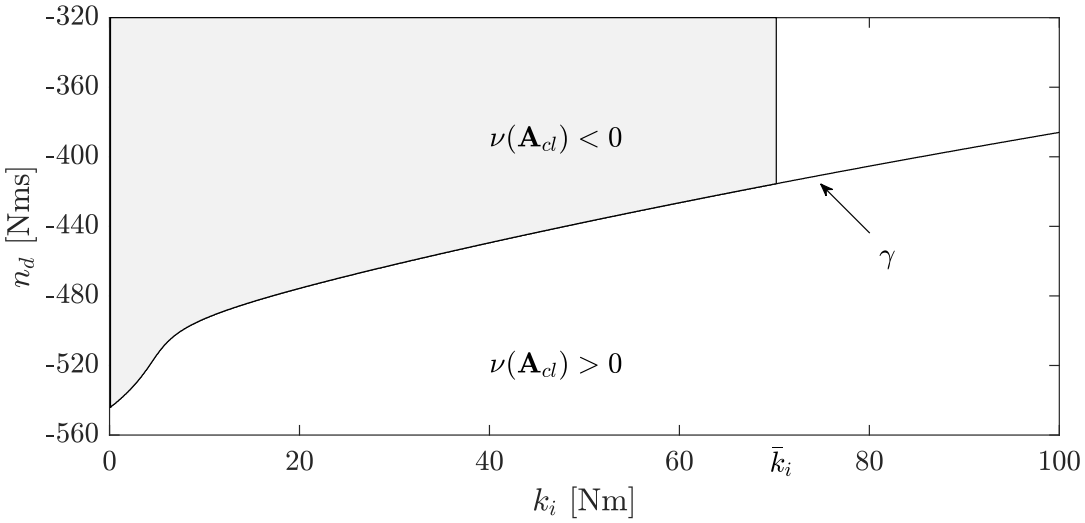

Figure 62 – Region of global stability of the operating point.

A last remarkable result of the NDBC happens in the region where the negative damping coefficient is lower than γ ($\nu(\mathbf{A}_{cl}) > 0$), for which the operating point is not asymptotically stable. Observing the simulation results shown in Figures 56-59 for the PI and OSOF controllers, we verify that for a tiny parameter variation, the system response ceases to converge to the operating point and exhibits large amplitude oscillations. Although these simulations refer to initial conditions far from the operating point, a similar behavior occurs when the equilibrium is not asymptotically stable, in which even small perturbations lead to the appearance of stick-slip oscillations. Figure 63 illustrates this statement by showing a simulation with the OSOF controller for a δa value slightly above that presented in Table 8, and considering a small perturbation at the equilibrium. This situation does not happen for the NDBC. Instead, when the negative damping coefficient crosses the region delimited by γ (by varying parameters like WOB or δa), a small-amplitude stable limit cycle branches from the equilibrium. This type of behavior is described in dynamical system theory as a supercritical Hopf bifurcation (KUZNETSOV, 2004). Figure 64 depicts this type of response for the NDBC with $k_i = 48.7$ by simulating a δa value slightly higher than δa^*. For δa closer to δa^*, the oscillation amplitude is smaller, but the convergence to the limit cycle is even slower. For k_i smaller than $\bar{k}_i$, simulations using other initial conditions suggest that the response converges to the limit cycle regardless of the initial condition, indicating a potential global stability of the small-amplitude limit cycle as well. Therefore, even when the operating point is not asymptotically stable, the closed-loop system with the NDBC still tolerates small parameter variations without exhibiting stick-slip oscillations, further increasing the safe operating region.

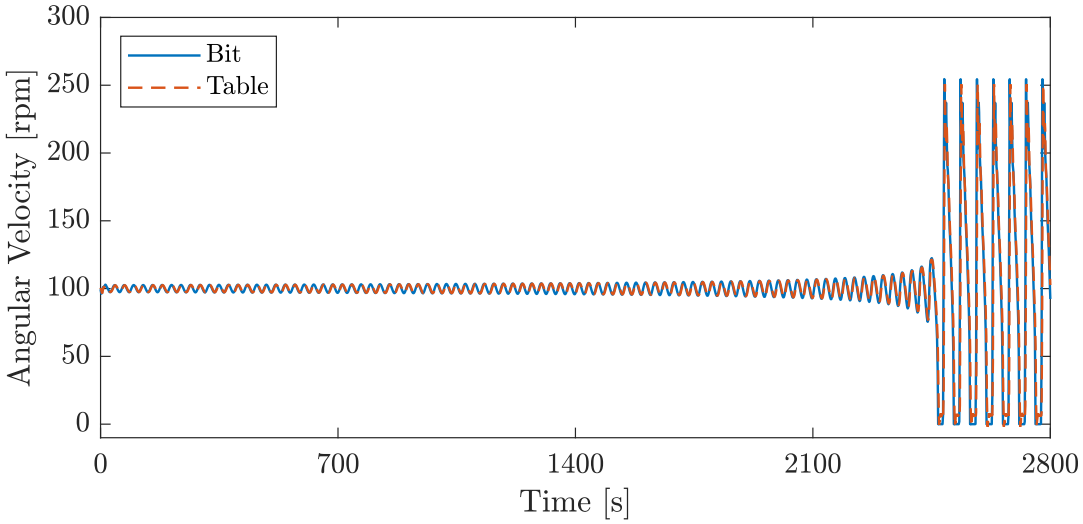

Figure 63 – Bit and rotary table velocities using OSOF controller with $\delta a = 22.29\%$ for a small perturbation at the equilibrium.

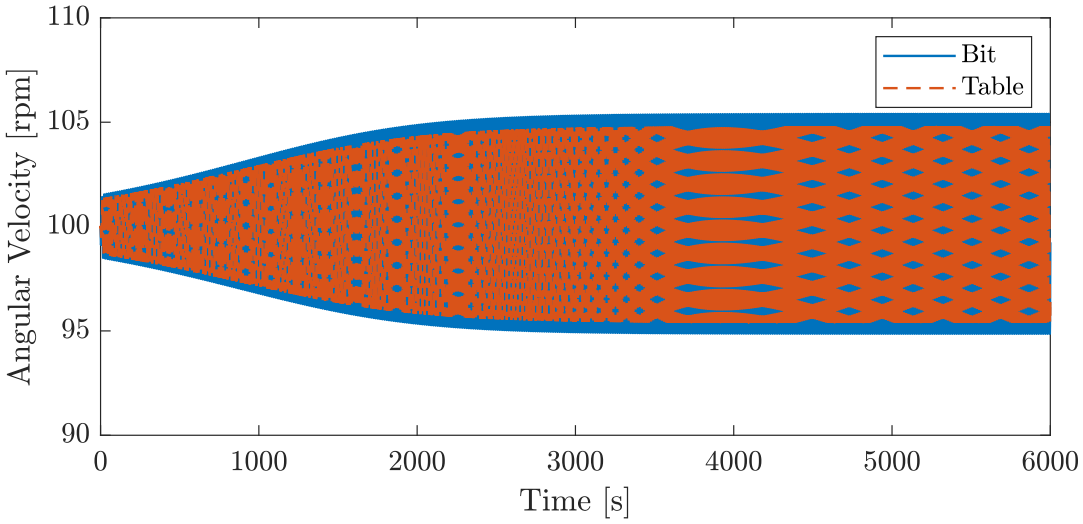

Figure 64 – Bit and rotary table velocities using NDBC with $\delta a = 27.35\%$ for a small perturbation at the equilibrium.

6.2 Performance

The previous section focused on investigating for which parameter variations the system response converged to the equilibrium point or exhibited stick-slip oscillations. As seen in some simulations, even in cases where the response converges to the equilibrium point, the system performance may not be acceptable. Thus, the objective of the present section is to evaluate the sensitivity of the system's performance and control effort with respect to parameter variations. Several metrics were employed to assess specific performance characteristics in chapter 5, such as stick phase duration, settling time and maximum overshoot. Considering that all these factors are compactly represented by the average deviation from drill bit target angular velocity (J), this metric is used in this

section as the main criterion for evaluating performance. For better comparison with the results of the previous section and chapter 5, the target speed is kept as 100 rpm and the standard initial condition is also used for the calculation of J. Similar to the last section, the cost function J is evaluated for the NDBC, OSOF and PI controllers determined for the WOB 140 kN configuration in chapter 5.

Figures 65 and 66 show J as a function of δa and WOB. In each case, only the parameter of interest is variable, while the others are kept constant according to the values given in Table 2 for the 140 kN WOB. A first aspect that stands out is the similarity between the graphs for each controller, which apart from a scale factor look almost identical. Another interesting aspect is that several instances of discontinuity in both graphs correspond to points that have equivalent values of the negative damping coefficient, highlighting the importance of this concept. For example, the highlighted points in the graphs, which indicate the critical value of the parameter of interest where persistent stick-slip oscillations are first observed, have very close negative damping coefficient values for each controller (values are equal by rounding to an integer). These values are -327, -381 and -441 Nms for the NDBC, OSOF and PI controllers, respectively. Note that these negative damping coefficient values for PI and OSOF are greater than the corresponding γ values given in Table 8, whereas the NDBC value is the only one that is smaller. These discrepancies are explained by the difference between the nonlinear system and its linear approximation for the PI and OSOF controllers and the supercritical Hopf bifurcation for the NDBC, which are both discussed in the previous section.

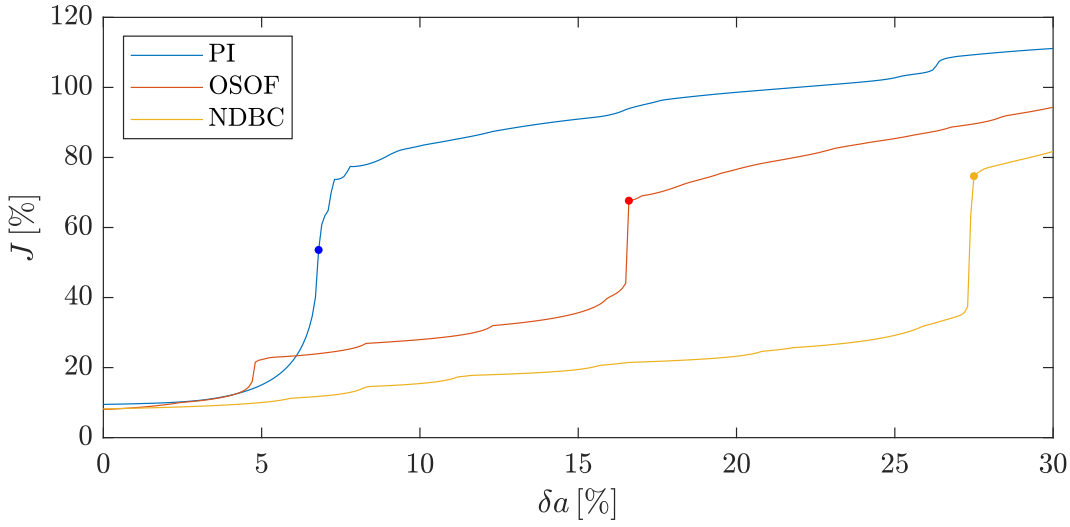

Figure 65 – Average deviation from the drill bit target angular velocity as a function of δa for the closed-loop system with NDBC, OSOF and PI controllers.

Figures 65 and 66 also emphasize the different performance sensitivities between the three controllers. Although the OSOF control has the best nominal performance, it also has the highest sensitivity for small values of δa and WOB. Indeed, for $\delta a > 0.7\%$, the

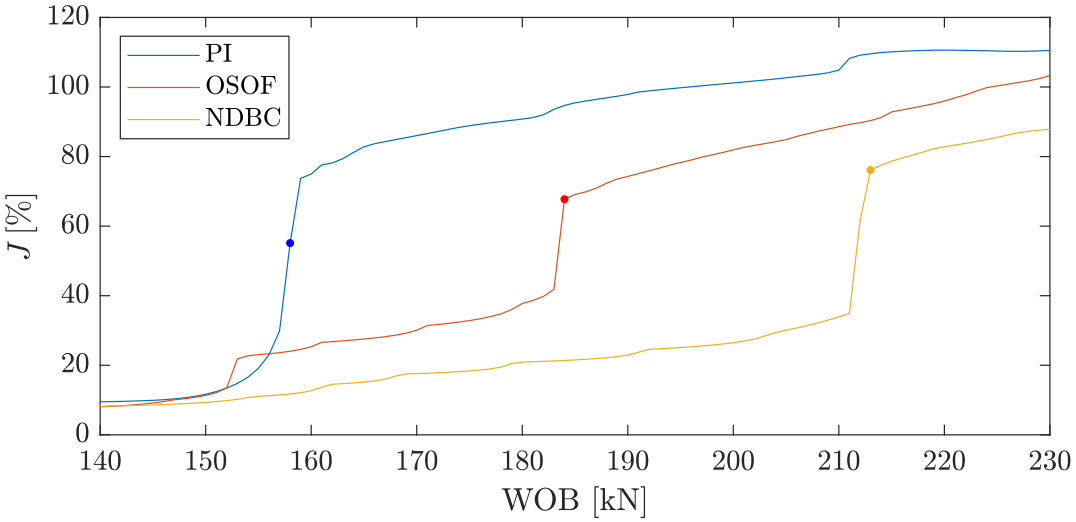

Figure 66 – Average deviation from the drill bit target angular velocity as a function of WOB for the closed-loop system with NDBC, OSOF and PI controllers.

cost function of the OSOF control is always greater than that of the NDBC, and in the interval $4.2\% < \delta a < 6.1\%$ the J value associated with the OSOF becomes even greater than that associated with the PI. At $\delta a = 4.8\%$, the OSOF controller passes through the stick phase twice, which justifies the first discontinuity in its curve and the consequent increase in the cost function value. To illustrate this result, the time responses with the OSOF control for δa values of 4.7% and 4.8% are depicted in Figures 67 and 68. Note that in addition to the increase in the stick phase duration, the drill bit velocity has a considerable increase in overshoot. As δa increases, the two separate stick regions collapse into a single large stick phase.

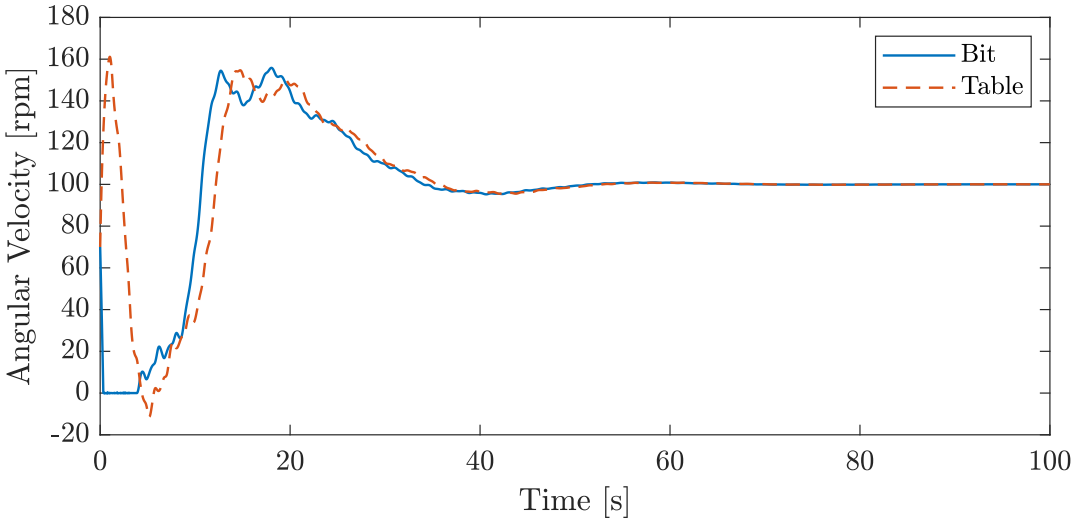

Figure 67 – Bit and rotary table velocities using OSOF controller with $\delta a = 4.7\%$ for the standard initial condition.

Figures 65 and 66 also show an apparently smoother transition between the con-

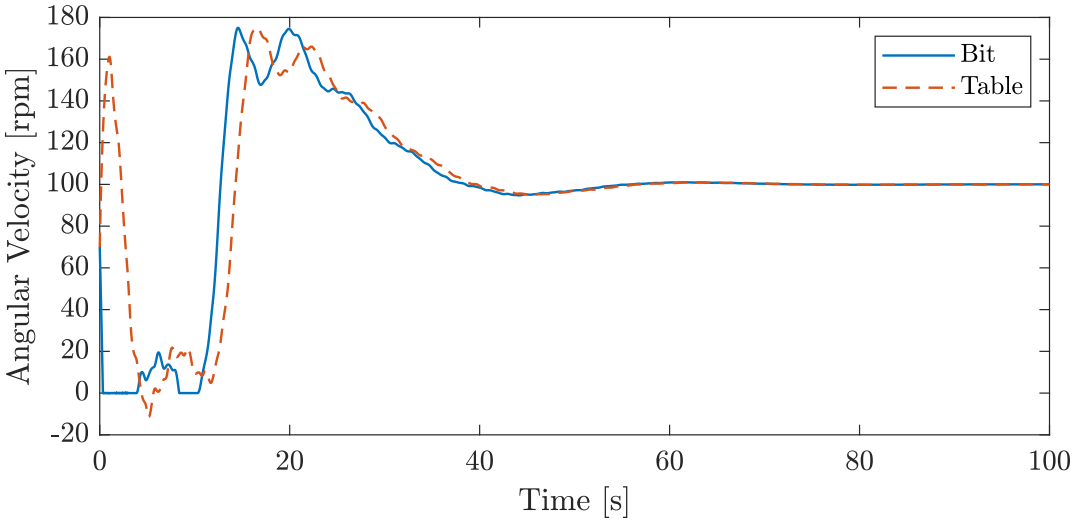

Figure 68 – Bit and rotary table velocities using OSOF controller with $\delta a = 4.8\%$ for the standard initial condition.

vergence to the operating point and the appearance of stick-slip oscillations using the PI controller. This fact happens because the PI control already displays large amplitude oscillations before the appearance of stick-slip oscillations, as illustrated previously in Figures 56 and 58. Due to the premature appearance of stick-slip oscillations, the PI controller displays the highest J values for the widest range of δa and WOB values. On the other hand, the NDBC presents the lowest values of J for virtually the entire range of parameters analyzed. Furthermore, when the derivatives of J with respect to δa are numerically approximated for each one of the controllers, it is verified that the NDBC obtains the smallest values for small parameter variations ($0\% < \delta a < 5.3\%$), in addition to having the widest range of parameter variations with the smallest derivatives. These observations reveal a remarkable result of the NDBC because, besides having the highest stability margins, this controller also has the lowest performance sensitivity, as qualified by the metric J.

As one of the strategies to avoid the occurrence of stick-slip oscillations using the NDBC is the reduction of the integral gain, it was also evaluated how this practice affected the system performance in terms of J. For comparison, the variation of J in relation to the integral gain was also evaluated for the other controllers, and the results are shown in Figure 69. Again, note that the NDBC has low sensitivity of J with respect to k_i, with values below 10% over the entire range $0 < k_i < 124.5$. Therefore, for the 140 kN WOB, it is verified that the reduction of k_i has negligible impact on the performance of the NDBC.

Finally, it was evaluated the impact of parameter variations on the maximum applied torque. Due to the similarities between WOB and δa, only the results for the latter are depicted in Figure 70. In this case, the OSOF controller had the better results for the entire parameter range considered. A similarity between the OSOF and NDBC is

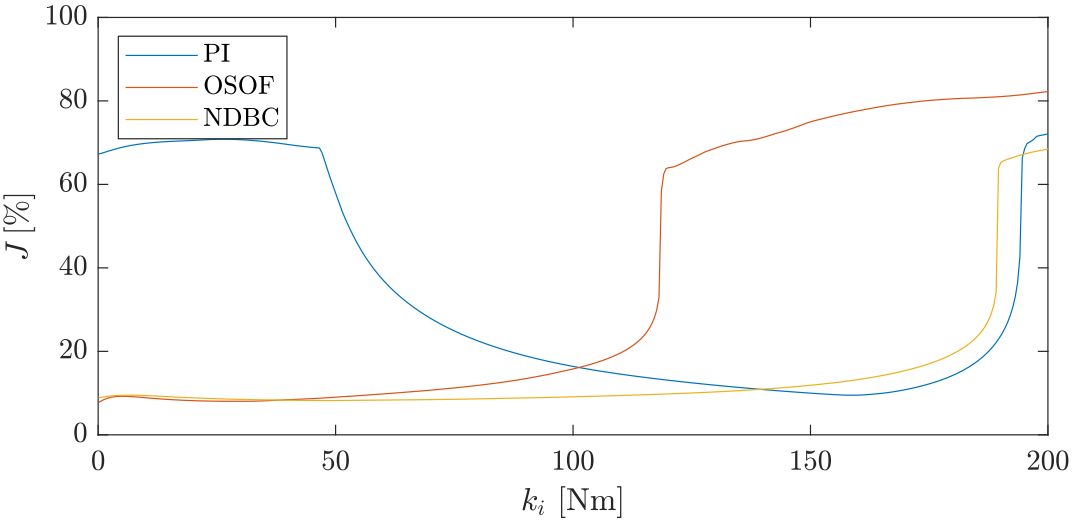

Figure 69 – Average deviation from the drill bit target angular velocity as a function of k_i for the closed-loop system with NDBC, OSOF and PI controllers.

that the maximum applied torque occurs immediately after the first stick phase, therefore independent of the occurrence of persistent stick-slip oscillations. Thus, unlike the metric J, the parameter values for which stick-slip oscillations occur for the OSOF and NDBC are not so clear from Figure 70. A different behavior is observed for the PI controller, for which the highest applied torques occur in the subsequent stick phases, justifying the discontinuity perceived at $\delta a = 6.8\%$. In addition to the maximum applied torque, the combination of high torque values with high angular speeds of the rotary table during stick-slip oscillations may result in high power demand, which may play a role in favor of the NDBC. Overall, combining all aspects concerning sensitivity analyzed in this chapter, it is considered that NDBC had the best results among all proposed control techniques.

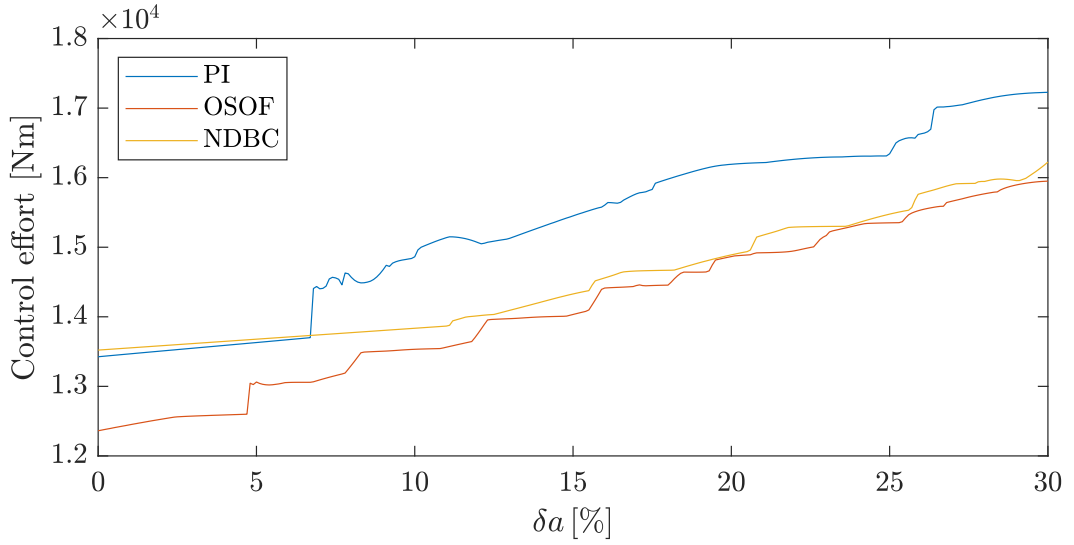

Figure 70 – Maximum applied torque as a function of δa for the closed-loop system with NDBC, OSOF and PI controllers.

7 Conclusions, future works and publications

This section summarizes the main steps taken in the development of this work, in addition to presenting the main contributions of this thesis and publications during the doctoral program.

7.1 Conclusions and future works

This thesis studied the problem of attenuation and suppression of torsional (stick-slip) vibrations in drill strings using active control. This study was organized into the following general steps: 1) Finite element modeling with non-regularized dry friction, reformulation of the equations of motion as a stabilization problem with addition of integral action; 2) Dynamic analysis of the drilling system in open- and closed-loop configurations; 3) Output matrix design to ensure asymptotic stability of the operating point and proposition of two control techniques based on the OSOF formulation and the negative damping coefficient; 4) Numerical simulations of the closed-loop system in the case of known parameters and in the presence of uncertainties, both scenarios considering comparisons with other control techniques. A detailed analysis of each one of these steps led to a series of original results and contributions:

- Development of a state-space model in translated modal coordinates that allowed a standard stability analysis of the operating point and a suitable design of the output matrix;
- Dynamic analysis identifying the primary limit sets of the drilling system in open- and closed-loop configurations;
- Definition of the concept of negative damping coefficient, which allowed a straightforward identification of the role of each drilling parameter in the stability of the operating point. This concept was also instrumental in the development of an extremely efficient control technique for the drilling system;
- Determination of which signals are relevant for feedback given the objective of ensuring asymptotic stability and assuming the constraint of static output feedback;
- Proposition of two novel control techniques for the drilling problem: one based on the OSOF control formulation developed in (CRUZ NETO; TRINDADE, 2019) focusing on nominal performance, and another based on the concept of negative damping coefficient focusing on robustness;

- Showing through numerical simulations that the proposed control techniques outperform an optimized PI controller with an equivalent control effort;
- Evaluation of the effects of varying the positioning of the second sensor on the performance and robustness of the proposed control strategies. It was found for the OSOF control that performance improves monotonically as the second sensor approaches the drill bit, while the stability margins of the NDBC increase drastically close to the rotary table, remain nearly constant for an intermediate length of the drill string and increase considerably close to the drill bit.
- Showing through a sensitivity analysis that the proposed controllers (especially the NDBC) tolerate much greater parameters variations while still ensuring stability than the optimized PI controller;
- Determination through simulations using several different initial conditions of an integral gain range for which the NDBC appears to provide global stability for the operating point;
- Identification of a supercritical Hopf bifurcation for the closed-loop system equipped with the NDBC, further increasing the safe operating region;
- Showing that the proposed controllers (especially the NDBC) are less sensitive to parameters variations in terms of performance and applied torque than the optimized PI controller.

Results obtained in this thesis motivate further research in the investigation of the apparent global stability provided by the NDBC, the application of the NDBC formulation for similar systems (Lure's problem) and the practical implementation of the proposed control strategies in laboratory setups or full-scale drilling rigs. Other aspects for further investigation are related to the drill string model, such as the inclusion of model dynamics in other directions and the study of other modal reduction techniques.

7.2 Publications

The following works were published during the doctoral program, some derived directly from the research developed in this thesis and others derived from the work developed during the author's master's degree.

1. CRUZ NETO, H. J.; TRINDADE, M. A. Reduction of Negative Damping Effects in the Drilling Process Using Active Control. DINAME 2023 - XIX International Symposium on Dynamic Problems of Mechanics. *Accepted*

2. CRUZ NETO, H. J.; TRINDADE, M. A. Control of drill string torsional vibrations using optimal static output feedback. Control Engineering Practice, v. 130, p. 105366, 2023.

3. CRUZ NETO, H. J.; TRINDADE, M. A. Output Feedback Control for Mitigation of Negative Damping Effects in the Drilling Process. In: Simpósio do Programa de Pós-Graduação em Engenharia Mecânica da EESC-USP (SiPGEM/EESC-USP), 6., 2022, São Carlos.

4. CRUZ NETO, H. J.; TRINDADE, M. A. A Novel Methodology for Controlling Stick-Slip Vibrations in Drill Strings. In: LACARBONARA, Walter; BALACHANDRAN, Balakumar; LEAMY, Michael J.; MA, Jun; TENREIRO MACHADO J. A.; STEPAN, Gabor (org.). Advances in Nonlinear Dynamics - Proceedings of the Second International Nonlinear Dynamics Conference (NODYCON 2021). Rome: Springer, 2022. p. 125-134.

5. CRUZ NETO, H. J.; TRINDADE, M. A. Comparison of controllers for stick-slip suppression in rotary drilling systems. In: ISMA conference on Noise and Vibration Engineering, 29., 2020, Leuven. Proceedings [...] Leuven: KU Leuven, 2020. p. 1419-1431.

6. CRUZ NETO, H. J.; TRINDADE, M. A. On the noncollocated control of structures with optimal static output feedback: Initial conditions dependence, sensors placement, and sensitivity analysis. Structural Control and Health Monitoring, v. 26, n. 10, p. e2407, 2019.

7. CRUZ NETO, H. J.; TRINDADE, M. A. Design and analysis of active control techniques for stick-slip suppression in rotary drilling systems. In: ABCM International Congress of Mechanical Engineering Proceedings (COBEM), 25., 2019, Uberlândia. Proceedings [...] Uberlândia: ABCM, 2019.

8. CRUZ NETO, H. J.; TRINDADE, M. A. Otimização do ganho e posicionamento de sensores para o controle de vibrações em estruturas. In: Congresso Nacional de Matemática Aplicada e Computacional, 38., 2018, Campinas. Proceedings [...] Campinas: SBMAC, 2018. p 010175.

Bibliography

AARSNES, U. J. F.; SHOR, R. J. Torsional vibrations with bit off bottom: Modeling, characterization and field data validation. *Journal of Petroleum Science and Engineering*, v. 163, p. 712 – 721, 2018. Cited on page 28.

ABDULGALIL, F.; SIGUERDIDJANE, H. Nonlinear control design for suppressing stick-slip oscillations in oil well drillstrings. In: *2004 5th Asian Control Conference (IEEE Cat. No.04EX904)*. [S.l.: s.n.], 2004. v. 2, p. 1276–1281. Cited 3 times on pages 27, 30, and 55.

ANDRONOV, A. A.; VITT, A.; KHAIKIN, S. E. *Theory of Oscillators (translated from Russian)*. [S.l.]: Pergamon Press, Oxford, 1966. Cited 2 times on pages 26 and 47.

AUBIN, J.-P.; CELLINA, A. *Differential inclusions: set-valued maps and viability theory*. [S.l.]: Springer Science & Business Media, 2012. v. 264. Cited on page 38.

BAILEY, J. J.; FINNIE, I. An analytical study of drill-string vibration. *Journal of Engineering for Industry*, v. 82, n. 2, p. 122–127, 1960. Cited on page 25.

BELLARBY, J. *Well completion design*. [S.l.]: Elsevier, 2009. v. 56. Cited on page 22.

BELOKOBYL'SKII, S. V.; PROKOPOV, V. K. Friction-induced self-excited vibrations of drill rig with exponential drag law. *Soviet Applied Mechanics*, v. 18, n. 12, p. 1134–1138, 1982. Cited on page 26.

BESSELINK, B. et al. Analysis and control of stick-slip oscillations in drilling systems. *IEEE Transactions on Control Systems Technology*, v. 24, n. 5, p. 1582 – 1593, 2016. Cited on page 30.

BOWDEN, F. P.; LEBEN, L. The nature of sliding and the analysis of friction. *Proceedings of the Royal Society of London. Series A. Mathematical and Physical Sciences*, The Royal Society London, v. 169, n. 938, p. 371–391, 1939. Cited on page 26.

Brasil, Ministério de Minas e Energia, Empresa de Pesquisa Energética. *Plano Decenal de Expansão de Energia 2026*. 2017. Cited on page 21.

BRESCH-PIETRI, D.; KRSTIC, M. Output-feedback adaptive control of a wave pde with boundary anti-damping. *Automatica*, v. 50, n. 5, p. 1407 – 1415, 2014. Cited on page 28.

BRETT, J. The genesis of torsional drillstring vibrations. *SPE Drilling Engineering*, v. 7, n. 3, p. 168 – 174, 1992. Cited 3 times on pages 26, 47, and 71.

BROGLIATO, B. *Nonsmooth mechanics: Models, Dynamics and Control*. [S.l.]: Springer, 2016. Cited on page 38.

CANUDAS-DE-WIT, C. et al. D-oskil: A new mechanism for suppressing stick-slip in oil well drillstrings. In: *Proceedings of the 44th IEEE Conference on Decision and Control*. [S.l.: s.n.], 2005. p. 8260 – 8265. Cited 2 times on pages 27 and 30.

CANUDAS-DE-WIT, C.; RUBIO, F. R.; CORCHERO, M. A. D-oskil: A new mechanism for controlling stick-slip oscillations in oil well drillstrings. *IEEE Transactions on Control Systems Technology*, v. 16, n. 6, p. 1177 – 1191, 2008. Cited on page 31.

CHARLEZ, P. A. *Rock mechanics: petroleum applications*. [S.l.]: Editions Technip, 1997. v. 2. Cited on page 22.

CHRISTOFOROU, A. P.; YIGIT, A. S. Fully coupled vibrations of actively controlled drillstrings. *Journal of Sound and Vibration*, v. 267, n. 5, p. 1029–1045, 2003. Cited on page 30.

CRAIG, R. R.; KURDILA, A. J. *Fundamentals of structural dynamics*. [S.l.]: John Wiley & Sons, 2006. Cited on page 33.

CRUZ NETO, H.; TRINDADE, M. Control of drill string torsional vibrations using optimal static output feedback. *Control Engineering Practice*, v. 130, p. 105366, 2023. Cited on page 57.

CRUZ NETO, H. J. *Otimização do Posicionamento de Sensores e Atuadores Para o Controle Ótimo com Realimentação de Saída Utilizando Critério de Desempenho Quadrático*. Dissertação (Mestrado), 2018. Cited 3 times on pages 59, 60, and 61.

CRUZ NETO, H. J.; TRINDADE, M. A. On the noncollocated control of structures with optimal static output feedback: Initial conditions dependence, sensors placement, and sensitivity analysis. *Structural Control and Health Monitoring*, v. 26, n. 10, p. e2407, 2019. Cited 6 times on pages 55, 60, 68, 70, 78, and 103.

DAREING, D. W.; LIVESAY, B. J. Longitudinal and angular drill-string vibrations with damping. *Journal of Engineering for Industry-Transactions of the Asme*, v. 90, n. 4, p. 671–679, 1968. Cited on page 25.

DONG, G. J.; CHEN, P. A review of the evaluation, control, and application technologies for drill string vibrations and shocks in oil and gas well. *Shock and Vibration*, 2016. Cited 3 times on pages 24, 25, and 36.

DOYLE, J. C. Guaranteed margins for lqg regulators. *IEEE Transactions on Automatic Control*, v. 23, n. 4, p. 756–757, 1978. Cited on page 58.

DUDLEY, B.; SWIFT, P. H. Lxxviii. frictional relaxation oscillations. *The London, Edinburgh, and Dublin Philosophical Magazine and Journal of Science*, Taylor & Francis, v. 40, n. 307, p. 849–861, 1949. Cited on page 26.

ERTAS, D. et al. Drillstring mechanics model for surveillance, root cause analysis, and mitigation of torsional and axial vibrations. In: *SPE/IADC Drilling Conference*. Amsterdam, The Netherlands: [s.n.], 2013. v. 1, p. 203 – 216. Cited on page 26.

FINNIE, I.; BAILEY, J. An experimental study of drill-string vibration. *Journal of Engineering for Industry*, v. 82, n. 2, p. 129–135, 1960. Cited on page 25.

FREEMAN, R.; KOKOTOVIC, P. Inverse optimality in robust stabilization. *SIAM Journal on Control and Optimization*, v. 34, n. 4, p. 1365 – 1391, 1996. Cited on page 30.

GACI, S.; HACHAY, O. *Oil and Gas Exploration: Methods and Application*. [S.l.]: John Wiley & Sons, 2017. v. 72. Cited on page 22.

GERMAY, C.; DENOËL, V.; DETOURNAY, E. Multiple mode analysis of the self-excited vibrations of rotary drilling systems. *Journal of Sound and Vibration*, v. 325, n. 1, p. 362–381, 2009. Cited on page 26.

GHASEMI, M.; SONG, X. Trajectory tracking and rate of penetration control of downhole vertical drilling system. *Journal of Dynamic Systems, Measurement and Control, Transactions of the ASME*, v. 140, n. 9, 2018. Cited on page 28.

GHASEMLOONIA, A.; RIDEOUT, D. G.; BUTT, S. D. A review of drillstring vibration modeling and suppression methods. *Journal of Petroleum Science and Engineering*, v. 131, p. 150–164, 2015. Cited 2 times on pages 24 and 27.

GRANT, R.; TEXTER, H. Causes and prevention of drill-pipe and tool-joint troubles. In: *Drilling and Production Practice*. New York: [s.n.], 1941. p. 9 – 48. Cited on page 25.

GUCKENHEIMER, J.; HOLMES, P. *Nonlinear oscillations, dynamical systems, and bifurcations of vector fields*. New York: Springer-Verlag, 1983. Cited on page 47.

HALSEY, G. W.; KYLLINGSTAD, A.; KYLLING, A. Torque feedback used to cure slip-stick motion. *SPE Annual Technical Conference and Exhibition*, p. 6, 1988. Cited 2 times on pages 29 and 55.

International Energy Agency. *Oil Market Report*. 2020. Cited on page 21.

JANSEN, J. D. *Nonlinear Dynamics of Oilwell Drillstrings*. Tese (Doctoral Thesis), 1993. Cited on page 24.

JANSEN, J. D.; VANDENSTEEN, L. Active damping of self-excited torsional vibrations in oil-well drillstrings. *Journal of Sound and Vibration*, v. 179, n. 4, p. 647–668, 1995. Cited 2 times on pages 27 and 30.

JARDINE, S.; MALONE, D.; SHEPPARD, M. Putting a damper on drillings bad vibrations. *Oilfield Review*, v. 6, n. 1, p. 15–20, 1994. Cited on page 24.

JAVANMARDI, K.; GASPARD, D. T. Application of soft-torque rotary table in mobile bay. *SPE/IADC Drilling Conference*, p. 6, 1992. Cited on page 30.

JOHNSON, M. A.; MORADI, M. H. *PID control*. [S.l.]: Springer, 2005. Cited 2 times on pages 29 and 73.

KAPITANIAK, M. et al. Unveiling complexity of drill-string vibrations: Experiments and modelling. *International Journal of Mechanical Sciences*, v. 101-102, p. 324 – 337, 2015. Cited on page 26.

KHALIL, H. *Nonlinear Systems*. [S.l.]: Prentice Hall, 2002. Cited 2 times on pages 44 and 48.

KHULIEF, Y.; AL-NASER, H. Finite element dynamic analysis of drillstrings. *Finite Elements in Analysis and Design*, v. 41, n. 13, p. 1270 – 1288, 2005. Cited on page 27.

KHULIEF, Y.; AL-SULAIMAN, F.; BASHMAL, S. Vibration analysis of drillstrings with self-excited stick-slip oscillations. *Journal of Sound and Vibration*, v. 299, n. 3, p. 540 – 558, 2007. Cited on page 27.

KREUZER, E.; STEIDL, M. Controlling torsional vibrations of drill strings via decomposition of traveling waves. *Archive of Applied Mechanics*, v. 82, n. 4, p. 515 – 531, 2012. Cited on page 27.

KRSTIC, M.; SMYSHLYAEV, A. *Boundary control of PDEs: A course on backstepping designs*. [S.l.]: SIAM, 2008. Cited on page 35.

KUZNETSOV, Y. A. *Elements of applied bifurcation theory*. 3rd. ed. [S.l.]: Springer-Verlag New York, 2004. v. 112. Cited on page 96.

KYLLINGSTAD, A. A comparison of stick-slip mitigation tools. In: *SPE/IADC Drilling Conference and Exhibition*. The Hague, The Netherlands: [s.n.], 2017. p. 619 – 634. Cited on page 65.

KYLLINGSTAD, A.; HALSEY, G. W. A study of slip/stick motion of the bit. *SPE Drilling Engineering*, v. 3, n. 04, p. 369–373, 1988. Cited on page 27.

KYLLINGSTAD, A.; NESSJØEN, P. J. A new stick-slip prevention system. In: *SPE/IADC Drilling Conference and Exhibition*. Amsterdam, The Netherlands: [s.n.], 2009. v. 2, p. 912 – 925. Cited on page 29.

LEINE, R. I.; CAMPEN, D. H. van; KEULTJES, W. J. G. Stick-slip whirl interaction in drillstring dynamics. *Journal of Vibration and Acoustics-Transactions of the Asme*, v. 124, n. 2, p. 209–220, 2002. Cited on page 25.

LEINE, R. I.; NIJMEIJER, H. *Dynamics and bifurcations of non-smooth mechanical systems*. [S.l.]: Springer Science & Business Media, 2013. v. 18. Cited on page 38.

LEVINE, W.; ATHANS, M. On the determination of the optimal constant output feedback gains for linear multivariable systems. *Automatic Control, IEEE Transactions on*, v. 15, n. 1, p. 44–48, 1970. Cited 2 times on pages 58 and 60.

LIN, Y. Q.; WANG, Y. H. Stick-slip vibration of drill strings. *Journal of Engineering for Industry-Transactions of the ASME*, v. 113, n. 1, p. 38–43, 1991. Cited on page 27.

LIU, X. et al. Spatial-temporal dynamics of a drill string with complex time-delay effects: Bit bounce and stick-slip oscillations. *International Journal of Mechanical Sciences*, v. 170, 2020. Cited on page 27.

LIU, X. et al. Coupled axial-torsional dynamics in rotary drilling with state-dependent delay: stability and control. *Nonlinear Dynamics*, v. 78, n. 3, p. 1891 – 1906, 2014. Cited on page 28.

LIU, Y. Suppressing stick-slip oscillations in underactuated multibody drill-strings with parametric uncertainties using sliding-mode control. *IET Control Theory and Applications*, v. 9, n. 1, p. 91–102, 2015. Cited 3 times on pages 7, 23, and 30.

LOBO, D. et al. On the stochastic bit–rock interaction disturbances and its effects on the performance of two commercial control strategies used in drill strings. *Mechanical Systems and Signal Processing*, v. 164, 2022. Cited 2 times on pages 27 and 29.

MEIROVITCH, L. *Principles and techniques of vibrations*. [S.l.]: Prentice Hall New Jersey, 1997. v. 1. Cited 2 times on pages 27 and 36.

MIHAJLOVIĆ, N. et al. Analysis of friction-induced limit cycling in an experimental drill-string system. *Journal of Dynamic Systems, Measurement and Control, Transactions of the ASME*, v. 126, n. 4, p. 709 – 720, 2004. Cited on page 47.

MLAYEH, R.; TOUMI, S.; BEJI, L. Backstepping boundary observer based-control for hyperbolic pde in rotary drilling system. *Applied Mathematics and Computation*, v. 322, p. 66 – 78, 2018. Cited on page 31.

MONTEIRO, H. L. S.; TRINDADE, M. A. Performance analysis of proportional-integral feedback control for the reduction of stick-slip-induced torsional vibrations in oil well drillstrings. *Journal of Sound and Vibration*, v. 398, p. 28–38, 2017. Cited 9 times on pages 7, 27, 29, 31, 33, 34, 36, 55, and 73.

MONTGOMERY, C. T.; SMITH, M. B. Hydraulic fracturing: History of an enduring technology. *Journal of Petroleum Technology*, v. 62, n. 12, p. 26–40, 2010. Cited on page 22.

NAVARRO-LOPEZ, E. M.; LICEAGA-CASTRO, E. Non-desired transitions and sliding-mode control of a multi-dof mechanical system with stick-slip oscillations. *Chaos, Solitons and Fractals*, v. 41, n. 4, p. 2035 – 2044, 2009. Cited 4 times on pages 27, 30, 55, and 67.

NAVARRO-LOPEZ, E. M.; SUAREZ, R. Practical approach to modelling and controlling stick-slip oscillations in oilwell drillstrings. In: *Proceedings of the 2004 IEEE International Conference on Control Applications*. [S.l.: s.n.], 2004. v. 2, p. 1454–1460. Cited 2 times on pages 27 and 34.

PAÏDOUSSIS, M.; LUU, T.; PRABHAKAR, S. Dynamics of a long tubular cantilever conveying fluid downwards, which then flows upwards around the cantilever as a confined annular flow. *Journal of Fluids and Structures*, v. 24, n. 1, p. 111 – 128, 2008. Cited on page 28.

PAVONE, D.; DESPLANS, J. Application of high sampling rate downhole measurements for analysis and cure of stick-slip in drilling. In: *SPE Annual Technical Conference and Exhibition*. New Orleans, Louisiana: [s.n.], 1994. p. 335 – 345. Cited on page 26.

PREUMONT, A. *Vibration control of active structures: an introduction*. [S.l.]: Springer Science & Business Media, 2011. v. 179. Cited on page 31.

RICHARD, T.; GERMAY, C.; DETOURNAY, E. A simplified model to explore the root cause of stick–slip vibrations in drilling systems with drag bits. *Journal of Sound and Vibration*, v. 305, n. 3, p. 432–456, 2007. Cited on page 26.

RITTO, T.; AGUIAR, R.; HBAIEB, S. Validation of a drill string dynamical model and torsional stability. *Meccanica*, v. 52, n. 11-12, p. 2959 – 2967, 2017. Cited on page 26.

RITTO, T.; SOIZE, C.; SAMPAIO, R. Non-linear dynamics of a drill-string with uncertain model of the bit-rock interaction. *International Journal of Non-Linear Mechanics*, v. 44, n. 8, p. 865 – 876, 2009. Cited 2 times on pages 27 and 28.

RITTO, T. G.; GHANDCHI-TEHRANI, M. Active control of stick-slip torsional vibrations in drill-strings. *Journal of Vibration and Control*, v. 25, n. 1, p. 194 – 202, 2019. Cited on page 27.

RUDAT, J.; DASHEVSKIY, D. Development of an innovative model-based stick/slip control system. In: *SPE/IADC Drilling Conference and Exhibition*. Amsterdam, The Netherlands: [s.n.], 2011. v. 1, p. 585 – 596. Cited on page 27.

RUNIA, D.; DWARS, S.; STULEMEIJER, I. A brief history of the shell "soft torque rotary system" and some recent case studies. In: *SPE/IADC Drilling Conference*. Amsterdam, The Netherlands: [s.n.], 2013. v. 2, p. 1492 – 1501. Cited on page 28.

SAGERT, C. et al. Backstepping and flatness approaches for stabilization of the stick-slip phenomenon for drilling. *IFAC Proceedings Volumes*, v. 46, n. 2, p. 779–784, 2013. Cited on page 28.

SALDIVAR, B. et al. Suppressing axial-torsional coupled vibrations in drillstrings. *Control Engineering and Applied Informatics*, v. 15, n. 1, p. 3–10, 2013. Cited 2 times on pages 28 and 47.

SALDIVAR, B. et al. A control oriented guided tour in oilwell drilling vibration modeling. *Annual Reviews in Control*, v. 42, p. 100–113, 2016. Cited on page 26.

SALDIVAR, B.; MONDIÉ, S.; VILCHIS, J. C. Ávila. The control of drilling vibrations: A coupled pde-ode modeling approach. *International Journal of Applied Mathematics and Computer Science*, v. 26, n. 2, p. 335 – 349, 2016. Cited 2 times on pages 28 and 31.

SAMPAIO, R.; PIOVAN, M.; LOZANO, G. V. Coupled axial/torsional vibrations of drill-strings by means of non-linear model. *Mechanics Research Communications*, v. 34, n. 5-6, p. 497 – 502, 2007. Cited on page 27.

SAYE, J.; RICHARDSON, T. Field testing of casing-string design factors. In: *Drilling and Production Practice*. [S.l.]: American Petroleum Institute, 1954. p. 23 – 38. Cited on page 25.

SERRARENS, A. et al. H_∞ control for suppressing stick-slip in oil well drillstrings. *IEEE Control Systems*, v. 18, n. 2, p. 19 – 30, 1998. Cited on page 27.

SKOGESTAD, S.; POSTLETHWAITE, I. *Multivariable feedback control : analysis and design*. 2nd. ed. Chichester, England ; Hoboken, NJ: John Wiley, 2005. 574 p. Cited on page 58.

STOER, J.; BULIRSCH, R. *Introduction to numerical analysis*. [S.l.]: Springer, 2002. v. 3. Cited on page 64.

TAUHATA, S. *Petrobras investe R$ 2 bi em pesquisa e volume aumenta a cada ano*. 2018. Disponível em: <https://valor.globo.com/brasil/noticia/2018/07/04/petrobras-investe-r-2-bi-em-pesquisa-e-volume-aumenta-a-cada-ano.ghtml>. Available from Internet: 11 of oct. 2019. Cited on page 21.

THOMAS, J. E. *Fundamentos de engenharia de petróleo*. [S.l.]: Interciência, 2001. Cited 2 times on pages 21 and 24.

TOUMI, S. et al. Stabilization of torsional vibration in oilwell drillstring system. *European Journal of Control*, v. 35, p. 19 – 27, 2017. Cited on page 31.

TRINDADE, M. Robust evaluation of stability regions of oil-well drilling systems with uncertain bit-rock nonlinear interaction. *Journal of Sound and Vibration*, v. 483, p. 115481, 2020. Cited 4 times on pages 27, 28, 29, and 55.

TRINDADE, M.; WOLTER, C.; SAMPAIO, R. Karhunen–loève decomposition of coupled axial/bending vibrations of beams subject to impacts. *Journal of Sound and Vibration*, v. 279, n. 3, p. 1015–1036, 2005. Cited on page 27.

TRÖLTZSCH, F. *Optimal control of partial differential equations: theory, methods, and applications*. [S.l.]: American Mathematical Soc., 2010. v. 112. Cited on page 35.

TUCKER, R. W.; WANG, C. An integrated model for drill-string dynamics. *Journal of Sound and Vibration*, v. 224, n. 1, p. 123–165, 1999. Cited 2 times on pages 27 and 28.

TUCKER, R. W.; WANG, C. On the effective control of torsional vibrations in drilling systems. *Journal of Sound and Vibration*, v. 224, n. 1, p. 101–122, 1999. Cited on page 30.

TUCKER, R. W.; WANG, C. Torsional vibration control and cosserat dynamics of a drill-rig assembly. *Meccanica*, v. 38, n. 1, p. 143–159, 2003. Cited 4 times on pages 31, 36, 55, and 67.

TZIMAS, E. et al. EUR - Scientific and Technical Research Reports, *Enhanced Oil Recovery using Carbon Dioxide in the European Energy System*. 2005. Cited on page 23.

U. S. Energy Information Administration. *International Energy Statistics*. 2022. Disponível em: <https://www.eia.gov/international/data/world/petroleum-and-other-liquids/annual-petroleum-and-other-liquids-production>. Available from Internet: 1 of may 2022. Cited on page 21.

VAZIRI, V.; KAPITANIAK, M.; WIERCIGROCH, M. Suppression of drill-string stick-slip vibration by sliding mode control: Numerical and experimental studies. *European Journal of Applied Mathematics*, v. 29, n. 5, p. 805 – 825, 2018. Cited on page 28.

VROMEN, T. et al. Mitigation of torsional vibrations in drilling systems: A robust control approach. *IEEE Transactions on Control Systems Technology*, v. 27, n. 1, p. 249–265, 2019. Cited on page 28.

VROMEN, T. et al. Nonlinear output-feedback control of torsional vibrations in drilling systems. *International Journal of Robust and Nonlinear Control*, v. 27, n. 17, p. 3659 – 3684, 2017. Cited on page 30.

WANG, J.; TANG, S.-X.; KRSTIC, M. Adaptive output-feedback control of torsional vibration in off-shore rotary oil drilling systems. *Automatica*, v. 111, 2020. Cited on page 28.

WASILEWSKI, M. et al. A new efficient adaptive control of torsional vibrations induced by switched nonlinear disturbances. *International Journal of Applied Mathematics and Computer Science*, v. 29, n. 2, p. 285 – 303, 2019. Cited on page 27.

YIGIT, A. S.; CHRISTOFOROU, A. P. Stick-slip and bit-bounce interaction in oil-well drillstrings. *Journal of Energy Resources Technology-Transactions of the Asme*, v. 128, n. 4, p. 268–274, 2006. Cited 4 times on pages 28, 30, 31, and 55.

ZHU, X.; TANG, L.; YANG, Q. A literature review of approaches for stick-slip vibration suppression in oilwell drillstring. *Advances in Mechanical Engineering*, v. 2014, 2014. Cited on page 25.